CCFE
CULHAM CENTRE FOR FUSION ENERGY

UK Atomic Energy Authority

UKAEA-CCFE-PR(21)26

J P Coad, M Rubel, J Likonen, N Bekris, S Brezinsek, G F Matthews, M Mayer, A M Widdowson, JET contributors

Material Migration and Fuel Retention studies during the JET carbon divertor campaigns

Material Migration and Fuel Retention studies during the JET carbon divertor campaigns

J P Coad, M Rubel, J Likonen, N Bekris, S Brezinsek, G F Matthews, M Mayer, A M Widdowson, JET contributors

This is a preprint of a paper submitted for publication in Fusion Engineering and Design

MATERIAL MIGRATION AND FUEL RETENTION STUDIES DURING THE JET CARBON DIVERTOR CAMPAIGNS

J P Coad[1], M Rubel[2], J Likonen[3], N Bekris[4], S Brezinsek[5], G F Matthews[1], M Mayer[6], A M Widdowson[1] and JET contributors*

EUROfusion Consortium, JET, Culham Science Centre, Abingdon, OX14 3DB, UK

[1]Culham Centre for Fusion Energy, Culham Science Centre, Abingdon, OX14 3DB, UK
[2]Royal Institute of Technology, SE-10044 Stockholm, Sweden
[3]VTT Technical Research Centre of Finland, P.O. Box 1000, FIN-02044 VTT, Finland
[4]Close Support Unit, EUROfusion Consortium, Culham Science Centre, Abingdon, UK
[5]Institut fur Energieforschung-Plasmaphysik, Forschungszentrum Juelich, D-52425 Juelich, Germany
[6]Max-Planck Institut für Plasmaphysik, 85748 Garching, Germany

*See the author list of X. Litaudon et al. 2017 Nucl. Fusion 57 102001

Contents

Abstract

The first divertor was installed in the JET machine between 1992 and 1994 and was operated with carbon tiles and then beryllium tiles in 1994-5. Post-mortem studies after these first experiments demonstrated that most of the impurities deposited in the divertor originate in the main chamber, and that asymmetric deposition patterns generally favouring the inner divertor region result from drift in the scrape-off layer. A new monolithic divertor structure was installed in 1996 which produced heavy deposition at shadowed areas in the inner divertor corner, which is where the majority of the tritium was trapped by co-deposition during the deuterium-tritium experiment in 1997. Different divertor geometries have been tested since such as the Gas-Box and High-Delta divertors; a principle objective has been to predict plasma behaviour, transport and tritium retention in ITER. Transport modelling experiments were carried out at the end of four campaigns by puffing ^{13}C-labelled methane, and a range of diagnostics such as quartz-microbalance and rotating collectors have been installed to add time resolution to the post-mortem analyses. The study of material migration after D-D and D-T campaigns clearly revealed serious consequences of fuel retention in the presence of carbon walls. They gave a strong impulse to make a fundamental change of wall materials. In 2010 the carbon divertor and wall tiles were removed and replaced with tiles with Be or W surfaces for the ITER-Like Wall Project.

Keywords

Fusion, JET, divertor, carbon, plasma-facing components

Acronyms and Abbreviations

AGHS: Advanced Gas Handling System

BeHF: Beryllium Handling Facility

CFC: Carbon Fibre Composite, or Carbon Fibre-reinforced Carbon composite

DTE or DTE1: Deuterium-Tritium Experiment (the first full experiment in 1997)

EFDA: European Fusion Development Agency

ELM: Edge Localised Mode

EPS: Enhanced Proton Scattering

FTS: Fast Transfer System

HFGC: High Field Gap Closure

GDC: Glow Discharge Carbonisation, or Glow Discharge Cleaning

GIM: Gas Injection Module

IBA: Ion Beam Analysis

ILW: ITER-Like Wall project (in JET)

ISP: Inner Strike Point

ITER: International Thermonuclear Experimental Reactor

JET: Joint European Torus

LBT: Load Bearing Tile

LCFS: Last Closed Flux Surface

MkI: Mark 1 divertor (1994-5)

MkII-A: Mark II-A divertor (1996-8)

MkII-GB: Mark II Gas Box divertor (1998-2001)

MkII-SRP: Mark II Septum Replacement Plate divertor (2001-4)

MkII-HD: Mark II High-Delta divertor (2005-9)

NBI: Neutral Beam Injection

NET: Next European Tokamak

NRA: Nuclear Reaction Analysis

OSP: Outer Strike Point

PIXE: Particle Induced X-ray Spectroscopy

PTE: Preliminary Tritium Experiment (in 1992)

RBS: Rutherford Back-scattering Spectrometry

RH: Remote Handling

RTE: Remote Tile Exchange

SAS: Surface Analysis Station

SIMS: Secondary Ion Mass Spectrometry

SOL: Scrape-Off Layer

SRP: Septum Replacement Plate

ToF-ERDA: Time-of-Flight Elastic Recoil Detection Analysis

1. Introduction

The purpose of this review is to outline the development of divertors in the Joint European Torus (JET) with a carbon wall, and particularly the contribution of post-mortem analysis of tiles removed from the divertor at each opportunity (usually at shutdowns to make modifications to the divertor design). However, it is first necessary to describe the development of the plasma-facing components in JET that provided the environment in which the divertors were to be installed. A timeline for the period from the first JET plasma in 1983 to the beginning of the JET ITER-Like Wall project (JET-ILW) in 2010 is shown in Figure 1.

Construction of JET was completed in 1983, and the first operational campaign was from 1983 to 1984. At that time the interior of the Inconel vacuum vessel was very plain – bare metal walls with discrete limiters at the outer mid-plane for controlling the minor radius of the plasma as shown in Figure 2. JET was designed to have nickel (Ni) limiters, and two can be seen at the outer mid-plane in Figure 2, but during the construction phase fusion experiments around the world were discovering the advantages of having carbon as the contact material with the plasma. Carbon can take very high power loads as it can operate to very high temperature and has excellent damage resistance. Furthermore, if carbon does get into the plasma by erosion (e.g. sputtering) a key advantage of low-Z PFMs is that they don't cause much radiative cooling of the core plasma, which can be a problem with high-Z PFMs. Therefore, at the last moment two carbon limiters were added at the outer mid-plane, and it was these limiters that were in contact with the plasma during 1983-4. (The distances of the limiters from the outer wall could be varied, so any particular limiters could be chosen to be the first contact points for the plasma.)

In the 1984 shutdown tiles were removed from each of the carbon limiters for analysis [1,2] and replaced with new tiles, and poloidal sets of long-term samples were installed around the vessel wall – these were ~1 cm^2 samples of nickel or graphite on a stainless steel holder screwed into "bosses" (M6 nuts welded to the surface of the Inconel wall) [3]. These were the first steps in the post-mortem analysis programme that has accompanied every shutdown in the history of JET.

During the 1983-4 operations, even though the discharges were purely ohmic as no additional heating had yet been installed, significant melt damage was observed at the inner vessel wall on bellows protection plates, which were the items at largest radius – i.e. closest to the plasma. To prevent such damage, during the 1984 shutdown carbon tiles were installed that covered the inner wall of JET. The tiles were flat graphite plates fitted so that every tile in each toroidal row was at the same major radius. This meant that the joint between adjacent tiles in the row were at slightly larger radius than the centres of the tiles, and ions travelling toroidally along field lines could impinge on the edges of each tile. As a result, in the subsequent campaign the most prominent edges received very high power loads leading to massive erosion and causing carbon impurity levels in the plasma to reach uncontrollable levels (referred to as "carbon blooms" [4]). In an emergency shutdown the carbon tiles at the inner wall were replaced with poloidal rows of ridged tiles, with the spaces between filled with (flat) tiles set back at a smaller radius, so that field lines were always incident at a small angle to the tangent to the tile surface.

Over the next few years the interior of JET was progressively covered with sets of carbon tiles, so that already by 1986 JET was referred to as an "all-carbon" machine [4], in that any ion in the confined plasma could only interact with a carbon surface at the periphery of the plasma; a view of the interior of the JET vessel in 1987 is shown in Figure 3. As can be seen in the figure, the poloidal sets of tiles were extended to the whole vessel. Two toroidal rings of tiles can also be seen in the figure, just above and just below the outer mid-plane: these "belt limiters" replaced the small discrete limiters at the outer midplane, with the intention of providing much greater surface area for plasma contact (and hence power handling capability). However, although the individual slices of the array were shaped poloidally, in the poloidal direction the slices provided a very large number of slight edges, and there was little or no improvement in actual power handling before carbon or (when one belt was replaced with Be slices) beryllium "blooms".

In Figure 3 it can be seen that about half of the Inconel wall was not covered with tiles, so that the wall remained a source of metal impurities (Ni, Cr, Fe) due to bombardment by charge exchange neutrals (CXN), which are high energy neutral particles that can escape the plasma and can travel in any direction. A method of covering all surfaces with carbon was employed in the period 1984-6 called Glow Discharge Carbonisation (GDC) [5,6] in which a glow

discharge is struck in the vessel in methane to deposit carbon everywhere. The coverage is very thin and probably non-uniform, so this can only be a short-term measure and was not continued.

Oxygen was present as a plasma impurity at a comparable level to carbon. To reduce the oxygen content in the TEXTOR tokamak in Germany, an oxygen gettering element (boron) had been deposited by using a glow discharge in a gaseous compound, diborane, incorporating the appropriate element, boron [7]. The boronisation greatly reduced the oxygen level (and also CO and CO_2) in subsequent plasma discharges. It was also found that the wall adsorbed hydrogen from the plasma, facilitating density control and the establishment of low recycling conditions [7]. Oxygen was also a problem in JET, but it was decided to experiment with an even lighter gettering element, beryllium. Beryllium (Be) is a malleable metal with high vapour pressure at ~900 ºC, so in JET Be was evaporated from four heads equi-spaced around the outer wall that were normally housed within ports protected from the plasma by limiters. They could be moved further into the vessel by about 50 cm during a break in plasma operations to positions beyond the limiters for evaporation over the majority of the vessel. The first evaporation was on 29th May 1989, and the evaporation was monitored with a probe on a sample insertion system called the Fast Transfer System (FTS). The probe provided a calibration point for the amount of material evaporated and hence deposited (which varied by inverse square law with distance from each head). Surface analysis of the probe demonstrated that the Be deposit was basically metallic, but that the deposit gettered any oxygen in the machine to form oxide, and that during subsequent plasma operations the carbon impurities could interact with the Be to form beryllium carbide [8]

The FTS allowed samples to be exposed at the plasma boundary near the outer mid-plane and to be returned under vacuum out of the machine and the Torus Hall to an analysis system called the Surface Analysis Station (SAS) in the Diagnostic Hall, but the system was very complex, and success rate was very low. Furthermore, the system had been designed when JET planned to use discrete limiters at the outer mid-plane, so these limiters would define the plasma boundary near the probe. However, by the time the system was operational belt limiters had been installed, as was shown in Figure 3, and typically the plasma would start in contact with both limiters but then drift out of contact with one during the heated phase of the discharge. As a result, the distance of the Last Closed Flux Surface (LCFS) from the probe position (which was fixed during the pulse) could vary by at least 10 cm during the pulse; as the probe cannot at any time protrude beyond the LCFS it meant during the interesting part of the discharge that

the probe was too far from the plasma for a meaningful measurement. When JET decided to install a divertor after the campaign ending in 1992, it meant the plasma boundary would be even more undefined at the outer mid-plane, and rather than make massive modifications the FTS and SAS were dismantled.

A drawback with using Be for density control is that it is a hazardous material. Since its introduction in 1989 work within the torus has been carried out using Remote Handling equipment, which was specially developed at JET for fusion applications, and if human intervention is essential workers are subject to rigorous Health Physics controls including use of full suits and piped air for breathing.

The consensus view of scientists working on fusion by the late 1980s using tokamaks was that a divertor would be essential for fuel and power exhaust in a power reactor, and the proposed ITER design incorporated such a divertor. However, it would be necessary to develop a satisfactory way of handling the power flux to the relatively small contact areas within the divertor, which might reach ~30 MW m^{-2} [9, 10]. It was clear that JET, as the world's leading research tokamak should therefore contribute to divertor development. Installation of a divertor within the JET vessel would require a major shutdown and complex internal engineering including in-situ winding of magnetic coils. It was decided therefore to first explore the production of plasma shapes with an X-point at the top of the JET vessel to create an open divertor (Figure 4). The roof of the vessel was covered with graphite tiles, and then in September 1991 specially designed carbon fibre reinforced carbon (CFC) dump plate tiles replaced these tiles where extra power handling was required (CFC tiles were to be used exclusively instead of graphite in JET after the divertor installation). Power fluxes up to 10 MW m^{-2} were experienced at the outer strike point. Post-mortem analyses showed that D retention and Be deposition were very low at both strike points (but lower at the outer), with most re-deposition occurring inboard from the inner strike point [11].

In 1992 in parallel with X-point experiments the first tritium was introduced into JET from the Active Gas Handling System (AGHS). During this Preliminary Tritium Experiment (PTE) a small amount (100 mg) was introduced in two pulses. All the tritium was absorbed into the wall (no tritium was pumped after either pulse), and the decrease in the amount recycling into the plasma was studied during subsequent discharges [12].

The shutdown for the installation of a divertor commenced in 1992, and operations with the MkI divertor began in 1994. The subsequent chapters deal with the developments in divertor design and operation in JET, and the lessons learnt through post-mortem analysis of samples taken from the divertor at each shutdown.

1.1. Conclusions from the pre-divertor phases

- There is unavoidable plasma interaction with the main chamber surfaces: ions in the SOL interact with the closest surfaces to the confined plasma, and CXN bombard all uncovered surfaces.
- Vessel damage can be avoided by installing poloidal rows of protection tiles
- Carbon tiles are a suitable protection material as they can withstand high power loads and any erosion has a minimal contribution to plasma dilution; however, shaping is essential to avoid interaction of ions with tile edges. CFC can withstand much greater power loads than graphite.
- Regular evaporations of beryllium improved plasma density control, facilitated low recycling conditions, and reduced oxygen impurity levels.

2. Operational campaigns with divertors in JET

2.1. The MkI divertor 1994-5

Installation of a divertor in JET was a major engineering task. Firstly, the interior of the vessel was contaminated with Be, so all interior fittings had to be removed to expose the vacuum vessel wall, which was then cleaned to remove any Be. The opportunity was then taken to remove one of the vessel Octants and replace it with the spare (ninth) Octant because one of its four toroidal field coils had failed previously - this required automatic cutting from inside and outside the double-walled vacuum vessel to remove the Octant, followed by automatic welding of the replacement. Four divertor field coils were then wound in-situ around the inside of the vessel to facilitate magnetic shaping of the plasma. It was realised that because of the power loading at the plasma contact regions of the divertor, cooling would be necessary. Maximum cooling can be achieved by having a coolant circulating through the very component in contact with the plasma. Design, development and construction of the ideal solution would have been a long-term project, but a compromise solution was installed in JET: a large number (193) of radial water-cooled pipes forming the shape of the divertor cross-section, with tiles

bolted to the pipes; Figure 5 shows one such divertor cross-section with the set of tiles (numbered 1-19) which are bolted to the pipe (which is in the plane of the drawing).

Following installation of the divertor structures, wall protection tiles and RF heating antennas were replaced, but with revised shaping to fit the outline of a single-null divertor plasma.

The MkI divertor was first fitted with graphite tiles, and operated from August 1994 to April 1995, when the graphite tiles were exchanged for Be tiles and operated during May and June 1995. The divertor tiles were mounted in a "roof-top" formation shown schematically in Figure 6, so that the edge of one tile shadows the edge of the next from the incident plasma ions - the vertical scale is exaggerated as the angle of incidence of the plasma ions is in reality ~5-7°. To allow for variations in the angle of incidence and for possible misalignments of the radial water-cooled support pipes, only 50 to 70% of each base tile was exposed to the plasma. There were also gaps of ~5 mm between each row of tiles, so as a result the exposed areas of tiles accounted for less than half of the circumferential distance round the divertor. Power handling in the MkI divertor was thus limited, and furthermore the cooling of the tiles by bolting to the pipes was not very effective. Following the MkI operations the divertor structure was removed and replaced with a unitary water-cooled structure, to which were fastened carbon-fibre composite (CFC) tile carriers fitted with much larger CFC tiles.

2.2. The MkIIA divertor 1996-8

The MkII divertor has been used with a number of different tile configurations. The first four divertor configurations used at JET are shown in Figure 7, whilst the final configuration of the carbon divertor (MkII-HD) is shown in Figure 8 and is compared to the proposed ITER divertor.

The MkIIA divertor was operated from 1996 to 1998. A deuterium-tritium experiment (DTE-1) was planned for 1997 wherein significant amounts of tritium would be introduced, so there was a short intervention at the end of 1996 (the first with the new divertor configuration) to remove diagnostics that did not have double containment for protection against a possible vacuum breach, or that might be damaged by the increased fluence of neutrons (i.e. not compatible with tritium operations) – as usual the opportunity was taken to remove some divertor tiles and this proved very interesting (see section 3.3). During the 1997 D-T campaign, 35g of tritium were introduced into the torus, mainly by gas puffing [13]. Following the DTE-

1 campaign during 1997 and a clean-up period of about three months, designed to remove as much tritium from the vessel as possible by running discharges in H or D, GDC (Glow Discharge Cleaning) and baking, etc, the machine was vented for the Remote Tile Exchange (RTE) [14, 15].

Since there was a significant amount of T still trapped in the vessel, and an increased radiation level due to the fast neutrons produced by D-T fusion reactions, all operations in the vessel during the RTE were performed using the remote handling equipment. All the divertor carriers were removed from the JET vessel, together with their CFC tiles (still mounted). Two poloidal sets of carriers plus tiles were retained for post-mortem analysis, whilst all the other carriers (plus tiles) were put into storage in two ISO-containers (at ambient temperature), with the ventilation pipes connected to the outlet stack from the gas handling system because of continuing chronic tritium release.

During the MkII-A campaigns the strike points were almost exclusively on the divertor base tiles, i.e. the inner strike points on Tiles 4 and 5, and the outer strike points on Tiles 6 and 7.

2.3. The MkII Gas Box divertor (MkII-GB) 1998-2001

New divertor tile carriers with a different configuration of CFC tiles were mounted during the 1998 RTE shutdown, called the MkII-GB divertor, as shown in Fig 7c. The inner carriers of the divertor support just two toroidal bands of (slightly wider) tiles (Tiles 1 and 3), whilst the outer wall of the divertor also comprises just two toroidal bands (Tiles 7 and 8). The most notable feature of the MkII-GB, however, is the septum at the centre of the divertor floor. This "septum" or so-called "Gas Box" is protected from the plasma by its own tiles, which are numbered 5, and the structure includes a complete wall separating the inner and outer divertor legs. Tile 4 is at the base of the inner divertor leg (and can be accessed by the plasma only over a limited area), whilst Tile 6 is at the base of the outer leg and, like Tile 4, can only be seen by the plasma in a limited region. The installation of the MkII-GB enabled the JET divertor to resemble the configuration planned for ITER (compare Figure 7c and Figure 8b). A view inside the JET vessel at this time is shown in Figure 9 (left-hand half of the figure).

During the period with the Mk-IIGB configuration there was an intervention in 1999 when a poloidal set of divertor tiles was removed from Octant 5D and replaced with a special set of

marker tiles (see section 3.3.1). Operations with the MkII-GB were completed in February 2001 when MkII-GB was replaced by MkII-SRP (see Fig. 7d).

The most common plasma configurations during the Mk-IIGB operations have the strike points on the vertical Tiles 3 and 7, as shown in Figure 10 (and as planned for ITER), though the location varies, as shown in Figure 11. The histogram in Figure 11 also shows that very occasionally the inner strike point was moved onto Tile 1, and the outer strike point onto Tile 8 (not included in Fig.10). If the X–point was lowered too much, then one or both of the strike points is intercepted by the septum tiles. It was avoided as far as possible, since the septum tiles did not have as high load-bearing capabilities as the other divertor tiles. However, there was a limited range of plasma configurations that allowed JET to run with the strike points on Tiles 4 and/or 6. Most of the surfaces of Tiles 4 and 6 can be seen from Fig. 10 to be horizontal, but the possible strike point positions were restricted to the sloping parts of the tiles between horizontal parts shadowed by the septum structure or by Tiles 3 or 7. These plasma configurations ("corner shots") were quite frequently run in studies of divertor physics, as they mean that access to the cryopump (which is via the louvres in the corners of the divertor) was from the scrape-off layer (SOL) rather than the private flux region. Corner shots were also believed to be very important for material transport and retention, as will be discussed in section 3.4.1.

The vast majority of discharges in JET were fuelled with deuterium and ran with a fixed direction for the toroidal magnetic field and plasma current. Occasionally there were periods of operation with protium (e.g. for H isotope changeover experiments) or helium fuelling. Such periods were usually at the end of the campaign prior to a shutdown, since protium or helium fuelling produces negligible neutrons, so the vessel activation is minimised. As an example, the four weeks of operation prior to the 2001 opening were in He [16], apart from the last three days when operations reverted to D fuelling. Unfortunately, such pre-shutdown deviations from normal running make the analysis of PFCs for retention of deuterium much more difficult, since the region best analysed is the near-surface which primarily reflects the latter stages of the plasma operations.

As will be shown later, the normal direction for the toroidal magnetic field and plasma current results in heavy deposition of impurities at the inner divertor, whereas most areas at the outer divertor exhibit small amounts of erosion. JET can also operate with the magnetic field

and the direction of the plasma current reversed (which is referred to as “reversed field” operations), and there was a short period of JET operation in this mode in 1998-1999 (just before the 1999 shutdown). In reversed field operations, ion temperatures and fluxes at the two divertor legs are more equitable; as a consequence it is believed that the deposition of impurities is also more equitable - more details are given in the description of the experiment during operations with the MkII-SRP (sections 2.4 and 4.2) [17]. However, JET has never run a complete campaign in this mode and, therefore, the pattern of deposition has not been clearly established. It may be that if there are small differences in deposition patterns between outer divertor tiles removed in 1999 and 2001, the reversed field experiment was responsible (see also section 3.5.2.1).

From the very first operations in 1983 until 2001, JET operated with a vessel wall temperature of 320°C throughout each campaign (usually last some months). The divertor structure is, however, water-cooled in order to protect the poloidal field coils that are situated within the vessel alongside the divertor to produce the necessary field shaping. The divertor carriers are fastened to the support structure, but there is limited thermal conduction between tiles and structure. The divertor tiles thus have a base bulk temperature intermediate between the water and vessel temperatures, which is measured with thermocouples embedded in a selection of tiles, the results of which are shown in Figure 12 for inner divertor wall tiles. During the MKII-Gas Box operations in 2000, Tiles 1 and 3 had base temperatures of 170°C and 160°C, respectively. During each plasma discharge (in the divertor configuration) power is deposited on the tile surfaces: the strike point region may reach 1000 °C or greater and the overall energy deposited in the divertor may be 10 MJ. Thus, during a day of plasma pulsing the bulk temperature of the tiles steadily increases, typically to 210 °C and 220 °C for Tiles 1 and 3 respectively, as seen in Figure 12, returning to the base temperature overnight. However, from the beginning of 2001 the vessel temperature was held at 200 °C throughout the two months’ operations in 2001 prior to the shutdown. As also shown in Figure 12, the mean tile temperatures for both Tiles 1 and 3 before and after a day of pulsing were then 80 °C and 140 °C, respectively. Values for the MkIIA inner divertor wall tiles are also included in Figure 12: the slightly higher values may be because the MkIIA carrier was different, and the tiles were farther from the cooling structure.

The integrated lengths of plasma pulses during MkII-GB operations were $6.1x10^4$, $1.02x10^5$ and $1.63\ x10^5$ seconds, including $3.7\ x10^4$, $5.7\ x10^4$ and $9.4\ x10^4$ seconds of X-point operation (i.e. the periods with the strike points in the divertor) for 1998-1999, 1999-2001 and (cumulatively) 1998-2001, respectively. Ion fluxes during discharges are routinely measured with divertor Langmuir probes. Integrated ion fluxes were calculated for the experimental periods 1998-1999 (discharges 44659-48596) and 1999-2001 (discharges 48597-54345), and hence for the combined period 1998-2001 (discharges 44659-54345). The results for the inner divertor wall probes 2-8 are given in Table 1. Unfortunately, Probe 1 was not working and is therefore not included in the table. Probes 2-4 and 5-8 correspond to Tiles 1 and 3, respectively. For Tile 1 numbering of the probes is the same as that for the mechanical measurement points shown in Figure 9. However, there are 5 probes in Tile 3 so the numbering of the probes does not quite correspond to the location of mechanical measurement points. Ion fluxes seem to be higher for Tile 1 during the 1999-2001 campaign than for the 1998-1999 campaign, possibly due to a change in the mean strike point position. For Tile 3 ion fluxes are quite comparable for both campaigns.

During the last session before the shutdown a series of identical L-mode pulses were run whilst ^{13}C-labelled methane was puffed into the vessel from a point at the top of the vessel during the X-point phase; the results are described in section 4.1.

2.4. The MkII divertor with Septum Replacement Plate (MkII-SRP) 2001-2003

Although the MkII-GB resembled the shape of the ITER divertor, with a septum and vertical strike points, in practice the range of plasma parameters that could be achieved using the divertor was restrictive and did not allow the closest simulation of ITER plasma parameters: the physical similarities turned out to be of secondary importance. Therefore, in the 2001 shutdown a changeover was made to the MkII-SRP divertor in which the septum was removed and replaced with a cover plate, which was termed the "septum replacement plate" (Fig. 7d). The cover plate was made of CFC but was just a flat plate with no shaping (e.g. to protect tile edges) and was thus intended not for power handling, but merely to protect the divertor base structure from short inadvertent movements of the strike points. A view of the interior of JET during the MkII-SRP phase was shown in Figure 9 (right-hand side).

The MkII-GB septum tiles and support structure became available for analysis, and the special marker tiles installed in 1999 were retrieved for analysis during the 2001 shut-down

and replaced with new tiles. At the same time, a new set of marker tiles was installed nearby; these comprised a poloidal set of tiles coated with stripes of W approximately 3 μm thick. As a result, two poloidal set of tiles became available for analysis in 2001 (see section 3.4.2).

JET continued to operate with a wall temperature of 200°C, compared with 320° for all previous operations except the last two months with the MkII-GB divertor (as shown in the previous section). In June/July 2003 four weeks of JET plasma operations were once again devoted to experiments with reversed magnetic field. In this configuration, as mentioned in section 2.2, plasma temperature and density in the inner and outer divertor legs are more similar. The drift velocity in the SOL from outboard to inboard seen for the normal field direction is greatly reduced [18] and the outer divertor also becomes a region of net deposition, as was demonstrated from infra-red spectroscopy measurements (the phenomenon is described in section 4.2) [17]: this may have affected the deposition observed on samples removed in 2004. Another $^{13}CH_4$ puffing experiment was carried out on the last day of the 2001-2004 campaign (see section 4.2).

Up to 2004 a number of different co-ordinate systems were employed to enable data to be allocated uniquely to poloidal positions on the divertor tiles. One such method was to plot data against the Z co-ordinate (distance above/below the vessel mid-plane), as used in Figure 10. However, this is unsatisfactory for measurements such as post-mortem analysis along tile surfaces as, for instances, horizontal surfaces have the same value, and there are inner and outer divertor tiles with the same value. From 2004 the "s co-ordinate" system was agreed between spectroscopists and post-mortem analysts that correctly defines the distance along the tile surfaces, starting at agreed reference points. The system is illustrated in Figure 13 for the MkII-HD divertor (next section). The measurements start at the inner edge of the High Field Gap Closure (HFGC) tile, which is located inboard from Tile 1 and labelled "0" in Figure 13 (but was not fitted in JET until 2004), then follow the tile contours all the way poloidally to Tiles B and C, which are located outboard from Tile 8, and are not attached to the main divertor structure. Tiles B and C are denoted as Tiles 9 and 10 in Figure 13. There are breaks in the continuity of the co-ordinates between some tiles (e.g. at inner and outer corners), where there are gaps between tiles. When the system is applied retrospectively to data from the JET MkII-

SRP campaigns, the SRP (which fits directly between Tiles 4 and 6) has co-ordinates for its top surface from 980 to 1260 mm.

Whilst the strike points in the MkII-GB divertor were expected to be on the vertical tiles, as in the ITER geometry, Tiles 4 and 6 are also shaped to handle the peak plasma power loadings at the strike point. Having removed the septum a wider range of discharge shapes with the strike points on Tiles 4 and 6 were enabled. Figure 14 is a histogram showing the distribution of strike point positions in the divertor during the MkII-SRP operations. The X-axis is the s co-ordinate: the changes from Tiles 1-3-4-5-6-7-8 occur at approximately 0.43, 0.7, 0.95, 1.32, 1.55 and 1.81 m. It is clear from the Figure 14 that marginally more discharges were run with the inner strike point on Tile 4 than on Tile 3, whilst there were clearly more discharges with the outer strike point on Tile 6 than on Tile 7.

On the last day of operation in 2004, $^{13}CH_4$ was puffed from gas nozzles in each of the outer modules, the gas emerging between Tiles 7 and 8, into 25 ELMy H-mode discharges (see section 4.2.1).

2.5. The JET MkII High Delta (MkII-HD) divertor 2005-2009

The Mk II-SRP divertor was a short-term measure to allow a wider variety of plasma shapes with a simple divertor modification. However, in 2004 a major shutdown commenced during which a well-designed divertor modification was installed. Replacing the SRP was a wedge-shaped unit with a load-bearing tile (LBT) correctly shaped for edge protection, and designed to be used as the outer strike point for high-δ discharges which simulate (at the JET scale) many of the important ITER parameters.

Figure 15 shows the cross-section of the JET-HD divertor installed in 2004 and used until 2009 with two different plasma configurations: (a) plasma cross-section for the high-delta configuration with the inner strike-point on Tile 1 and the outer strike-point on the load bearing tile (sometimes referred to as Tile 5): (b) an example of other configurations used with the MkII-HD divertor with strike-points more symmetrically placed, e.g. as here, on Tiles 3 and 7. Figure 15 (a) is a rather extreme version of the HD configuration – more usually the inner strike point was at the top of Tile 3, as can be seen for the histogram of strike point positions given in Figure 16.

As was seen in Figure 16, there were actually two operational periods with the carbon MkII-HD divertor, which were separated by a shutdown in 2007 to complete installation of the ICRH antenna and upgrades to the Neutral Beam systems - as usual the opportunity was taken to remove tiles for post-mortem analysis. We may note that in Figure 16 there do not appear to be many pulses with the strike point on Tile 5 compared to Tiles 6 and 7. However, the integrated power loadings to divertor Tiles 5, 6 and 7 in 2005-7 (taken from thermocouple data) were 9.5, 18 and 9.2 MJ, respectively. For comparison the power loadings with the MkII-SRP divertor for the equivalent tiles were <1, 16 and 12 MJ, respectively.

Tracer experiments with puffed $^{13}CH_4$ were carried out before the shutdowns in 2007 and 2009. The puffing in 2007 was from a plenum at the outer mid-plane alongside the Lower Hybrid antenna, but was not very successful because the gas supply line was found to be contaminated with air, so the experiment was abandoned after just a few pulses. In 2009 the gas was puffed from nozzles set in each tile 6D (24 toroidal locations); the results are described in section 4.3.

3. Analysis of tiles removed during JET shutdowns

3.1. Analysis methods

As mentioned previously, tiles are removed at every shutdown for post-mortem analysis. Although toroidal uniformity is usually assumed when analysing data, it is worthwhile appreciating the locations of the tiles being analysed. Figure 17 is a floor plan of the divertor which consists of 24 modules, numbering anti-clockwise from Octant 1. Each module has Wide and Narrow carriers (the wide carrier has electrical connections), and there are Outer, Base and Inner carriers. So, for example, a tile designated as 2IN G1A is in Module 2, on the Inner carrier and is a Tile 1 (one of four with labels “A”, “B”, “C” or “D”).

The main methods of analysis were the Ion Beam (IBA) techniques, whilst thicker films were analysed by sputter profiling using Secondary Ion Mass Spectrometry (SIMS), or by making cross-sections for optical microscopy or nuclear microprobe (IBA using a micro-beam [19]). The aim of the analysis was to determine the quantitative composition and structure of the surface and near-surface layer of PFCs, i.e. usually CFC tiles in the case of JET. The amount and distribution (spatial and depth) of deuterium, carbon (^{12}C and ^{13}C), beryllium, boron and metals (Re or W markers and Inconel® components: Ni+Cr+Fe) were of primary interest. No single analysis method can possibly provide the complete data required, and in any case there

would be a benefit in comparing analyses from different techniques. Because of problems with beryllium and tritium contamination in samples coming out of JET, equipment within dedicated facilities was required: special chambers and sample handling facilities were developed for the two main SIMS and IBA laboratories located at VTT, Espoo in Finland, and at the University of Sussex in the UK (equipment later moved to the University of Lisbon, Portugal). These techniques are almost unique in their ability to analyse H-isotopes, but alternative techniques such as Auger electron spectroscopy and scanning electron microscopy combined with wavelength dispersive X-ray spectroscopy also proved helpful.

As stated in the previous paragraph, all materials retrieved from the JET vessel are contaminated with beryllium and tritium. Therefore, ex-situ examination of tiles is carried out in controlled areas equipped with glove boxes for transfer and handling of samples. IBA, in most cases, could analyse entire tiles without cutting them into smaller pieces, because of the large loading port and large volume of the analysis chamber. Smaller samples required for SIMS analysis (cylinders 17 mm in diameter) were machined by a coring technique. Each core was cut by drilling through the tile with a hollow drill with an outside diameter of 20 mm and 1.5 mm wall thickness, producing a core sample of 17 mm in diameter. A poloidal line of holes was drilled every 20 mm across the tile. For cross-sectional analysis the samples were then cut in half and polished to provide a poloidal cross-section for 17 out of every 20 mm of the tile. The sections were examined with a Nikon optical microscope.

IBA methods used in the study include Nuclear Reaction Analysis (NRA), Rutherford Backscattering Spectrometry (RBS), Enhanced Proton Scattering (EPS), Particle Induced X-ray Emission (PIXE) and Time-of-Flight Elastic Recoil Detection Analysis (ToF-ERDA). Data in Table 2 summarise the most typical parameters of the IBA methods. In this work the most demanding was the analysis of ^{13}C in the presence of significant ^{12}C background in the tiles. Therefore, the quantity of ^{13}C re-deposited on the tiles was cross-checked with several independent methods. In the case of materials from JET the most convenient was the use of NRA technique based on the $^{13}C(^{3}He,p)^{15}N$ reaction [20]. Very reliable results were also obtained using enhanced proton scattering $^{13}C(p,p)^{13}C$ with a 2.5 MeV proton beam [21]. The greatest sensitivity is achieved with a proton beam at the resonance energy (1.442 MeV) but reliable quantification in this case was possible only for very thin films containing the ^{13}C isotope [22].

Nuclear Reaction Analysis (NRA) reaction cross-sections vary with beam energy, and data were typically recorded with a ^{3}He ion beam at 2.5 MeV when the three elements of interest at JET (C, Be and D) could be simultaneously measured using the reactions ^{9}Be(^{3}He,p)^{11}B, ^{12}C(^{3}He,p)^{14}N and d(^{3}He,p)^{4}He, where "p" and "d" are protons and deuterons, respectively. The threshold energy for measuring Be and C is ~1.8 MeV and the cross-section increases with energy to well beyond the 3 MeV that was attainable at the University of Sussex. The analysis depth also depends on the reaction energy and is greater for Be than for C by approximately a factor of two. In the NRA results, therefore, if the film thickness is greater than the analysis depth (1-2 μm) the Be signal has been reduced by a factor of two to compensate, so that the Be/C values plotted are the atomic ratios in the outermost micrometres of the surface film. This correction is only accurate if the ratio of Be to C remains constant through at least the outer 2-3 μm; variation in the composition of the outer layers can be seen by RBS and detailed evaluation of that data may indicate whether some correction to the NRA ratios is necessary in the future. The reaction cross-section for D however is quite different, with a threshold at ~0.5 MeV and a peak at ~0.8 MeV - the cross-section at 2.5 MeV is about one-third the peak value. Thus the amount of D is an approximate integration over the first ~8 μm into the surface, based on the D peak shape (which reflects the variation in composition with depth) and taking into account the variation in cross-section with incident energy. However, a rigorous quantitative solution is difficult due to limits in the inherent resolution, and the resulting values for thick films may be in error by about ±30%.

SIMS analysis was made with a double focussing magnetic sector instrument (VG Ionex IX-70S). A 5 keV O_2^+ primary ion beam was used and the ion currents of a selection of secondary ions such as H^+, D^+, $^{9}Be^+$, $^{11}B^+$, $^{12}C^+$, $^{13}C^+$, ^{28}Si, $^{58}Ni^+$ and $^{185}Re^+$ were profiled. Since the surface topography of the CFC tiles varies, SIMS measurements are performed at several points on each sample, covering an area larger than the fibre plane separation. Surface profilometry measurements of a re-deposited carbon layer and a Be-rich layer allowed the determination of the layer thicknesses and, therefore, the assessment of sputter rates in SIMS. Relative uncertainty of the sputter rates is estimated to be ± 15%. The roughness of the CFC surface causes the rounded shape and broadening of the SIMS depth profiles, because secondary ion signals come from different depths. This induces variation in the apparent layer thickness and may also change the signal intensities slightly.

Some selected samples that had been analysed by SIMS were also measured with TOF-ERDA to obtain elementary concentrations at the near surface region [23]. In the measurements, the 5 MV tandem accelerator (EGP-10-II device) of the University of Helsinki was used with a 53 MeV beam of $^{127}I^{10+}$ ions. The maximum measured depth is different for every element and for each matrix. However, as an example, ToF-ERDA gives quantitative data for deuterium up to a depth of about 1100 nm in a carbon-based matrix with 53 MeV I^{10+} ions when a density of 1.6 g/cm^3 is assumed.

3.2. MkI divertor 1994-5

Complete poloidal sets of divertor tiles were removed after the carbon divertor phase and after the beryllium divertor phase.

Figure 6 (right) showed the Be, C and D concentrations across an individual tile exposed during the C divertor phase near the outer strike point (position 13 in the upper part of Figure 5). As mentioned in section 2.2.1, the fractional area of each tile exposed to the plasma varied, and in Figure 6 “Tile C” had the largest fraction of surface shadowed from direct plasma impact at that location. The tile has been eroded in the plasma-exposed region, with a sharp peak of re-deposited material in the shadowed region.

Figure 5 showed a comparison of the D retention between the C and Be phases, with the amount averaged (toroidally) across a whole tile. Firstly, there is a peak in the D retention at the inner corner of the divertor, which is approximately of similar extent for both the C and Be divertors. Analysis shows the retention is due to co-deposition of D with C, even in the case of the Be divertor since there was very little Be present in the deposits. Assuming that the D:C ratio in the deposits at the inner divertor corner was similar for both divertors, then it implies the amount of C deposited was also similar. Clearly the source of the carbon cannot be the divertor in the Be case. Based on common assumptions, modelling of material migration in tokamaks for divertor plasmas predicts that the main impurity source is the divertor, with only a relatively small main chamber source. It also predicts that re-deposition should be approximately equally split between inner and outer divertor. These first JET post-mortem results from the divertor clearly contradict these standard modelling results. The C must arise from sputtering in the main chamber, the C then being transported to the divertor along the plasma SOL. The fact that there is not a similar deposition from the outer SOL in the Be case

became evidence for the drift in the SOL from outboard to inboard (which had not been observed at the time of the experiment but was proposed later [24]).

In the case of the C divertor, the peaks in D retention near the inner and outer strike-points, are due to C being sputtered from the exposed part of tiles and promptly re-deposited in the adjacent shadowed areas as shown in Figure 6. This also led to very significant carbon transport and fuel trapping in the gaps (6-10 mm wide) between the small tiles. The inventory in gaps was at least twice greater than on the deposition regions on plasma-facing surfaces [25]. However, in the Be divertor either the Be is not sputtered and re-deposited, or if it is sputtered it does not trap a significant amount of D before its re-deposition. These analyses were made on the top surfaces of the divertor tiles. The analyses of gaps between the tiles (6-10 mm) revealed smaller fuel inventory than in the carbon divertor. The deposition and inventory in narrow (0.6 mm) grooves of the castellations was approximately two orders of magnitude smaller than that in wider gaps separating the Be divertor tiles, thus indicating a relatively small contribution of retention in such narrow gaps to the overall inventory. However, in all cases (wide or narrow gaps) the fuel trapping was related to the co-deposition with carbon [25]. It should also be stressed that no accumulation of dust particles was observed in the castellated structure.

The main science and technology lessons from the operation of the MkI divertor are:

- Sharp edges of PFC should be avoided or eliminated in the design of a reactor wall. They are prone to macroscopic erosion.
- The importance of shadowed regions as areas of heavy deposition and fuel inventory has been revealed. The increase of deposition/retention with the increasing gap width has been shown. Therefore, small tiles and wide (mm size) gaps separating the components should be avoided.
- A comparison of the C and Be divertors has clearly demonstrated the impact and importance of the local carbon source on the total inventory in the divertor.

3.3. MkIIA divertor 1996-8

Pumping of the plasma fuel during a discharge is either dynamically by the plasma-facing surfaces (mostly to be released at the end of the pulse), or by the liquid-nitrogen cooled divertor cryopump, which is situated at the outboard side, underneath the divertor structure. The

poloidal gaps in the MkI divertor structure allow pumping throughout the divertor, whereas the MkII structure only allows gas to exit through the inner and outer corners of the divertor. Regions of marked re-deposition were found in the region shadowed by the roof-top effect (see Fig. 6) on each of the small MkI divertor tiles near the strike zones [26]. The MkII divertor tiles, though much bigger, also have shadowed regions from their roof-top design, so it was assumed that heavy deposition would also be found in such regions near the strike points. However, this was not the case. Heavy deposition occurred in the inner corner of the divertor shadowed from any plasma bombardment, on the inboard end of Tile 4, on the bottom edge of Tile 3, and on the inner louvres. Films 40 μm thick were found in each of these regions on tiles removed in 1996 [27]. There was some spalling of the film from the louvres, which must have occurred as the machine was vented to air, since the spalling revealed a pristine copper surface. (The louvres are angled copper plates secured between water-cooled vertical pipes that block the line-of-sight from the divertor field coil housing to the divertor target tiles which would be a source of radiated heat and of CXN). Post-mortem IBA showed that the films consisted of carbon with very high deuterium contents (D/C ~1), thus it appears that carbon is transported in the direction of the gaseous fuel flow at the inner divertor corner. Furthermore, the explanation for the much higher Be:C ratio (~1:1) found on the inner divertor Tiles 1, 2 and 3 than expected from the plasma impurities flowing to those tiles (Be/C = ~0.1) is that much of the carbon is selectively removed by chemical sputtering by deuterium and then migrates towards the divertor corner [28, 29]. The conclusion is that the local re-deposition seen in the MkI divertor requires the movement of fuel through the adjacent gaps in the structure - in the MkII divertor there is no such movement between the divertor tiles (see section 4.2).

There appears to be no equivalent movement of impurities to the outer divertor corner (which is much closer to the cryopump), although significant deposition mostly of carbon was demonstrated on Tile 7 by stripping deposits off the tiles using adhesive tape.

During the deuterium-tritium experiment (DTE1) in 1997, a total of 35 g T were injected into the torus. A careful assessment of the tritium balance was made, based on the amount of T returned to the Advanced Gas Handling System (AGHS): ~40% of the input was still retained within the torus by the end of the DT-fuelled campaign. Methods of reducing this hold-up were extensively studied [13, 14]. Firstly, there were three months of non-intrusive in-vessel clean-up experiments (e.g. running pulses in hydrogen, glow discharge cleaning etc) which reduced the amount of retained T by about one-half (to 6.2 g). Secondly the vessel was vented

to air and the airborne release was measured (including the chronic release during the following shutdown) which re-claimed 2.5 g. Thirdly all the divertor tiles were removed and their T content estimated by analysis of representative samples, and the likely content of T in the carbon tiles remaining in the vessel was also estimated from samples, as shown in Figure 18. Allowing for these retained amounts, 3.5 g T were missing from the inventory [13,29].

There was a significant accumulation of flakes and dust on the divertor floor next to the inner louvres, much of which appeared to have resulted from spalling of deposits from the louvres themselves; there were no flakes observed on or near the outer louvres. All the flakes from the inner divertor corner were collected after the tile carriers were removed (all round the torus) using a vacuum cleaner, weighed and a sample analysed at AEA, Winfrith. The analysis showed that the flakes were carbon with a very high D and T content: based on the sample analysed, the 152 g collected contained 0.52 g tritium, giving a specific activity of 1.3 TBq g^{-1} for the flakes [30]. This reduced the missing T to ~3 g. The way the louvres are angled, most material spalling from their blades would fall into the void under the divertor. If it is assumed that all the missing T is in flakes that have fallen below the divertor, there would need to be ~1 kg of flakes similar to those collected at the inner divertor corner [31]. In the next intervention (in 1999) an endoscope was fed through the louvres to see if there were indeed flakes in the sub-divertor volume. As the endoscope was being fed through the gap between the divertor structure and the inner divertor coil housing flakes could be seen balanced on each bolt head and ledge, and on the floor of the vessel (which under the inner divertor is sloping towards the lowest point which is approximately beneath the outer divertor) there were piles of flakes behind every obstacle, for example divertor support legs as seen in Figure 19. In the 2001 shutdown there was a plan to remove all the flakes from one sector of the sub-divertor in order to assess their T content and, by extrapolation of the mass of flakes recovered, the total T inventory. Some flakes were recovered by inserting a metal pipe attached as an extension to a vacuum cleaner hose through 15 mm diameter holes in the base structure (exposed by removing tiles 4A and 4B in Octant 5). Movement of the pipe was directed from an endoscope inserted through a nearby hole. However, manoeuvring the pipe was very difficult, and the flakes had spread all over the divertor floor in the intervening years: regrettably the analysis of the flakes retrieved was not attempted for several years and the results after that period of time were inconclusive.

3.3.1 Summary of results from MkI and MkIIA divertors

- Apart from local erosion and re-deposition near strike-points, most of the deposition in the divertor comes from erosion in the main chamber.
- There is much more deposition at the inner divertor that at the outer divertor, which implies drift in the SOL from outboard to inboard.
- Carbon migrates preferentially from strike point regions towards areas shadowed from the plasma.
- 35 g T were injected in DTE1 in 1997 with ~40% retained in the vessel. Half of the retained T (6.2 g) could not be released by non-intrusive methods, but a further 2.5 g were released by exposure to air.
- ~3 g were believed to be retained in C flakes formed at the inner divertor.

In conclusion, all experimental campaigns with MkI (CFC and Be) and MkIIA served to emphasis the seriousness and consequences of material migration and fuel inventory on the economy and safety of reactor operation. The role of shadowed regions as deposition zones was revealed. These lessons pointed to the need for development and application of erosion-deposition diagnostics based on tracer techniques to determine the extent of PFC erosion and the mechanism of material transport to shadowed regions.

Techniques for measuring the supply of T to JET, and for analysing T retained in the dust, tiles and other components removed from JET after DTE-1, allowed the overall retention of T in the machine to be assessed: more sophisticated measurements outside, and importantly within, the ITER vessel will be required to fulfil the legal requirement to know its in-vessel inventory. None of the work within the Be-contaminated and radioactive JET machine would be possible without the years of development of complex Remote Handling equipment at JET, giving a basis for such equipment for ITER.

3.4. MkII-GB divertor 1998-2001

Operations with the Gas Box divertor were from 1998 to 2001, and there was an intervention in 1999 when a poloidal set of divertor tiles was exchanged. Further sets of tiles were of course removed in 2001, so that tiles were analysed that had been in the vessel 1998-1999, 1998-2001 and 1999-2001. There were new elements in the programme of erosion-deposition studies: (i) application of marker tiles described in the next paragraph and (ii) tracer puffing using methane labelled with ^{13}C to determine carbon transport; details for all campaigns are in Chapter 4.

3.4.1. Marker tiles exposed during the MkII-GB campaign

In the evaluation of the MkIIA data it was clear that there is a difficulty in fully describing material migration in the tokamak if only deposition is known, but not the erosion sites. During the 1999 intervention, a special poloidal set of tiles was inserted that had been measured with a micrometre using carefully engineered slots along one edge, as shown in Figure 20. These marker tiles also had bands of rhenium (Re) deposited on them along the poloidal direction, with a ~10 μm layer of carbon including a small boron (B) content on top of the Re. The idea was that if a small amount of erosion occurred the C/B layer would be partially removed and the Re would appear closer to the surface when IBA data before and after exposure were compared [32]. If a lot of erosion occurred the marker layer would have disappeared, but there would then be a difference in the mechanical measurements of the tile. The 24 poloidal positions of the mechanical measurement points were illustrated in Figure 10. The results of the mechanical measurements and also SIMS profiling data are shown in Figure 21. Normally the micrometer measurements were repeatable, but on the sloping parts of Tiles 4 and 6 each measurement was smaller than the preceding one showing that the coating was of low density and being compressed by the micrometer - grey shading shows the amount of compression in the measurements.

Analysis by SIMS of the coated stripes on the marker tiles installed at the outer divertor wall (Tiles 7 and 8) and exposed 1999-2001 showed no evidence of the C+B coating at any point, and only a small amount of Re remained at some points on the surface, and none remained at others. The mechanical measurements confirmed erosion at all positions for Tile 8, but indicated a mixture of net erosion and deposition on Tile 7. It appeared that the C+B layer did not survive plasma exposure (a lesson repeated in 2004-2007), which meant that the measurement of small amounts of erosion using the layer was not possible; small amounts of erosion of Re cannot be extrapolated to an equivalent erosion of the carbon substrate. Nevertheless, the micrometer measurements gave clear evidence that the extent of the *erosion* at the outer divertor wall was much less than the *deposition* measured at the inner. It is worth mentioning that in order to sputter Re atoms we have to assume that some of the erosion must be by impurity ions, or by high energy ions (~200 eV) of the fuelling gas.

3.4.2 Analysis of divertor tiles

Inner divertor wall tiles removed in 2001 were covered with a duplex film. IBA showed that the deeper of the two layers was very rich in metallic impurities, with Be/C ~1 and H-isotopes only present at low concentrations, whereas in the near-surface layer D/C was ~0.4 and Be/C was ~0.14 – much higher concentrations of D than the normal for plasma-facing surfaces measured previously in JET. The duplex nature of the deposit is clearly seen by SIMS analysis in Figure 22, recorded from near the bottom of Tile 1 after exposure 1998-2001: the near-surface layer is about one-half the thickness of the deeper layer, and the ratio of ^{9}Be to ^{12}C (for example) is very much greater at depths of 4 to 12 μm than at the surface. Figure 23 shows another example of SIMS profiles from a tile removed in 2001, this time from a thicker deposit at the middle of a Tile 3 also exposed 1998-2001. The origin of this near-surface layer might have been the result of the lower JET vessel (and divertor tile) temperatures for the last three months of the MkII-GB campaign (as mentioned in section 2.3), or from the He-fuelling campaign during much of the same period. The deeper layer is similar in composition to that seen on MkIIA inner divertor wall tiles, and also to MkII-GB tiles removed prior to 2001; the disparate near-surface layer does therefore not result from different behaviour for the two divertors. JET continued to run at reduced wall temperature in subsequent campaigns and Be/C values on Tiles 1 and 3 returned to values of unity, or greater (see section 3.5.2), so the low Be/C value in this near-surface layer must be due to deposition during the He campaign. If total erosion in the main chamber remains comparable for He as for D plasmas, then there will be a similar impurity fluence to the inner divertor wall (now Tiles 1 and 3). However, if chemical sputtering of C is "switched off" then all the impurities will remain as deposit on Tiles 1 and 3, rather than up to ~80% of the deposit being transported to the inner corner of the divertor. This would explain the low Be/C ratio and the fact that the deposit thickness in two months is about half the amount in the previous two years. The large D content of the deposits must be a result of infilling of the (porous) films during the last days of operations before the shutdown when discharges were again fuelled with deuterium to convert the Neutral Beam Boxes.

Figure 24 shows the mechanical structure of the septum of the MkII-GB divertor, viewed from the inner divertor side. The location of narrow deposition belts on the support plates is indicated with arrows. Local re-deposition on Tiles 5 is indicated with shading. The septum dividing plates provide almost complete separation of the inner and outer divertor legs (a very small flow may be possible within the private flux region over the septum tiles if the X-point is high enough). Since there is erosion from Tiles 1 and 3 (mostly of carbon) and the septum is

a large adjacent shadowed volume, significant deposition was expected on surfaces of the structure. Deposition monitors (silicon boxes with just a small entrance slit in one face) were placed in the inner divertor corner (slit facing outboard) and in the septum (slit facing Tile 3) to aid comparison of deposition in the two regions [33].

Surface morphology of all the vertical support and dividers plates of one module was studied with IBA. A dusty deposit was observed near the plate edge facing towards the inner divertor channel. Moreover, there were areas partly eroded by arcing. Some deposition occurred in narrow belts (15-20 mm wide) near the plate edges on the inner divertor side where the deposit was predominantly a deuterated carbon film with the fuel content reaching 2.3 x 10^{19} D atoms cm^{-2}. The amount of trapped fuel on the outer divertor side was distinctly lower, generally not exceeding 2 x 10^{18} D atoms cm^{-2}. The deposit thickness was everywhere in the range that can be probed by IBA, i.e. not exceeding 7-8 μm. The deposits contained some beryllium, in the range 0.1-2 x 10^{18} Be atoms cm^{-2}. Low levels of deuterium and beryllium (less than 1.5 x 10^{18} atoms cm^{-2}) were found on both sides of the divider plates. Therefore, the results for the support and divider plates were consistent. Moreover, no ^{13}C – above the background level – was detected on any part of the gas box plates, showing that the material retention in that region was limited (see later section on ^{13}C puffing experiments). The results gave a clear indication that the gas box components cannot be considered as a major place for fuel retention. However, the deposition monitor in the gas box trapped a comparable amount of carbon-containing particles to the one at the inner divertor corner (where heavy deposition was observed - see next paragraph) [33]. The likely explanation is that carbon was sputtered from the target tiles towards the septum, as it had to be, but deposition was clearly offset by re-erosion by deuterium ions and radicals (but which cannot remove particles from within the deposition monitors).

MkII-GB tiles showed thick films of high D/C ratio (approximately =1) with no Be nor any other metallic impurities on the part of Tile 4 shadowed by Tile 3 [34-36]. Similar films were seen in MkIIA and were about 50 μm thick [27] Somewhat thinner films (~ 15 μm) were also seen in the region of the MkII-GB Tile 4 shadowed by the septum. In this region the films had a D/C concentration ratio of ~0.4 and negligible Be and other metallic impurities. In the more central sloping region of Tile 4 there was a very thick friable (i.e. easily crumbled) deposit (~200 μm) seen with the micrometer and SIMS. The D contents were much lower and sometimes concentrated at the surface, and traces of Be were visible. A similarly friable film

was present at the equivalent point in the MkIIA divertor and showed up clearly in infra-red [37] and tritium experiments [38], but its thickness was not determined.

Tiles from three different periods were examined (but not all from the same toroidal location), and logically the thickness of tiles exposed 1998-2001 should equal the sum of the thicknesses of tiles exposed for 1998-1999 and for 1999-2001 - however this was not quite the case, and it appeared there was some toroidal variation in deposition rate at Tile 4 (seen again in 2009).

The outer base MkII-GB Tile 6 also had a narrow thick, friable band on the sloping region (Point 16: Note that the arrows on the tiles in Figure 10 denote each measuring point – the numbers run consecutively from the top of tile 1 poloidally to the top of tile 8 – some numbers are omitted for clarity, but point 16 is thus immediately to the left of point 17, for example). This is the extreme point of access for the plasma into the corner of the outer divertor, analogous to Point 10 for the inner divertor. A sharp change of film structure was visible by eye towards one edge of this tile. From the NRA spectra it was clear that there was a thick film with rather high D/C ratio on the sloping part of Tile 6, but this rapidly attenuated to a surface film (~2 μm) near Point 17. This contrast between the deposition at the inner and outer corners of the divertor precisely mirrored the behaviour of the MkIIA divertor. Towards the septum (from Point 15 to 14), all samples showed just a surface film of modest D concentration. The RBS and SIMS spectra from this region indicated that over the 1999-2001 campaign there had been little net erosion or deposition. However, the composition of the surface region indicated that there has been some intermixing of the marker film and plasma impurities through the outer ~2 μm.

Tiles 7 and 8 were clearly areas of modest erosion; the tiles appeared clean by eye, and according to IBA and SIMS analysis there were very low levels of surface impurities. However, the mechanical markers indicated surface changes that were near the limits of detection - the total net erosion from the seven measurement points on Tiles 7 and 8 was only 20 μm, i.e. average erosion over the surfaces of 3 μm, with a measurement error of ±10 μm. Further data on the MII-GB analysis may be found in [39].

3.4.3 Summary of results from the JET MkII-GB divertor

- Marker tiles exposed 1999-2001 showed deposit ~50 μm thick on Tile 3 and the part of Tile 4 shadowed by Tile 3, together with friable deposits up to 200 μm thick on the sloping parts of Tiles 4 and 6
- The septum (Gas Box) blocked transport between inner and outer divertor legs, but did not act as a significant deposition zone, although impurity flow to a deposition monitor located therein was similar to that to the inner divertor corner.
- SIMS showed qualitatively that C:Be ratios were much reduced in deposits during operation with He fuelling.

In conclusion, the inclusion of marker tiles, puffing of $^{13}CH_4$ tracer gas (all details in Chapter 4) and the helium campaign all deepened the knowledge of material migration, and indicated the need for installing more wall diagnostics including a new generation of tools capable of providing time-resolved information. However, the most important lesson was that the distinct change of the divertor configuration (MkII-A to MkII-GB) did not lead to any significant change of the erosion-deposition pattern and the level of retained fuel inventory. The greatest inventory was in the inner divertor. All these findings gave a strong impulse to thinking and preparation towards the major step in the reactor wall technology: replacement of carbon wall by metal PFC.

3.5. MkII-SRP divertor 2001-3

3.5.1. Quartz Micro-balance (QMB) and Deposition Monitors

During the period of JET operations between shutdowns, there are discharges with a wide variety of plasma configurations, power levels, magnetic fields, etc. A justified criticism of post-mortem analyses is that in general they only give a net picture of deposition (and perhaps erosion) for the entire period. Apart from the unsuccessful FTS/SAS prior to 2001, JET had no system/device for measuring erosion/deposition on a shorter timescale equivalent to the DIMES system on the DIII-D tokamak [40]. However, in 2001 a Quartz Micro-Balance (QMB) was installed in the shadowed area at the inner divertor. QMBs are regularly used to monitor thin film deposition in coating plants, and operate by exposing a thin crystal of nickel to the flux of deposit. The resonant frequency of the crystal decreases with increasing weight of the crystal, so by calibrating the amount of deposit against frequency change, the deposition can be monitored. The frequency also changes with temperature, so QMBs are normally water-cooled to eliminate this effect - this is not possible in JET, so comparisons were made after

several minutes (normally just before the next pulse) to allow the crystal heating by the plasma to dissipate, and in comparison with another crystal that had not been exposed to the plasma. The QMB was fitted with a shutter, which was normally closed but could be programmed to open for a number of seconds during the pulse. Typically the shutter was open for the entire pulse, but the opening period could be restricted to one or more seconds (e.g. during Additional Heating in the X-point phase), if required. The amount of deposition during the opening period was calculated from the frequency change before and after the opening (having corrected for the crystal temperature).

This first experimental QMB operated for about one year. It demonstrated that the largest deposition per pulse occurred when the strike point was first moved to the sloping part of Tile 4 after some time low on Tile 3; subsequent but consecutive pulses with the strike point on Tile 4 gave progressively less deposition. Periods with the strike point higher up on Tiles 1 and 3, followed by moving to Tile 4 also gave less deposition. This indicates a two-step migration: migration from Tiles 1 and 3 to the plasma-accessible part of Tile 4 followed by ejection into the shadowed inner corner [41].

Deposition monitors (silicon boxes with just a small entrance slit in one face, as used during the MkII-GB campaign) were fitted in the shadowed regions at both inner and outer divertor corners [33].

3.5.2 Analysis of tiles from the JET MkII-SRP divertor

3.5.2.1 Analysis of Tiles 7 and 8

A poloidal set of clean CFC divertor tiles was coated with a stripe of W along the poloidal direction, prior to mounting in JET during the 2001 shutdown [42]. The thicknesses were measured at IPP, Garching using IBA and were typically 3 μm. At the end of the 2001-2004 campaign the W coatings on Tiles 7 and 8 were still clearly visible by eye, though there were some toroidal bands of deposition on Tile 7 that in some places appeared to overlay the W. A photo of Tile 7 after the campaign, and after one poloidal set of samples had been cut at VTT, is shown in Figure 25.

The W stripe on Tile 8, in particular, appeared by eye to have survived the campaign intact. The RBS spectra from certain parts of the stripes on each tile appeared similar to that prior to exposure confirming that the coating here had indeed survived intact: Figure 26 is an example,

taken from near the bottom of the front face of Tile 8 (exposed 201-4). However, this spectrum was not reproduced all over the tiles. Figure 27 is an RBS spectrum from about one-third the way up the Tile 7 surface as shown in the sketch (also exposed 2001-4). This spectrum is quite different to that of Figure 26. There is W visible, and the energy of the edge (just under 2.5 keV) indicates it is present right at the surface. However, the peak height is only about 25% of that in Figure 26 indicating only a quarter of the surface is covered with W. Furthermore, the energy of the carbon edge (~1.8 keV) indicates C was also present at the surface. Several areas of Tiles 7 and 8 had both W and C at the surface, notably the strike point areas on Tile 7, the upper half of the front face of Tile 8 and, surprisingly, the apron (horizontal surface) of Tile 8. Thus, although the stripes looked intact by eye, in fact carbon was exposed over much of the coated area. If these coatings were used for the ITER-like wall, and erosion rates were similar, then there would have been breakthrough over much of the outer divertor after less operational time than in the 2001-2004 campaigns at JET.

SEM analyses showed that for a sample cut from a region such as that analysed for Figure 27, a thinner remaining W coating was in islands, with the CFC exposed in between, as shown by SEM imaging as in Figure 28, and the RBS spectra were consistent with this picture. On the other hand, for areas with spectra such as in Figure 26, SEM confirmed there was still a continuous W film over the whole surface

Although the most common strike point region on Tile 7 was the most logical area to find erosion of the W stripes, the top of the front face of Tile 8 was always well back from the last closed flux surface (LCFS) into the SOL. The apron of Tile 8 was even deeper into the SOL, but in compensation the field lines have a larger angle of inclination to the surface. Although Langmuir measurements showed fluxes strongly peaked at the LCFS, this flux is mostly deuterium. However, D cannot erode W, as the threshold energy for physical sputtering is ~200 eV, and the plasma electron temperature (T_e) was not high enough for D ions to have this energy. Nevertheless, we do observe W erosion on Tile 8, which can only be sputtered by multiply charged impurity ions heavier than deuterium. The peak contribution of carbon impurities following methane puffing to the SOL flux is ~25 mm from the LCFS [43]. It may be erosion by these impurity ions that caused the erosion at the top of Tile 8.

In the RBS spectra recorded along the W stripe, ^{13}C peaks were seen such as indicated on Figure 27. However, due to the interference with the W peak, in many cases the quantification

is easier from spectra recorded off the W stripes. The strike point for the series of discharges into which the ^{13}C was puffed was about two-thirds the way up Tile 7, as shown in Figure 29. A peak of ^{13}C, determined by RBS just off the W stripe, was just above this region (i.e. just inside the SOL), and a dark film can be seen in Figure 25 on top of the W stripe in this area. The thickness of the layer (which seems to be a mixture of roughly 60% ^{12}C and 40% ^{13}C) is about 1.5 μm and was discussed with respect to the IR data in section 2.4. A smaller ^{13}C peak was also seen near the centre of Tile 7, where there was a brownish deposit running toroidally across the tile. The NRA for Tile 7 **(**Figure 30) showed the same ^{13}C peaks and associated D peaks. A small amount of Be is present on Tile 7 as seen in Figure 30 (and a Be peak was also indicated in the RBS spectrum from Tile 7 in Figure 27), despite the fact that the tile is usually a net erosion zone. Be atoms are continually arriving and being re-eroded from the outer divertor, as is seen by spectroscopy, so at any instant in time there will be a transitory concentration of Be on the surface, which will vary with the contours of the rough surface. It is also possible that some Be on the tile surface may come from contamination of the surface during handling in the BeHF.

The position on Tile 7 of the W stripe was about 200 mm away toroidally from the puffing location. It will be seen later (section 4.2.1) that quite different analyses were found adjacent to the puffing location.

Tile 8 was generally very clean, however, NRA (and RBS) showed increased levels of ^{13}C on the top section of the front face, and particularly on the apron. Nevertheless, on Tile 8 the ^{13}C behaviour was not mirrored by the D levels which were particularly low on the apron.

3.5.2.2 Analysis of Tiles 1 and 3

In Figure 31 the Be/C ratios from NRA are plotted against position on a Tile 1 removed in 2004 and compared with data from two tiles removed in 2001. The s co-ordinates of the tile apron are 162 to 222 mm, and the front face is from 222 to 431 mm. The ratios are similar after each campaign: on average, there seems to be a slight increase in the Be/C values with exposure time

Films on Tile 3 were thicker than on Tile 1, and reached thicknesses of 60 μm, as shown in the polished cross-section in Figure 32. The film composition is not uniform through the film - SIMS reveals large variations in the C/Be ratio in the film, but this cannot be assessed

quantitatively. Changes in composition can be simulated from RBS spectra over the first 10-20 μm.

Figure 33 shows RBS spectra from the upper part of the front face (sample position 3.7) for a Tile 3 removed in 2001 and one removed in 2004. Here there is clearly a large Be concentration in the spectra from 2004, whilst the spectrum from 2001 is dominated by carbon at the surface. Be is the principal metallic impurity that is eroded in the main chamber and travels along the SOL to the inner divertor with the predominant C flux; it is thus the element used in assessment of the amount of chemical re-sputtering of C taking place on Tiles 1 and 3. However, there are other metallic impurities reaching the plasma following erosion in the main chamber, notably Ni, Fe, Cr from the inconel used as the vessel wall and for tile fixings etc [43]. These elements are also entrained in the SOL flow and deposited on Tiles 1 and 3. SIMS shows clear parallels in the behaviour of these elements with Be in the deposited films. Thus the much larger contribution of Ni, Fe and Cr in the 2004 spectrum shown in Figure 33 is another indication of the greater metal content of the near-surface part of the deposit on Tile 3 removed in 2004. Note the ^{13}C peak in the 2001 spectrum which comes from the puffing in 2001 – see Section 4 – and that the D feature is very much smaller.

On the tile removed in 2004, Be concentrations were higher than in 2001, and indeed were comparable with the levels seen in the inner layer formed in 1999-2001 or in earlier campaigns. It is clear, therefore, that chemical sputtering of C at the inner divertor returned for the majority of the 2001-2004 operations from the reduced rate at the end of the 1999-2001 campaign to its earlier value, despite the similar JET wall temperature.

The difference in surface analysis between a Tile 3 removed in 2001 and one removed in 2004 is also apparent in NRA. Figure 34 shows NRA spectra from samples cut from the same relative position towards the top of Tile 3, one exposed 1998-2001 and the one exposed 2001-2004 as analysed in Figure 33. The most obvious difference in the NRA spectra is in the D signals, with approximately 15 times more counts in the D feature in the 2001 spectrum (note: the 2004 spectrum is expanded by a factor two along the Y-axis to reduce overlapping with the 2001 spectrum). The D peak size varies to some extent over Tile 3, probably being related to the strike point position for the last pulses prior to the shutdown, but is everywhere much smaller than on tiles removed in 2001. It is clear that the Be/C peak ratios are much less from

the 2001 tile, and a ^{13}C peak can be seen on the 2001 tile, again in agreement with the RBS results.

The surface analyses of Tiles 1 and 3 removed in 2001 were abnormal compared to Tiles 1 and 3 measured previously; Be/C ratios were very high, as was the D concentration. Before the shutdown in 2001 there were four weeks of operation with He-fuelling, and He-fuelled discharges will cause chemical sputtering to cease, thus the Be/C ratio of films deposited on divertor Tiles 1 and 3 during that campaign should remain close to the ratio found in the plasma and in deposits in the main chamber, as observed. But this would not be expected to be accompanied by higher D levels, which encouraged the view at that time that the main reason for the reduction in chemical sputtering was because the vessel temperature was reduced from 300 °C to 200 °C during 2001, since D retention is a strong function of temperature. However, it will be shown below that in subsequent campaigns with the vessel temperature at 200 ºC high Be/C values were once more observed, so the effect is more likely to have been due to the He campaign. A possible explanation for the high D concentration is that the He discharges resulted in a more porous film structure, and that after the He-fuelling campaign when D-fuelling was resumed just for the last 3 days of the campaign (a requirement for the Neutral Beam systems) the lattice filled up with deuterium.

3.5.2.3 Analysis of divertor base tiles

In the 2001 shutdown the septum and its support structure were removed, and in their place was put a Septum Replacement Plate (SRP). This CFC plate covers the divertor support structure between Tiles 4 and 6 and could be seen in outline in Figure 29. The plate itself had limited power handling capability, but it was then possible to run with inner and outer strike point locations on much of Tiles 4 and 6 (respectively), whilst before only the sloping sections of these tiles were accessible to the plasma. A deposited film was visible as coloured fringes on the inboard and outboard bevelled edges of the SRP tile, and a thick deposit on the inboard and outboard vertical sides of the tile (shadowed from the plasma). The D/C ratio in the film on the inner edge was similar to that found typically on the shadowed region of Tile 4 (D/C=1), and there was also a large D concentration at the outboard edge. Significant concentrations of metal impurities characteristic of inconel were also observed on the outboard edge. However, over the majority of the top surface of the SRP little deposition was found.

Figure 35 shows C, Be and D concentrations derived from NRA measurements on Tile 3BW G4B after exposure 2001-4. As seen for tiles from previous campaigns, the section of the tile shadowed by Tile 3 (~700-750 mm) had very high D concentration and the Be level was very low. The cross-section in Figure 36 shows that the film here was about 70 μm thick and had a well-defined layer structure. However, some Be was found on the plasma-exposed part of the tile, probably reflecting the significant number of plasma pulses run with a horizontal target during 2001-2004, whereas during 1998-2001 the region was shadowed by the septum support structure. Note that the Be concentration in this figure is enhanced x10 relative to D and C, so Be/C ratios on the exposed part of Tile 4 were still not comparable to those on Tiles 1 and 3.

At first glance the C, D and Be concentrations on Tile 6 seen from the NRA data plotted in Figure 37 appear as a mirror image of those for Tile 4 in Figure 35. There was a film of high D/C ratio on the section of the tile nearest the outer louvres shadowed by Tile 7. The D/C ratio was similar to that on the shadowed region on Tile 4, and the film thickness at the points analysed was greater than the analysis depth (~7 μm). However, coloured fringes in the shadowed region suggest the film probably thinned closer to the louvres, and was unlikely to be as thick as the 50 – 100 μm typically found on Tile 4 (e.g. as seen in Figure 36) – SIMS profiling confirmed this impression.

Thus, more deposition was seen on the shadowed section of Tile 6 than in previous campaigns. This may have been due to the two weeks operating with reversed toroidal field and plasma current in 2003, which has the effect of making plasma parameters in the inner and outer divertor legs more equitable, and greatly reducing the drift in the SOL that under normal conditions sweeps impurities from outboard to inboard [44]. However, the amount deposited on Tile 6 approached 50% of that seen on Tile 4, which is in agreement with the relative amounts of hydrocarbons collected in the deposition monitors in the respective corners. Although the D concentration was low on the sloping part of the tile, there was in fact a thick powdery film there, as seen also on Tile 4, and following previous campaigns [35].

Cross-sections cut from this region such as in Figure 38 show a more fractured deposit, which is consistent with a friable film. Note also in Figure 38 the thin bright band at the interface between the substrate and the deposit - this tile was one of the marker tiles with a W interlayer. Some deposit was also seen on the exposed flat section of Tile 6 (distances on the

tile from 0 to ~100 mm), as witnessed by the presence of Be. These Be concentrations were comparable to those found on the equivalent region of Tile 4. The data in Figure 37 were taken on the part of the tile that was coated with the W stripe. Towards the inboard edge of the tile (0-40 mm) the Be, D and C levels decreased where the film deposited onto the W was thinner; close to the inboard edge no film was evident, and the W stripe was clearly visible. This was to be expected, as the tile in this area was shadowed from field lines by the SRP plate.

3.5.2.4. Summary of results from the MkII-SRP divertor

- The Be/C ratios in deposits on Tiles 1 and 3 were high, indicating it did not depend on vessel temperature
- There was now significant deposition at the outer divertor corner, though less than at the inner divertor corner.

In conclusion, the transition from the closed (MkII-GB) to the open divertor resulted in only relatively small changes of the deposition and fuel retention pattern. However, the main lesson was related to a clear progress in understanding of material transport to shadowed regions. This was possible due to the application of QMB and, as detailed in Chapter 4, experiments with ^{13}C tracer. As a consequence, data obtained in such activities facilitated enhanced cooperation with modellers. It also emphasised the need for new wall probes to be installed in various toroidal and poloidal positions.

3.6 Analysis of the JET MkII-HD divertor 2005-9

3.6.1 Divertor diagnostics installed in 2004

The JET Mk-II HD divertor was installed in 2004, along with the limiters for an ICRH antenna and a number of other modifications. For the HD-divertor (see cross-sections in Figures 8, 13 and 15) the SRP plates were replaced with a triangular wedge comprising a sloping Load Bearing Tile (LBT – equivalent to a Tile 5) and a wedge plate facing Tile 3 to complete coverage of the support structure. Prior to the shutdown an exercise throughout the Fusion Associations was carried out to design diagnostics to fit within the JET divertor to improve the measurement of erosion, deposition, migration and retention with an emphasis on time resolution. As a result the following diagnostics were installed in the shadowed divertor corners in 2004: more QMBs and deposition monitors, louvre clips on the inner and outer louvres, witness samples, mirror samples and holders, and rotating collectors. The last-named was a

disc-shaped collector inside a housing with a slit facing the plasma that rotated a magnetically-triggered step at the start of each pulse for 3000 pulses covering ~320°, at which point rotation ceased. Details of all these diagnostics can be found in [45], whereas a diagram showing their location is given in Figure 39.

Diagnostics cannot be fitted to plasma-interacting surfaces in JET, but special tiles were used to measure erosion/deposition. Firstly, a poloidal set of tiles from the divertor and also the main chamber were coated with a set of marker stripes and were physically measured accurately with a tile profiler [46]. Previous markers had been W or Re stripes on the tiles [32]. This may measure the erosion of the metal, but says little about erosion of carbon, since the processes are totally different. This time the markers comprised a thin W interlayer covered with 10 μm of carbon, with the idea that this time C erosion could be assessed.

3.6.2 Load-bearing SRP tile (LBSRP or LBT)

3.6.2.1 LBT 14WR exposed 2005-7

One LBSRP tile was initially coated with a thin W interlayer and ~10 μm of C in a 20 mm strip along one edge, as part of the poloidal set of marker coatings for the divertor to be mounted in 2004, the tile due to be positioned within module 14W (Tile 14WR). However, as this tile can be photographed from the Upper Main Vertical Port (UMVP) at Octant 5 directly above it, it was decided to use it also to investigate the lifetime of W coatings for a future ITER-like Wall (ILW). The tile was therefore additionally coated with two wide strips of W, one 1.5 μm thick and the other 0.7 μm thick (about one-half the thicknesses that had been planned). Figure 40 is a photograph of the tile ready for mounting in JET, whilst Figure 41 is a photograph taken from above the LBSRP Tiles 14WR and 14NL, *in situ*, at the end of the 2005-7 operations. The W-coated stripes can still be clearly seen on Tile 14WR.

All the RBS spectra from the thinner W coating showed a mixture of W and C being present at the surface, as in spectrum JET11822 in Figure 42; this indicates that the plasma has eroded W from some areas and, as seen from Tiles 7 and 8 removed in 2004 (Figure 28), W coating (appearing white in the photograph) remains intact in areas shadowed from the plasma by the surface roughness. Part of the thicker W coating is shadowed from the plasma by the adjacent tile toroidally to the left (Tile 14WL), and part is exposed fully to the plasma. A spectrum from

the shadowed area is included in Figure 42 (JET11838) together with a spectrum from the exposed part of the thicker W coating (JET11832). This latter spectrum shows that the C concentration steadily increases up to the surface, whilst the W concentration decreases; this indicates that different areas are eroding at different rates, and that the W layer has almost disappeared from some areas (in fact in JET11832 there may already be a small denuded area). Thus the 1.5 μm W coating was just about adequate to protect the central part of the CFC tile during the 2005-7 campaign.

When making analysis scans of the tile toroidally, it was apparent that there was some W present on the region between the thinner stripe and the edge of the tile. Plasma ions are incident approximately toroidally from the left at a small angle to the surface (viewing as in Figure 41), and material sputtered from the surface tends to be re-deposited some distance to the right of its origin. One might therefore expect the amount of W to decrease with the distance from the W stripe. This is seen in the RBS spectra in Figure 43 selected from an analysis series across the centre of the tile (JET11868 was recorded as a reference from the thicker stripe). JET11870 and JET 11874 were recorded from the gap between the two W stripes, JET11874 having been recorded 6 mm to the right of 11870. Even in this narrow gap the deposit decreases towards the right by more than a factor of two over a distance of 6 mm (i.e. an e-folding length of~6 mm) – PIXE analysis gave the same result. JET11890 was recorded 27 mm to the right of the thinner stripe (close to the edge of the tile): this is the region where the W+C marker stripe had been deposited on the tile. No evidence of the coating could be found, implying that the 10 μm C coating was completely eroded and if any of the thin W interlayer remains it is incorporated in the small tail of the re-deposited W profile following erosion of the stripes.

Methane ($^{12}CH_4$) was puffed near the end of the campaign from a gas nozzle that is visible in Figure 41 between Tiles 14WR and 14 NL, approximately mid-way along the gap (poloidally) between the two tiles, into a series of high-delta discharges, with the strike point towards the inner edge of the LB-SRP (so that the gas was injected into the outer SOL). Thereafter plasmas were only run with strike points on the vertical targets, so that re-deposition on the tiles near the nozzle lay within the private flux region (PFR) and would not be disturbed by the plasma. IBA analyses of this re-deposition have been modelled by Brezinsek [47]. The tile up-stream was the W-coated LB-SRP tile, and a deposit up to 15 μm thick with a high D/C ratio was found on the tile within 2-3 mm of the edge, but this decreased very rapidly a few more millimetres away from the injection point. An extended plume was visible downstream

on the adjacent LB-SRP tile. Analysis reveals films up to ~2 μm in thickness, also with high D/C, but decreasing with distance from the source at an order of magnitude lower rate than on the up-stream tile.

3.6.2.2. LBT tile exposed 2007-9

The Load Bearing Tile 14WR removed in 2007 described above was replaced with a tile coated with 10 μm W, and a photograph of that tile after exposure 2007-9 is shown in Figure 44. For about 20 % of the discharges during the 2007-9 operations, the Outer Strike Point (OSP) was on the LBT. The W coating is intact everywhere over the tile and was still too thick to tell from RBS if there had been any thinning. The darkening of the right-hand (outboard) half of the tile corresponds to a (small) amount of deposited C, but the tile was generally quite clean; the maximum amount of carbon was ~2.5 10^{18} atoms cm^{-2} in the stripe at s co-ordinate ~1189 mm and at the outboard edge (s = 1289 mm). There was also a peak in ^{13}C seen by NRA at s ~1189 mm, and this stripe (which is clearly visible in Figure 44) was seen with the IR camera to develop during the puffing experiment on the last day of operation (see Section 4.3); the OSP was at s ~1170 mm during the inter-ELM periods.

3.6.2.3. Summary of results for the LBT tiles of the MkII-HD divertor

- During the 2005-7 operations ~1.5 μm of W coating on an LBT were eroded
- Eroded W was re-deposited off the coated stripes with an e-folding distance of ~6 mm
- Methane puffed into the private flux region was re-deposited with a range of millimetres up-stream, but of centimetres downstream

3.6.3 Analysis of divertor tiles 1 and 3

3.6.3.1. Tiles removed during the 2007 shutdown

During 2005-7 many plasmas were run in the “High-delta” configuration wherein the inner strike point was on Tile 1 and the outer strike point was on the LB-SRP tiles. As a result the inner SOL could be further inboard than before, and significantly greater fluxes fell onto the apron of Tile 1. When JET was vented for the 2007 shutdown and Remote Handling operations commenced, it was noticed that there was a very rough appearance to all the aprons of Tiles 1 around the vessel. It became clear that this was spalling deposit which extends over about two-

thirds of the apron, with the film still being adherent on the right-hand side of the tile (viewing radially inwards) that was slightly shadowed by the adjacent tile. There was also a little spalling on the left-hand upper part of the tile, just around the corner from the apron, as can be seen in Figure 45, which is for a tile that had been in the vessel since 1998. The spalling was also visible on Tiles 1 that had been mounted new in 2004, but the extent of the spalling was noticeably less.

Figure 46 shows RBS spectra from the apron (JET12860) and low on the front face of a Tile 1 that was only in from 2005-7. The Be concentration was very low on the apron (e.g. JET12860, in which the spectrum is dominated by carbon from the surface and extending into the bulk, with just a small protuberance on top due to the Be), and increased on the front face, with a maximum just below the bend (s co-ordinates 309-329 mm), and again near the bottom of the tile (400-430 m). Spectrum JET12924 was recorded at 409 mm and shows that the outer few microns are dominated by Be together with some O, D and transition metals with just a little C at the surface, then returning to C in the bulk: in general the D concentration was very low on Tile 1 except near the bottom of the front face. An adjacent tile that had been in JET 1998-2007 was also analysed, and it was clear that there was a considerable difference between the two data sets. On the apron of the tile exposed 1998-2007 there was significantly more retained D, and the Be/C ratio was factors 2 - 4 higher than on the tile only exposed 2005-7; D and Be levels were more similar on the front faces of the tiles. It may be that the analysis of the tile exposed for the longer period has been affected by the spalling of the deposit.

The spalling clearly indicates that there were thick deposits on the apron of Tile 1. However, in this region the IBA techniques showed that the Be was not enhanced relative to the C by chemical sputtering to the same extent as on the front face of the tile where high Be/C ratios could be found. Thus, chemical sputtering was restricted beyond the corner of Tile 1 to the apron – and the fact that C was not being removed from the film means that almost all the deposition from the SOL remained on the surface, increasing the rate of build-up in comparison to deposits on the front face of the tile where chemical sputtering was evident. The particle flux was also greater on the apron than just around the corner on the front face, since the poloidal component of the angle of incidence was much greater (even if toroidally ions were incident on both faces at a small angle of incidence). The reason for the low D content is unclear, since deeper into the SOL one might expect lower ion temperatures so greater D/C ratios.

Tile 3 showed a big variation in surface composition from top (high Be/C ratio of ~2.5, quite low D concentration) to bottom (lower Be/C ratio of ~0.6). During this campaign many pulses were run in the high-delta configuration, i.e. with the inner strike point at the top of Tile 3 or on the lower part of Tile 1 (see Figure 15a). The top of Tile 3 was a popular point for the strike-point because this particular region is well diagnosed with Langmuir probes and has a sight-line to the Infra-Red camera system. Thus, the top and bottom of Tile 3 were frequently in rather different plasma regions, with the top at the strike-point and the bottom of the tile in the private flux region Note, however, that there were many more pulses with the strike-point at the bottom of Tile 3 when conditions across Tile 3 would be more uniform (Figure 16). For the final day of operations the strike point was on Tile 3, just above centre.

3.6.3.2. Tiles exposed 2007-9 (removed in 2010)

Tiles 1 and 3 removed in 2010 after exposure 2007-9 have been analysed [48], and Figure 47 shows the ratio of Be/C in the surface layer and the D content on Tiles 1 and 3 derived from NRA. In order to calculate the correct Be/C ratio in thick films such as on these tiles, the concentration for Be derived from the NRA signal count rate (using values calibrated using thin films) has been reduced by a factor of two since the analysis depth for Be is about a factor of two greater than for C at the analysis beam energy employed. The top edge of Tile 3 was shadowed from the plasma by the bottom of Tile 1 which explains the lower first two Be/C values on Tile 3. Thus, the band of very high Be/C ratios straddling the change of tiles coincides with the maximum plasma flux levels at the ISP for HD discharges (and just within the inner SOL). There is another maximum in Be/C at the top of the front face of Tile 1 (s ~250 mm), just before the corner to the horizontal part of the tile (the "apron"). The high Be/C ratios on tiles removed in 2010 (with a maximum on Tile 1 of 4.4 and averages for Tiles 1 and 3 of 1.5 and 1.12) compare with average values for Tiles 1 and 3 removed in 2007 of 0.94 and 1.24, and for tiles removed in 2004 of 0.83 and 0.81, respectively. The increase in the Be/C ratio may be due to the increased number of HD discharges in 2007-9 (i.e. with the ISP at the top of Tile 3 or bottom of Tile 1). The NRA Be/C data are in agreement with profiles calculated from RBS spectra using the Data Furnace simulation programme [49], and by SIMS measurements of the tiles. The increase in the Be/C ratio cannot be attributed to an increase in the amount of Be entering the vessel, as the number of Be evaporations during the campaign was only 58 in 2007-9 compared with 73 in 2005-7, and the integrated collection of Be from a probe near an evaporator [46] was 1.3 x 10^{19} atoms cm^{-2} during 2007-9 compared with 4 x 10^{19} atoms cm^{-2}

in 2005-7. The D concentrations on Tile 1 (i.e. in the SOL) correlated with the Be/C ratio, whereas on Tile 3 levels were low near the strike point on the last day of operations. The explanation for this pattern is not immediately clear, and in some aspects conflicts with RBS data.

3.6.4 Analysis of Tiles 4 and 6

3.6.4.1 Analysis of tiles removed in 2007

Tile 4 appeared generally as usual – a-C:D in the area shadowed by Tile 3 with a very high D/C ratio of ~1, a very thick deposit on the sloping part of the tile with low D, then a thinner deposit on the upper horizontal section that was difficult to access by the plasma due to the proximity of the LBSRP unit. Figure 48 shows the Be/C ratio (corrected for the different analysis depths) across the Tiles 4 that were removed after the previous three JET campaigns (in 2001 after the MkII-Gas Box, in 2004 after the MkII-SRP, and in 2007 after the MkII-HD divertor campaign). There was clear evidence that the Be/C ratio on the sloping part was greater than in the earlier campaigns.

On Tile 6 interference fringes were visible on the horizontal part of the tile shadowed by Tile 7. As sectioning shows a thick film of up to 40 μm in this region, this clearly does not indicate a thin (sub-micron) film but rather a smooth dense coating with some optical effect within the outermost micrometre. The high D concentration in this region showed that the coating was an a-C:D film of similar nature to the film on the region of Tile 4 near the inner louvres (shadowed by Tile 3); however the D:C ratio within the film appeared to be slightly lower than in the equivalent region of Tile 4. A denser film with lower D:C ratio may indicate greater ion flux and higher surface temperatures. A thick deposit was obvious on the sloping part of Tile 6 (accessible to the plasma if the outer divertor corner is in the outer SOL), with one or two small regions of spalling evident. The Be concentration was higher than previously observed on Tile 6 (as was the case with Tile 4); Figure 49 shows a comparison for tiles that had been removed after the previous three JET campaigns: note the different scale for the Be to that in Figure 48. The two peaks in the Be concentration for the tile removed in 2007 roughly correspond to the two positions on Tile 6 most favoured as the OSP for the 2005-2007 campaigns.

Figure 50 is a photograph of the bottom of an inner divertor carrier, after removal from the torus in 2007. At the top of the picture is the bottom part of Tile 3. Three of the CFC carrier

ribs can be seen projecting below Tile 3, and between two of these is the front of a mirror test unit, which holds three 1 cm^3 mirrors, one flush with the front of the unit (though indistinguishable in the photo from the holder), the others recessed into channels (and not visible). The mirror test unit was only in the torus from 2005-7 and serves as an example of how much deposition takes place at the inner corner of the JET divertor.

The increase in Be on Tile 6 over the years was even more striking than for Tile 4, however the reason for the increase is not clear. Kreter et al [50] have suggested that deposition occurred on the QMB at the outer shadowed region when the ISP was on Tile 1 or high on Tile 3 when there is a line-of-sight across to the outer QMB, irrespective of where the OSP might be, implying cross-divertor transport. This might be correlated with the increased level of Be on Tile 3 during this period. However, deposition on the outer QMB was much less than at the inner divertor corner, and was balanced by erosion in other pulses, whereas on other surfaces in the outer shadowed region thick films were deposited, comparable to the overall deposition seen at the inner louvre region.

3.6.4.2 Analysis of Tiles 4 and 6 removed in 2010

Figure 51 shows the surface concentrations of D and Be by NRA across a Tile 6 exposed 1998-2009: note that again there are two peaks in the Be profile shown in the figure. However, during the 2007-9 campaigns the strike point when on Tile 6 was concentrated at the outer of these two positions, at an s co-ordinate of ~1440 mm, and it is clear that the Be peak had moved outward beyond the strike point location and was in the region shadowed from the plasma by Tile 7. Deposits on Tile 6 can reach ~100 μm in the vicinity of the Be peak (and up to 800 μm at certain areas on the sloping part of the tile), so as NRA is only measuring the Be at the surface, the analysis was of material deposited during the latter stages of the 2007-9 operations. Ion microprobe analysis of cross-sections through films on Tile 6 from previous campaigns had shown distinct bands of higher Be concentration within the deposit [51, 52]. The whole issue of erosion and deposition at the JET outer divertor corner needs further investigation and modelling with the ERO and 3D-GAPS codes.

There was a high D concentration on the outer part of Tile 6 (>1490 mm), which is the region shadowed by Tile 7, but there was also a peak near the inboard edge of these tiles (~1320-1330mm). This was associated with a toroidal belt of local re-deposition resulting from the $^{13}CH_4$ puffing on the last day of the campaign (see Section 4.3).

Tile 4 removed in 2010 again showed a Be peak at the inboard end of the sloping part of the tile, but less than on the tile removed in 2007 [38] and with no second peak as seen previously. The averaged amounts of Be seen on tiles removed in 2010, 2007 and 2004 were 0.4, 1.5 and 0.6 10^{17} atoms cm^{-2}, respectively. The amount of Be on Tile 4 deposited in 2005-7 may be the anomalous value of the three, because a number of experiments were carried out during that period to understand the factors controlling migration of impurities to the QMB located at the inner corner of the JET divertor [50, 53]; these experiments involved sweeping the plasma from Tile 3 to Tile 4, which may have encouraged migration of Be.

Thicknesses of the deposited layers on the divertor tiles, as measured with SIMS and optical microscopy, are given in Table 3 for tiles removed in 2009 after various exposure periods. The measurements were made on cores cut from the tiles: cores from Tile 1 are numbered from the bottom of the tile (and core 10 was cut from the apron); cores from Tile 3 were also numbered from the bottom of the tile: cores from Tile 4 are numbered outboard to inboard: cores from Tile 6 are numbered inboard to outboard. The deposition patterns after the 1998-2009 and 2007-2009 operations were similar to those determined after previous campaigns. There was heavy deposition on the apron of Tile 1 while on the plasma facing surface of Tile 1 the deposits were notably thinner. Tile 3 had clearly thicker deposits than Tile 1. Tiles 4 and 6 had very thick deposits especially on the sloping part and shadowed areas. Tables 4 and 5 give thicknesses of the deposited films for tiles exposed in different periods – on the inner divertor Tiles 1 and 3, and Tiles 4 and 6, respectively.

Deposition monitors (DM) were present at the inner and outer divertor corners for the period 2007-9 [33]. The amount of C collected in each DM was virtually identical, with maxima facing the entrance slit of each element reaching ~10^{24} atoms cm^{-2}, allowing for an extrapolation over the central part of the lower plate of the outer DM where the deposit had spalled; D was co-deposited with the C at a ratio of 1:1. Be was present at uniform concentrations over the interior surfaces of both DMs, but at a very low level of ~$2x10^{15}$ atoms cm^{-2}.

3.6.5 Analysis of divertor Tiles 7 and 8

3.6.5.1 Tiles removed in 2007

A Tile 7 that was only exposed in JET during the 2005-7 campaign appeared quite clean apart from a poloidal band where the tile was shadowed from the plasma by the adjacent tile

(toroidally, to the right of this tile). Tile 7 was frequently deep in the outer SOL in 2005-7 when high-δ shots were being run. However, on the last day of operations before the 2007 shutdown a series of pulses were run with the outer strike point at the centre of Tile 7 (and the inner strike-point at the centre of Tile 3) and ^{13}C-doped methane was puffed at the outer mid-plane. Only small amounts of Be were found on the tile, in contrast to the amounts on Tile 6, for example. Small amounts of ^{13}C were also found across the tile, but with a maximum near the centre of the tile - the largest concentration of ^{13}C found by IBA in the HD divertor. The ^{13}C was also clearly visible by RBS as shown in Figure 52 recorded from samples 10 mm below (spectrum 13926) and 10 mm above the middle of the tile (spectrum 13924, recorded for only half the beam fluence of 13926 for clarity).

A Tile 7 exposed 1998-2007 was also analysed. In 2004 every Tile 7 showed the features of a toroidal band of (brownish) deposit just above the centre of the tile and a narrow region of very heavy ^{13}C-H deposition near the top edge in the left-hand half of the tile (appears silvery) - see Section 3.4. This second tile was present in the vessel at this time and must have appeared similarly marked before the 2005-7 campaign. All traces of the deposits visible in 2004 have been eroded from the tile during the 2005-7 period of operations.

The Tile 8 analysed in 2007 was also new in 2005, so was only exposed from 2005-7. The tile appeared very clean.

3.6.5.2 Tiles removed in 2010 (after operations concluding in 2009)

As shown in sections 3.4.2 and 3.5.2.1 the outer divertor Tiles 7 and 8 are normally a region of slight net erosion, and the tiles appear very clean. However, there is a pattern of ^{13}C deposition on the tiles removed in 2010, with the largest concentration (~10^{17} atoms cm^{-2}) occurring at the bottom of Tile 7, decreasing by two orders of magnitude at the Tile7/Tile 8 junction, and rising again to ~10^{17} atoms cm^{-2} at the top of Tile 8 [54]. This must result from the ^{13}C puffing (as CH_4) on the last day of operations: more details are given in Section 4.3.

3.6.6. Summary of results for MkII-HD divertor Tiles 1, 3, 4, 6, 7, 8

- Be/C ratios on Tiles 1 and 3 increased steadily during the period 1998-2009, reaching 4.4 on Tile 1 exposed 2007-9
- Be/C ratios on Tiles 4 and 6 also increased, but were at a lower level with the level on Tile 6 twice that on Tile 4 (0.1-0.2 after 2005-7)

- DM data indicated fluxes of C (and co-deposited D) were the same to both inner and outer divertor corners.
- Tiles 7 and 8 were in erosion zones, except during methane puffing experiments.

In conclusion, the operation of the High Delta divertor was a crucial step in the test of divertor configuration and operation scenarios for JET with the ITER-like wall. Therefore, the determination of erosion-deposition pattern was at the heart of that test. Results obtained with W-coated marker tiles helped understanding of high-Z erosion and, by this, contributed to the R&D process for ILW. The other lesson was connected with application of numerous wall probes which provided detailed information regarding erosion-deposition and could be approved as diagnostics for JET-ILW.

4. Carbon-13 puffing experiments

4.1. ^{13}C puffing in MkII-GB in 2001

To study transport of impurities in the tokamak, JET carried out a series of experiments over the years injecting material transport tracers into the last pulses before shutdowns, then using post-mortem analyses to study the migration, following procedures developed on TEXTOR [22, 55]. The first such experiment was in 2001, during the last operation session with the MkII-GB divertor [56]. ^{13}C labelled methane ($^{13}CH_4$) was puffed into the SOL from the gas inlet module (GIM-5) at the top of the vessel. The key objective for the experiment was to assess the direction of material migration and the resultant location of re-deposition. During fifteen ohmic pulses 1.3 x 10^{23} $^{13}CH_4$ molecules were injected, which was judged to be close to the maximum that could be injected without seriously modifying the discharge parameters. The number of ^{13}C atoms puffed into the SOL (assuming no loss of material by deposition local to the nozzles) was therefore also 1.3 x 10^{23}. ^{13}C is a natural isotope of carbon (abundance 1.1%). This small amount does not influence the quantitative analysis of the injected tracer, however it does provide a background, which limits the sensitivity of detection in the presence of carbon surfaces.

A poloidal section of divertor tiles were analysed for ^{13}C by EPS and by SIMS, together with a selection of tiles from the main chamber. If there is a significant amount of ^{13}C in the outer monolayers it can be seen in RBS as a small peak ahead of the ^{12}C edge, as seen previously in Figure 33 and 52, and in NRA (Figure 34). In SIMS the masses 12 and 13 are separately

plotted: normally the mass 13 signal is two orders of magnitude smaller than mass 12 (natural abundance), but after puffing experiments the ^{13}C is manifested as an increase (relative to mass 12) at the surface as was clearly visible in Figure 22 and Figure 23 and has been calibrated.

Table 6 gives the amounts of ^{13}C detected in the divertor: The amounts have been extrapolated by integrating toroidally to the whole divertor and expressed as a percentage of the ^{13}C-labelled methane gas input. The vast majority of ^{13}C was found on the inner Tiles 1 and 3 (45% out of 46.2%), which is to be expected because of the known drift of impurities such as C and Be to these tiles along the SOL. What is perhaps surprising is that following 15 discharges there is virtually no migration of ^{13}C to Tile 4. Either this process is relatively slow, or requires heated discharges rather than the ohmic pulses of this experiment. Relatively small amounts were found on main chamber tiles such as the IWGL tiles.

4.2 ^{13}C puffing experiments in the JET MkII-SRP divertor in 2004

4.2.1 Distribution of ^{13}C in the divertor

On the last day of operations in 2004 a total of 4 x 10^{24} atoms of ^{13}C in the form of $^{13}CD_4$ were injected from a toroidally symmetric gas supply at the outer SOL, between Tiles 7 and 8 (Figure 53), into 25 identical ELMy H-mode discharges from 63405 to 63445 with the plasma configuration shown in the Figure. The amount of ^{13}C was measured over a complete poloidal scan of the divertor, and the amounts detected extrapolated toroidally around the vessel and expressed as a percentage of the amount puffed in. The results are given in Table 6. The total percentage (21.3%) is only a small fraction of the input, and less than found after the 2001 puffing [39]. Although a significant amount was found in the private flux region, it was clear that some ^{13}C was transported around the SOL, as ^{13}C was measured on a probe inserted into the SOL at the top of the machine [57]. ^{13}C was found at the intersection of the inner divertor with the SOL (i.e. on Tiles 1 and 3), however the level was quite small, and much less than the peak levels deposited locally on Tiles 7 and 8. The ^{13}C concentrations on the SRP tile were generally low, especially towards the centre of the tile. A hollow profile of this type was predicted by the modelling of Strachan et al [58-61], however the ^{13}C values towards the centre of the tile are far lower than predicted, suggesting that there is an erosion mechanism in the private flux region that is not correctly included in the modelling.

As mentioned in Section 3.5, the highest concentrations of ^{13}C have been seen in the outer SOL just above the strike-point on Tile 7 where a deposited film was clearly visible, as seen in the poloidal slice shown in Figure 54 (but shown horizontally) and on the horizontal section (apron) of Tile 8. A plot of D concentration from top to bottom of Tile 7 is also given in Figure 54, and an RBS spectrum from the W stripe where the deposited ^{13}C is at a maximum is shown in Figure 55 which was recorded using a beam energy of 4 MeV. The narrow ^{12}C and ^{13}C peaks in Figure 55 indicate a thin film comprising 1.6×10^{19} atoms cm^{-2} ^{12}C and 1.4×10^{18} atoms cm^{-2} ^{13}C on top of the remaining W film. The amount of deposited ^{13}C is similar off the W stripe, but it is not then possible to distinguish the deposited ^{12}C from that of the underlying carbon-based substrate.

A number of possible explanations may be proposed to explain the ^{13}C on the horizontal surface of Tile 8: Firstly, a material transport loop for ^{13}C may be established in the SOL from the outer divertor close to the separatrix, migrating into the main chamber and returning to the far SOL: Secondly, ELMs may be responsible for the movement of ^{13}C: Thirdly, there may be a leakage path for the puffed gas from the supply manifold to the top of the outer divertor, so that gas may enter the far SOL close to the deposition site as indicated by an arrow in Figure 53.

An interesting additional feature of the ^{13}C deposition was noticed after the initial survey analyses, when a second Tile 7 (2ON G7A) was analysed, with the poloidal scan aligned with the position of one of the 48 injection nozzles between Tiles 7 and 8. Visible near the top edge of Tile 7 was a silvery cigar-shaped deposit shown schematically in Figure 56. When this region was analysed by IBA it was discovered that there was a thick deposit at the top of the front surface of Tile 7 with the maximum aligned with the edge of the region normally protected from incident ions by the slightly prominent lower edge of Tile 8 (3-5 mm from the edge of the tile).

Figure 56 shows a 2-dimensional plot of the ^{13}C deposit in this region of the second tile. The thickness of the deposit was determined by RBS, but there is the possibility of the layer being a mixture of ^{13}C and ^{12}C by this technique. ^{13}C and ^{12}C concentrations measured by NRA across the tile aligned with the centre of this deposit at the top edge showed that it was almost exclusively ^{13}C and not ^{12}C (Figure 57). The deposition is symmetric about the injection point and extends for about 3 cm in each direction. The deuterium and ^{13}C concentrations across the

Tile 7 reported previously (on Tile 14OWG7B) were taken along a poloidal line 20 cm away from the gas port, so this peak was not seen in that scan: subsequently a similar deposit was found on the part of Tile 14OWG7B that aligns with the gas introduction point. Although the ^{13}C concentrations were very high, the effect was very localised, so that no adjustment of the estimated ^{13}C inventory in the machine is required, therefore, as a result of this further analysis.

The whereabouts of the remaining ^{13}C is unknown. Since there was a significant level seen on the horizontal apron section of the divertor Tile 8, the next tile outboard in a poloidal direction (called Tile B) was analysed, but no measurable ^{13}C level was found. Furthermore, no significant ^{13}C was found on the OPL tiles. It should be noted that the divertor cryopump is situated just outboard of the outer divertor support structure. The cryopump is fully toroidal, has a very large pumping speed, and there is a large conductance to the injection point in the outer divertor via the gap between Tiles 6 and 7. Deuterium streams along the SOL over Tiles 7 and 8 towards this sink, and much of the $^{13}CD_4$ may go with it.

4.2.2 Effect of ^{13}C deposition on the IR divertor signal

The pulses used for the puffing experiment were ELMy H-mode discharges. Viewing with the IR camera, the highest surface temperatures were observed during the ELMs, and were located just above the strike point, for both inner and outer divertor legs. The upper part of Figure 58 shows the maximum temperature at any point in the outer divertor during the discharge – the red curve is for pulse 63415 (one of the early pulses of the puffing experiment) and the blue is for pulse 63438 (the penultimate pulse of the experiment). The red curve overwrites the blue, so the blue spikes for each ELM have the same base level as that for each red spike, i.e. for pulse 63438 the apparent surface temperature rise for each ELM is about three times as large as for 63415. By contrast, the lower part of Figure 58 shows the maximum temperature at any point in the inner divertor during the discharge – again the red curve is for pulse 63415 and the blue is for pulse 63438. In this case the temperature excursions for each ELM are similar for pulses 63438 and 63415.

The temperature rise observed with the IR camera for a short pulse of given power input is greater if a film with poor thermal contact to the substrate is present at the surface [62, 63]. What is being seen at the outer divertor is therefore the growth of a thin film during the puffing experiment. Such a film just above the strike point of Tile 7 was described in Section 3.4. and

is where the maximum ^{13}C is observed. The RBS analysis shows the film to comprise approximately 60% ^{12}C and 40% ^{13}C and be ~1.5 μm thick.

The mean temperature rise during an ELM (ΔT) for pulses 63405 to 63415 was ~70 °C (63415 was in fact the eighth pulse with $^{13}CD_4$). From pulse 63415 onwards there was a steady, approximately linear rise in ΔT to 330 °C at pulse 63438. Thus, assuming the deposited film growth was uniform for all the pulses containing $^{13}CD_4$, there appears to be a minimum film thickness for which no change is observed, after which the effect is progressive. Since the induction period covered the first 8 of the 25 pulses, the minimum film thickness may be ~0.5 μm. This was the first time such a correlation between the thermal response of a surface film and its analysis had been made. No difference was observed at the inner divertor, since there was already a very thick film on Tile 3.

4.3. ^{13}C-puffing into the MkII-HD divertor

There was a puffing experiment on the last day of operations in 2007 when ^{13}C-labelled methane was puffed through nozzles in the ICRH antenna surround at the outer mid-plane. However, due to a problem whilst operating the gas control modules, nitrogen was inadvertently mixed with the methane, and after 4 discharges the experiment was abandoned: nevertheless some ^{13}C does appear in IBA spectra from tiles removed in 2007.

On the last day of operations in 2009 another ^{13}C-labelled methane puffing experiment was performed. This time the plasma was in the high-δ configuration with the OSP on the LBSRP tiles. The ^{13}C-labelled methane (i.e. $^{13}CH_4$) was puffed into the divertor via 24 puffing holes equally spaced around the torus at the location on Tile 6 shown in Figure 59. The discharges were 2.5 T, 2.6 MA H-mode shots with 15 MW auxiliary heating and the ELMs were of type I with an average core energy loss of about 400 kJ. A total of 3.3 x 10^{23} $^{13}CH_4$ gas molecules were injected, however 30% of this injected gas was pumped directly by the divertor cryopump [64]. There is a pattern of ^{13}C deposition on the tiles removed in 2010, with the largest concentration (~10^{17} atoms cm^{-2}) occurring at the bottom of Tile 7, decreasing by two orders of magnitude at the Tile 7/tile 8 junction, and rising again to ~10^{17} atoms cm^{-2} at the top of Tile 8 [61]. The outer divertor leg is sensitive to small changes of plasma parameters and can easily switch from net erosion to net deposition as shown during the Reverse Field campaign in 2003

when films were shown to grow on previously clean outer divertor surfaces by IR camera observations [63]. Also on the last day of the 2001-2004 operations when $^{13}CH_4$ was puffed into the outer divertor between Tiles 7 and 8 a deposit formed near the strike point on Tile 7 as was observed with the IR camera [65]: this deposit was eroded away during the subsequent 2005-7 operations. Clearly on the last day of operation in 2009 the injection of impurities into the outer divertor has again temporarily changed the region into a net deposition zone.

4.4 Summary of results of ^{13}C-labelled methane puffing experiments

- When puffed from the top of the machine, 46.2% of the ^{13}C input was located in post-mortem analyses of divertor tiles - 45% of this on inner divertor Tiles 1 and 3 (extrapolated values) confirming drift in the SOL
- When puffed from the divertor, only 21.2% of re-deposited ^{13}C was discovered (extrapolated value) – probably due to pumping of the methane by the cryopumps
- Puffing in the outer divertor turned the region from net erosion to net deposition.

5. Dust and flakes

5.1 Introduction

As has been shown in previous sections, deposition occurs invariably in some parts of the divertor regardless of the divertor configuration, and these deposits may be very thick - for example in the MkII-GB divertor deposits reached over 250 μm in thickness (Section 3.4.2 and Figure 21). The deposits generally have a layered structure (e.g. Figures 32 and 36) and are often of rather fractured structure (e.g. Figure 38): they are therefore prone to spalling of all, or part of, the coating. Flakes of spalled coating were first observed at the inner corner of the MkII-A divertor in 1996 [27], and at the start of the shutdown in 1998 following the DTE1 campaign 150g of flakes were collected from the inner corner of the entire divertor.

The amounts of dust/flakes would be important for future larger tokamaks such as ITER and JT-60SA in two ways. Firstly, do deposits reach a critical thickness, so that any further deposition will result in flaking or conversion to dust: there is an overall limit to the amount of debris that is allowable in the tokamak? Secondly, one of the critical safety issues for ITER is the accumulation of dust in the machine which could become airborne during an accident scenario and result in a fire or a positive pressure within the vessel. To be fully mobilizable dust must be of micron or sub-micron size, so size distribution of the collected material is of

interest. At the final shutdown with the C divertor in 2010 when all the CFC divertor and first wall tiles were removed to install the JET-ILW [66] detailed studies of the flakes/dust were carried out.

5.2 Experimental and Results

A cross-section of the JET MkII-HD divertor was shown in Figure 15, which shows the configuration in use in 2005-9. As has been described previously, the Load Bearing Tile (LBT) and its support structure were installed in the 2004-5 shutdown, as were the High Field Gap Closure (HFGC) tiles, but most of the JET carbon divertor tiles had been in place continuously from 1998 to 2009, so deposition could be assessed after 11 years of film accumulation on these tiles.

The conversion of deposits into dust and flakes was assessed by comparing the increase in total deposition during the campaign period 2007-2009 with the amount of dust accumulated over the same period. The dust in the JET divertor was collected in January 2010 using cyclone vacuum cleaners with exchangeable collection pots in six stages: 1) the outer divertor tiles LBT, 7 and 8, 2) the inner divertor tiles HFGC, 1 and 3, 3) the inner and outer divertor support structures, 4) the outer divertor floor tile 6, 5) the inner divertor floor tile 4, and 6) the inner and outer louvre regions. Sample 1 is the dust collected in the pot during stage 1, etc: very fine particles that might not be collected in the pots were collected in dust bags. The total amount of dust produced in the 2007-9 period was 248.4 g. To compare with the deposition in the divertor, the weight of dust was converted to volume by taking the last measured density of dust removed from JET (in 1998) of 1.69 $g.cm^{-3}$ [31]: the resulting value was 147 cm^3. The density of the dust collected in 2010 has not been measured and may differ: it should be noted that much lower density values have been reported for re-deposited material in tokamaks; the lowest value reported is 0.8 $g.cm^{-3}$ derived by comparing RBS and sectioning data [68].

The size distribution versus mass of the collected dust particles was measured for all samples except Sample 1 due to insufficient amount of material for measurements. The dust bags seemed to contain smaller particles than the other samples (distribution peaked at ~2 μm, compared with maxima at ~100 μm). The reason for the different size distributions is not quite clear. This could be related to the operation of the vacuum cleaner, i.e. very small particles remain suspended in the airflow and go to the dust bag instead of the pot where the rest of the dust is collected. The dust particle size distributions (i.e. fraction of the sample at a given size)

for all samples would be somewhat misleading because the distribution for the sample from dust bag 3 has a dominating peak at ~2 μm, yet the mass of this sample was much smaller than most other samples. Therefore, in Figure 60 the size distributions have been multiplied by the mass of the corresponding sample. Only a very small fraction of the mass of dust collected fell in the size range up to 1 μm considered by ITER to be "mobilizable". It should be mentioned that some of the dust/flakes may have been trapped in the hose to the vacuum cleaner.

The vast majority of the dust was carbon, with the next largest components being the elements Ni, Fe and Cr in the correct relative amounts for Inconel varying from 16% from Tiles 1 and 3 to 3% at the louvres. Beryllium was analysed at 2.4% and 0.1% for these same samples, respectively.

The amount of deposits on the divertor tiles was derived by measuring the film thicknesses by optical microscopy from cross-sectional samples covering Tiles 1, 3, 4 and 6: the outer divertor Tiles 7 and 8 were areas of net erosion for all JET campaigns and deposition on the central divertor tile (Tile 5 or LBT) was negligible (<1 μm) (see Section 3.6.2.2) so they were not analysed. The increase in the quantity of deposits on tiles exposed in 1998-2009 over the amount found on tiles that had been removed in 2007 (and exposed 1998-2007) gives the amount deposited and still adhering to the tiles during the 2007-9 campaigns.

Although the comparison of dust/flakes and deposition is calculated for 2007-9, data were also collected for tiles exposed in 1998-2004, 1998-2009 and 2005-9. The deposition on the apron of Tile 1 exposed in 1998-2009 is close to the sum of the deposits in 1998-2004 and 2005-2009 as shown in Figure 61. Note also that the profile on the front face of the Tiles 1 (s = 236-423 mm) is similar for all the three periods. The mean film thicknesses on Tile 3 exposed during the periods 1998-2004, 1998-2009 and 2005-9 in a similar toroidal location were all comparable (55, 54 and 44 μm, respectively). This indicates that the deposit on Tile 3 and the front face of Tile 1 reached an equilibrium value wherein deposition and erosion rates were equal.

The thickest deposits occur on the base divertor Tiles 4 and 6, and isolated spots of spalling were observed. Very thick films (~500 μm) accumulated at the bottom of the sloping part of Tile 4 and even thicker on Tile 6, extending into the shadowed region as shown in Figure 62 which gives the profiles for Tile 6 for 1998-2007, 1998-2009 and 2007-9, with a deposit over 1 mm thick in one area.

The thickness profiles such as in Figures 61 and 62 have been integrated across each tile to give the volume of deposits in cm^3. This is then integrated toroidally to give the overall deposition in the torus. The increase in adherent deposits following the 2007-9 campaign was 197.5 cm^3. Thus, including the dust, the total impurity flux to the divertor during 2007-9 was 197.5 +147 = 344.5 cm^3. Possible errors may be due to the following causes *inter alia*: incorrect dust density value, statistical variations in coating thicknesses within the divertor, and corrections for deposition in other parts of the divertor.

5.3 Discussion

Some of the loose materials in the divertor that could be seen prior to vacuum cleaning were flakes of coating that had become detached, and some of these were millimetres in size. Figure 60 shows that the most abundant particle size for all the "dust" was about 100 μm in diameter, which must include the previously observed flakes that had broken up within the vacuum cleaner. If passing through a vacuum cleaner can be regarded as a test of the material friability, and ITER are particularly concerned about mobilizable dust of ≤1 μm diameter, then very little of the "dust" collected from JET in 2010 qualifies.

No "critical thickness" at which deposits are liable to spall has been observed – films up to >1000 μm remained adherent, whilst in other areas spalling of films <30 μm thick were observed. On Tile 3 and the front face of Tile 1 deposits were not accumulated beyond certain thickness levels, despite the continual arrival of impurities along the inner SOL, as shown in Fig. 61 for s co-ordinates 236-423 mm. It appears that the film and the plasma were in equilibrium so that the incoming impurity flux was balanced by the outgoing flux of sputtered material (sputtering coefficient equal to unity).

New tiles were introduced at each JET shutdown to act as "marker" tiles to witness the erosion/deposition at that location over a limited period. There is clear evidence from these investigations that this does not necessarily measure the correct deposition typical for this location. For example, the combined film growth during 2007-9 plus the accumulated dust was 344.5 cm^3, yet tiles only exposed in 2007-9 accumulated more than twice this amount (799.5 cm^3). Another example is Tile 3: there was no net deposition at that location between 2004 and 2009, yet clean tiles inserted at that position accumulated deposition until they were indistinguishable from the surrounding tiles.

5.4 Summary of results from studies of dust and flakes accumulation

- Only a very small fraction of the collected dust/flakes was in the 0 to 1 μm size range considered “mobilizable” by ITER
- There was no universal critical film thickness for flaking – deposits were observed up to 1000 μm thick, yet some deposits <30 μm in thickness spalled.
- In the period 2007-9 approximately 344.5 cm^3 C arrived in the divertor, of which approximately 197.5 cm^3 remained adhered to tiles, the rest becoming dust/flakes
- New tiles inserted between campaigns (e.g. as markers) can accumulate deposit at quite different rates to their neighbours.

6. Discussion

The precise details of the deposition and retention patterns in the JET divertors from 1994 to 2010 have changed, but a few fundamental trends have remained constant. The basic picture of transport within JET is unaltered: impurities such as C, Be and metals such as Ni eroded from the main chamber are deposited on the inner divertor wall tiles, then C is preferentially sputtered and transported towards the inner divertor corner. At the outer divertor, the vertical tiles are areas of net erosion, and there is a lot of deposition on the outer base tile accessible by the plasma. However, as is well-known, the "devil is in the detail".

The first results that caused a major rethink in tokamak understanding, and forced an interest in plasma boundary physics, were: 1) The main source of the material deposited in the divertor is the main chamber: 2) The behaviour of the inner divertor is quite different to that of the outer divertor. Both points were in opposition to common modelling assumptions. The first point was proven already in 1995 when the deposition in the all-Be divertor was carbon, which had to have come from the main chamber [24]. There was always an in-out asymmetry in deposition in JET, but the result that galvanised interest was when the vast majority of the retained T was found to have accumulated at the channel from the inner divertor corner to (or through) the inner louvres during the DTE1 experiment in 1997 [27].

The preferential removal of C from the MkII inner divertor tiles (i.e. Tiles 1, 2 and 3 for MkIIA, just Tiles 1 and 3 subsequently) leaves a Be-rich (and Ni-rich) layer on the tiles. Up to 2001 it appeared that the greatest Be/C ratio was ~1, and it was thought that BeC might be forming which was stable. BeC had been seen in JET with the Fast Transfer System [8], but BeC has never been satisfactorily identified on inner divertor tiles - a task made doubly difficult by the inevitable exposure to air prior to analysis. However, from 2001 the greatest values of

the Be/C atomic ratios observed at the surface of the deposits steadily increased. After the 2009 operations the greatest values were near the bottom of Tile 1 and top of Tile 3 (Be/C up to 4.5 [40]), and the average Be/C ratio over Tile 1 had almost doubled compared with tiles removed in 2004 (0.83). This was the region of the ISP during the high-delta discharges that formed a significant part of the 2007-9 operations, and (perhaps significantly) also for the last day of operations. There would be a maximum in deuterium flux in that region, so a maximum in the amount of carbon chemical sputtering was not unexpected.

At the divertor base, some patterns of deposition remained constant, that is heavy deposition on the sloping parts of Tile 4 and 6 and in the inner shadowed area. However, there were drastic changes between different MkII configurations at the outer divertor corner, in the region shadowed from the plasma by Tile 7. For the MkIIA divertor, although estimates of 1 kg of carbon are thought to have reached the inner louvres, yet the outer louvres appeared clean. During the MkII-GB campaigns the outer louvres also appeared clean. It was anticipated that there would be heavy deposition within the Gas Box structure, also shadowed from the plasma. However, although deposition monitors showed similar fluxes of carbon and hydrocarbons peaks to the structure and the inner divertor [33], there was no significant deposition on either the inner or outer parts of the structure. Note that the dividing plates of the Gas Box form an almost complete separation between inner and outer divertor legs. During the MkII-SRP phase deposition was observed at the outer divertor corner, of approximately half the amount seen at the inner corner for the same period - this time in agreement with deposition monitor data. There was a short period of reversed field operations in JET in 2003 (when plasma parameters in the inner and outer divertor legs were more similar), but the same ratio was found for components exposed during MkII-HD operations 2005-9, so there appears to have been a more fundamental change in divertor behaviour. Throughout, however, there was a similar or slightly greater deposition on the sloping part of Tile 6 to that of Tile 4. The deposition on Tile 4 was predominantly C with very little Be, but the deposition on Tile 6 contained a little more Be, and the amount steadily increased from 2001 to 2007, when peaks of Be/C at the surface of 0.8 and 0.75 were observed (Figure 49). The latter of these two points also appeared to be in the region shadowed from the plasma by Tile 7, thus beyond the strike-point: deposition in this region is not at all understood and might benefit from modelling with the ERO and 3D-GAPS programmes. Observations from a QMB placed in the outer shadow region during MkII-HD operations seemed to show that material arrived at the QMB when the inner ISP was at the top

of Tile 3 or on Tile 1, that is, with a line of sight from the ISP into the outer divertor corner [50]. Although this is consistent with results from MkII-GB (plate blocking movement from the inner leg to the outer corner) and MkIIA (OSP invariably on a base tile facing slightly inboard), it is difficult to imagine a large flux of impurities travelling across the divertor.

Is there a pattern to the instances of heavy re-deposition? For all JET divertors there has been heavy deposition at the inner divertor corner. In the MkI divertor there was also deposition in locally shadowed areas adjacent to erosion zones for the carbon (but not beryllium) targets. In MkIIA deposition was anticipated in the region shadowed by the roof-top geometry for each of the tiles in an erosion zone, such as on Tiles 7 and 8. However, analysis did not reveal any significant deposition in these areas. Again, for the MkII-GB divertor the septum support structure seemed an obvious location for deposition, but none was observed. The conclusion is that deposition only occurs where there is flow of gas, such as towards the pumps: in MkI flow is possible between each of the poloidal divertor elements, whereas in MkII it is only possible through the divertor corners. The MkII divertor tiles are mounted on solid supports and there are no direct pumping routes through the poloidal gaps between tiles. Likewise, there is no escape route for gas particles from the Gas Box. As this re-deposition in shadowed regions is a characteristic of carbon, perhaps the carbon-containing species require some trigger to initiate deposition which is present in gas flowing through gaps. One should note that flow of gas into the divertor can also trigger deposition, as occurred between Tiles 7 and 8 during ^{13}C puffing experiments in 2004 (Section 4.2.1); controlled experiments into the movement of impurities could prove very valuable. The behaviour at the outer divertor corner is still unexplained.

Although the general picture is of net erosion on Tile 7 and 8 (for normal field directions), injection of small amounts of impurities into the outer divertor can change the outer divertor into a region of net deposition. This was clearly demonstrated by the ^{13}C-puffing experiments in 2004 (Section 4.2) and 2009 (Section 4.3). In 2004 the development of a band of deposition across Tile 7 near the strike point was recorded by IR cameras because the heating/cooling properties of clean surfaces and deposited films have quite different properties, as well as being obvious by eye and analysis during the following shutdown. There were also small regions of intense deposition near the injection points as the gas emerged from the shadow of Tile 7. The features disappeared after operations resumed in 2005 demonstrating that the area was again a region of net erosion.

Many experiments have been made with metallic coatings in the divertor. These experiments provided important information for the JET ITER-like Wall operations when it was important to eliminate carbon from all plasma-facing surfaces, including the divertor, most of which was tiled with W-coated CFC [65]. Particularly relevant was the test of an LBT that was coated with ~10 μm W and exposed 2007-9: the LBT during high-δ discharges receives the greatest power density of any of the divertor tiles. The test showed that the W coating remained intact at all places, despite the large number of discharges run with the OSP on the LBT during 2007-9 operations.

The amount of dust/flakes accumulated in the divertor during the operating period 2007-9 was 248.4 g (or 147 cm^3, using a density derived for JET dust from 1998 of 1.69 $g.cm^{-3}$) whilst over the same period the overall growth of deposited films was determined to be 197.5 cm^3. The erosion of this material from (predominantly) the main chamber walls was of little consequence to JET. However, for a larger carbon-walled machine with a heavier duty cycle and non-uniform erosion it would be necessary to calculate material erosion rates for specific areas. Fortunately analysis of the collected dust indicated most particle sizes were from 10 to 100 μm, so most of the material would not be liable to in-vessel mobilisation. No critical film thickness for spallation to occur was seen for deposits onto the CFC tiles - deposits up to 1 mm thickness were observed, yet spalling was observed in other areas for films <30 μm thick.

The dust analysis revealed a concern for the routine analysis of samples retrieved from JET during shutdowns. The integrated amount of deposition on the "marker" tiles exposed 2007-9 was found to be more than twice the amount expected from film growth on other tiles plus the dust. This is because the plasma responds differently to the new tiles, so care must be taken when interpreting the analysis of "marker" tiles.

The studies of erosion/deposition and H-isotope retention in the JET divertors led the world in trying to understand the behaviour of this most critical part of a tokamak. Much was learnt about the nature of deposited films, flows and migration that influenced the directions of fusion research (such as in the design of ITER and JT-60SA). There are still many unknowns but hidden in the vast database collected since the first JET divertor operated in 1994 are many answers that may emerge with improved modelling and analysis.

7. Concluding remarks

The main scientific mission of JET is to develop plasma operation scenarios for a reactor-class machine such as ITER. It is to test the performance of plasma-facing components and to contribute to the best-possible assessment of fuel retention (tritium retention). Therefore, detailed examination of PFC after different operation periods is the only way to approach this goal. This review covers the JET operation with a series of consecutive divertors, but broad studies of erosion-deposition and fuel retention started at JET already in 1984. All this work has provided a comprehensive and coherent picture of material migration and fuel retention in the carbon environment. It also contributed to the further development and large-scale application of tracer techniques and wall probes, which have assisted in this process, and the use of such tools is now considered by ITER [69].

JET has always been a benchmark for modelling. The JET data (particularly from MkI) debunked the common assumptions in modelling at the time, demanding consideration of main chamber interaction, re-sputtering processes and SOL drift, though it was the catastrophic implications of MkIIA data that gave impetus to new developments such as the ERO code for divertor transport [70] and EDGE2D/NIMBUS for consideration of SOL drift [44]. Modelling is laborious work and manpower is limited – but JET continues to provide a vast reservoir of data available to check theories as they develop.

An important conclusion from the JET carbon wall experience is that there is significant erosion from the main chamber walls, and that this material migrates to the divertor corners where it traps large amounts of the fuelling gas (mostly D in JET, but equally of tritium if operating in a DT mixture): the deposits are beyond the reach of the confined plasma, and have no discernible effect on operations. Comparing the various JET divertor configurations also shows that the eventual route for the eroded material is where the fuelling gas streams out of the divertor towards the pumps: the significance of this experimental result deserves further research and modelling. Data from JET can be extrapolated to large-scale devices to estimate the erosion rates of first wall surfaces, incorporating peaking factors for components most at risk if a carbon wall is ever to be contemplated. Fuel inventory is also recognised to have a serious impact on the safety and economy of operating a D-T reactor. Reactors must generate at least as much T as they burn or otherwise consume through retention/losses, since T is an expensive commodity in very short supply. Thus a system for recovery of trapped T is essential for any reactor. ITER was first designed with a Be wall and a carbon divertor, which would also have resulted in some C migration to the corners with concomitant H-isotope trapping,

though of a much lesser amount than for an all-carbon machine. Unfortunately ITER was designed without any system of collecting the carbon and trapped fuel from under the divertor, and suggestions to install such a system were considered impractical leading to a debate on whether to change to a tungsten (W) divertor. In order to contribute research relevant to the design and operation of ITER, JET has been re-configured with a Be first wall and a W divertor (the ITER-like Wall Project, JET-ILW [66]). The resulting JET-ILW demonstrated a significant reduction (by a factor of ~15) in fuel retention and contributed to the decision to use only tungsten in the ITER divertor. This had an impact not only on scientific and technological matters but also had a strong financial aspect; it facilitates a saving of approximately 300 million EUR, i.e. the foreseen cost of one divertor.

The clean-up exercise following DTE-1 demonstrated the difficulties in determining the T inventory in a fusion device: more sophisticated measurements outside, and importantly within, the ITER vessel will be required to fulfil the legal requirement to know its in-vessel T inventory. None of the work within the Be-contaminated and radioactive JET machine would have been possible without the years of development of complex Remote Handling equipment at JET, providing a basis for (whilst indicating the difficulties in developing) such equipment for ITER.

Acknowledgements

This work has been carried out within the framework of the EUROfusion Consortium and has received funding from the Euratom research and training programme 2014-2018 under grant agreement No 633053 and from the RCUK Energy Programme [grant number EP/P012450/1]. To obtain further information on the data and models underlying this paper please contact PublicationsManager@ccfe.ac.uk. The views and opinions expressed herein do not necessarily reflect those of the European Commission.

References

[1] R. Behrisch, J. Ehrenberg, H. Bergsaker, J.P. Coad, L. de Kock, B. Emmoth et al., J. Nucl. Mater. 145-147 (1987) 731.

[2] H. Bergsaker, R. Behrisch, J.P. Coad, J. Ehrenberg, B. Emmoth, S.K. Erents et al., J. Nucl. Mater. 145-147 (1987) 727.

[3] R. Behrisch , J. Ehrenberg, M. Wielunski, A.P. Martinelli, H. Bergsaker, B. Emmoth et al., J. Nucl. Mater. 145-147 (1987) 723.

[4] J.P. Coad, R. Behrisch, H. Bergsaker, J. Ehrenberg, B. Emmoth, J. Partridge et al., J. Nucl. Mater. 162-164 (1989) 533.

[5] J. Winter, J. Nucl. Mater. 145-147 (1987) 131.

[6] J.P. Coad, K Behringer and K.J. Dietz, J. Nucl. Mater. 145-147 (1987) 747.

[7] J. Winter, H-G. Esser, L. Koenen, V. Philipps, H. Reimer, J. v. Seggern et al., J. Nucl. Mater. 162-164 (1989) 713.

[8] J.P. Coad, H. Bergsaker, S. Burch, G. Kaveney, F. Lama, J. Partridge et al., J. Nucl. Mater. 176&177 (1991) 145.

[9] M.F.A. Harrison and E.S. Hotston, J. Nucl. Mater 176-177 (1990) 256

[10] J. Brooks, J. Nucl. Mater. 170 (1990)164]

[11] J.P. Coad and B. Farmery, Vacuum 45 (1994) 435

[12] P. Andrew, C.J. Caldwell-Nichols, J.P. Coad, K.J. Dietz, J. Ehrenberg, D.H.J. Goodall et al., J. Nucl. Mater. 196-198 (1992) 143.

[13] P. Andrew, D. Brennan, J.P. Coad, J. Ehrenberg, M. Gadeberg, A. Gibson et al., Fusion Eng. Des. 47 (1999) 233.

[14] D. Stork (Ed), Technical Aspects of Deuterium–Tritium Operation at JET (special issue), Fusion Eng. Des. 47 (1999).

[15] A.T. Peacock, P.L. Andrew, D. Brennan, J.P. Coad, H. Hemmerich, S. Knipe et al., Fusion Eng. Des. 49–50 (2000) 745.

[16] R.A. Pitts, P. Andrew, Y. Andrew, M. Becoulet, I. Coffey, D. Coster et al., J. Nucl. Mater. 313-316 (2003) 777.

[17] P.A. Andrew, J.P. Coad, Y. Corre, T. Eich, A. Hermann, G. Matthews et al., J. Nucl. Mater. 337-339 (2005) 99.

[18] S.K. Erents, R.A Pitts, W. Fundamenski, J.P. Gunn and G.F. Matthews, Plasma Phys. Control. Fusion 46 (2004) 1757.

[19] H. Bergsaker, J.P. Coad, B. Emmoth, J. Likonen, G. Possnert, T. Renvall et al., J. Nucl. Mater. 362 (2007) 215.

[20] J.P. Schiffer, T.W. Bonner, R.H. Davis and F.W. Prosser, Nucl. Phys. 15 (1956) 1064.

[21] E.A. Milne, Phys. Rev. 93 (1954) 762.

[22] M. Rubel, P. Wienhold and D. Hildebrandt, Vacuum 70 (2003) 423.

[23] J. Likonen, S. Lehto, J.P. Coad, T. Renvall, T. Sajavaara, T. Ahlgren et al., Fusion Eng. Des. 66-68 (2003) 219.

[24] J.P. Coad, P.L. Andrew, J.D. Elder, S.K. Erents, H.Y. Guo, C.F. Maggi et al., 26th EPS Conf. Controlled Fusion and Plasma Physics, Europhys. Conf. Abstracts 23J (1999) 57, Maastricht, June 1999.

[25] M. Rubel, J.P. Coad and R.A. Pitts, J. Nucl. Mater. 367-370 (2007) 1432

[26] J.P. Coad, M. Rubel and C.H. Wu, J. Nucl. Mater. 241-243 (1997) 408.

[27] A.T. Peacock, P. Andrew, P. Cetier, J.P. Coad, G. Federici, F.H. Hurd et al., J. Nucl. Mater. 266-269 (1999) 423.

[28] R.A. Penzhorn, N. Bekris, U. Berndt, J.P. Coad, H. Ziegler and W. Nagele, J. Nucl. Mater. 288 (2001) 170.

[29] J.P. Coad, N. Bekris, J.D. Elder, S.K. Erents, D.E. Hole, K.D. Lawson, et al., J. Nucl. Mater. 290-293 (2001) 224.

[30] S.J. Knipe, A.C. Bell, P.D. Brennan, J.P. Coad, C.J. Manning and A.Perevezentsev, Fusion Eng. Des. 58-59 (2001) 383.

[31] N. Bekris, J.P. Coad, R-D. Penzhorn, S. Knipe, L. Doerr, R. Rolli et al., J. Nucl. Mater. 337–339 (2005) 659.

[32] M.J. Rubel, J.P. Coad, P. Wienhold, G. Matthews, V. Philipps, M. Stamp et al., Phys. Scr. T111 (2004) 112.

[33] S. Krat, Yu. Gasparyan, A. Pisarov, M. Mayer, U. von Toussaint, J.P. Coad et al., J. Nucl. Mater. 463 (2015) 822.

[34] J.P. Coad, P. Andrew and A.T. Peacock, Phys. Scr. T81 (1999) 7.

[35] J.P. Coad, P. Andrew, D.E. Hole, S. Lehto, J. Likonen, G.F. Matthews et al., J. Nucl. Mater. 313-316 (2003) 419.

[36] M. Rubel, J.P. Coad, N. Bekris, D. Hole, G.F. Matthews and R-D. Penzhorn, J. Nucl. Mater. 313-316 (2003) 323.

[37] E. Gauthier, S. Dumas, J. Matheus, M. Missirlian, Y. Corre, L. Nicholas et al., J. Nucl. Mater. 337-339 (2005) 960.

[38] T. Tanabe, N. Bekris, J.P. Coad, C.H. Skinner, M. Glugla and N. Miya, J. Nucl. Mater. 313-316 (2003) 478.

[39] J.P. Coad, J. Likonen, M. Rubel, E. Vainonen-Ahlgren, D. Hole, T. Sajavaara et al., Nucl. Fusion 46 (2006) 350.

[40] C.P.C. Wong, R. Junge, R.D. Phelps, P. Politzer, F. Puhn, W.P. West et al., J. Nucl. Mater. 196-198 (1992) 871.

[41] H-G Esser, V. Philipps, M. Freisinger, J.P. Coad, G.F. Matthews, G. Neill et al., Phys. Scr. T111 (2004) 129.

[42] S. Lehto, J. Likonen, J.P. Coad, T. Ahlgren, D.E. Hole, M. Mayer et al., Fusion Eng. Des. 66-68 (2003) 241.

[43] J. P. Coad, N. Bekris, J.D. Elder, S.K. Erents, D.E.Hole, K.D. Lawson et al., J. Nucl. Mater. 290-293 (2001) 224.

[44] A.V. Chankin, G. Corrigan, S.K. Erents, G.F.Matthews, J. Spence and P.C. Stangeby, J. Nucl. Mater. 290–293 (2001) 518

[45] J.P. Coad, H-G. Esser, J. Likonen, M. Mayer, G. Neill, V. Philipps et al, Fusion Eng. Des.74 (2005) 745.

[46] A.M. Widdowson, S. Brezinsek, J.P. Coad, H-G. Esser, D.E. Hole, J. Likonen et al., Phys. Scr. T138 (2009) 014005.

[47] S. Brezinsek, A. Pospieszczyk, D. Borodin, M.F. Stamp, R. Pugno, A.G. McLean et al., J. Nucl. Mater. 363-365 (2007) 1119.

[48] J.P. Coad, S. Gruenhagen, D.E. Hole, A. Hakola, S. Koivuranta, J. Likonen et al., Phys. Scr. T145 (2011) 014003.

[49] C. Jeynes, N.P. Baradas, P.K. Marriott, G. Boudreault, M. Jenkin, E. Wendler et al., J. Phys. D: Applied Physics 36 (2003) R97.

[50] A. Kreter, S. Brezinsek, J.P. Coad, H-G. Esser, W. Fundamenski, V. Philipps et al., J. Nucl. Mater. 390-391 (2009) 38.

[51] P. Petersson, H. Bergsaker, G. Possnert, B. Emmoth, J.P. Coad, S. Koivuranta et al., Nucl. Instr. Meth. B268 (2010) 1838.

[52] I. Bykov, H. Bergsaker, P. Petersson, J. Likonen and G. Possnert, Nucl. Instr. Meth. B332 (2014) 280.

[53] A. Kreter, H-G. Esser, S. Brezinsek, J.P. Coad, A. Kirschner, W. Fundamenski et al., Phys. Rev. Lett. 102 (2009) 045007.

[54] J. Likonen, A. Hakola, S. Koivuranta, M. Airila, J.P. Coad, A. Widdowson et al., Phys. Scr. T145 (2011) 014004.

[55] P. Wienhold, H-G. Esser, D. Hildebrandt, A. Kirschner, M. Mayer, V. Philipps et al., J. Nucl. Mater 290-293 (2001) 362

[56] M.J. Rubel, J.P. Coad, K. Stenstrom, P. Wienhold, J. Likonen, G.F. Matthews et al, J. Nucl. Mater. 329-333 (2004) 795.

[57] M. Rubel, J.P. Coad and D.E. Hole, Vacuum 78 (2005) 255.

[58] J.D. Strachan, J.P. Coad, G. Corrigan, G.F. Matthews and J. Spence, 31st EPS Conference on Plasma Physics, London, Europhys. Conf. Abstracts G28, P1.136, London, UK

[59] J.D. Strachan, J.P. Coad, G. Corrigan, J. Spence, G.F. Matthews, J. Likonen et al., 48th APS Conference, NP1.00035, Philadelphia, USA, October 2006. http://meetings.aps.org/Meeting/DPP06/Session/NP1.35

[60] J.D. Strachan, J.P. Coad, G. Corrigan, J. Spence, G. Matthews, M. Airila et al, 34th EPS Conf. Plasma Physics, Europhys. Conf. Abstracts 31F (2007) P1-030, Warsaw, Poland, July 2007

[61] J.D. Strachan, J. Likonen, J.P. Coad, M. Rubel, A. Widdowson, M. Airila et al., Nucl. Fusion 48 (2008) 105002.

[62] P. Andrew, J.P. Coad, T. Eich, E. Gauthier, A. Herrmann, G.F. Matthews et al., J. Nucl. Mater. 313-316 (2003) 135.

[63] P. Andrew, J.P. Coad, Y. Corre, T. Eich, A. Herrmann, G. Matthews et al., J. Nucl. Mater. 337-339 (2004) 99.

[64] S. Gruenhagen, P.D. Brennan, S. Knipe, R. Stagg, J. Yorkshades and JET-EFDA contributors, Fusion Sci. Technol. 60 (2011) 631.

[65] J.P. Coad, P. Andrew, D. Hole, J. Likonen, M. Mayer, M. Rubel et al., J. Nucl. Mater. 363-365 (2007) 287.

[66] G.F. Matthews, M Beurskens, S. Brezinsek, M. Groth, E. Joffrin, A. Loving et al., Phys. Scr. T145 (2011) 014001

[67] A.M. Widdowson, C.F. Ayres, S. Booth, J.P. Coad, D. Ivanova and J. Likonen, J. Nucl. Mater. 438 (2013) S827.

[68] S. Krat, J. P. Coad, Yu. Gasparyan, A. Hakola, J.Likonen, M. Mayer et al., J. Nucl. Mater. 438 (2013) S742.

[69] Ph. Mertens, O. Neubauer, V. Philipps, S. Ciattaglia, A. Huber, A. Kirschner et al., Phys. Scr. T159 (2014) 014004.

[70] A. Kirschner, V. Philipps, D.P. Coster, S.K. Erents, H-G. Esser, G. Federici et al., J. Nucl. Mater. 337-339 (2005) 17

Table Captions

Table 1: Cumulative ion fluxes measured with Langmuir probes for experimental campaigns 1998-1999, 1999-2001 and 1998-2001.

Table 2: Characteristic parameters for accelerator-based ion beam analysis

Table 3: Thickness of the deposits on the divertor tiles removed in 2009 after different exposure periods.

Table 4: Thickness (in μm) of the deposits measured on cores cut from Tiles 1 and 3 after different experimental campaigns and after different exposure periods.

Table 5: Thickness (in μm) of the deposits on the samples from Tiles 4 and 6 exposed in 1991-2001, 2001-2004, 1998-2007 and 1998-2009. Layer thicknesses were determined with SIMS, micrometer and optical microscopy.

Table 6: Amounts of ^{13}C found on divertor tiles (extrapolated to the whole divertor) following the puffing experiments in 2001 and 2004, expressed as a percentage of the ^{13}C-labelled methane gas input

Table 7: Average film thicknesses for each tile in Module 2, and the volume of coatings obtained by integrating film thicknesses toroidally.

Table 1: Cumulative ion fluxes measured with Langmuir probes for experimental campaigns 1998-1999, 1999-2001 and 1998-2001

Tile	Probe	Ion flux (10^{26} m^{-2}) 1998-1999	Ion flux (10^{26} m^{-2}) 1999-2001	Ion flux (10^{26} m^{-2}) 1998-2001
1	2	0.086	0.840	0.926
1	3	0.142	0.799	0.941
1	4	0.090	0.650	0.740
3	5	0.959	2.98	3.94
3	6	4.25	4.39	8.64
3	7	4.96	3.69	8.65
3	8	4.55	5.78	1.03

Table 2: Characteristic parameters for accelerator-based ion beam analysis

Element / Isotope	Reaction/Method	Energy (MeV)	Sensitivity (atoms cm^{-2})	Remarks
D	$D(^3He,p)^4He$ / NRA	0.7 - 3	1×10^{14}	Depth profiling Very high selectivity
Be-9	$^9Be(^3He,p)^{11}B$ / NRA	2.5	1×10^{17}	Cross-section not well known
B-11	$^{11}B\ (p,\alpha)^8Be$ / NRA	0.7	4×10^{14}	No depth profiling
C-12	$^{12}C(^3He,p)^{14}N$ / NRA $^{12}C(p,p)^{12}C$ / EPS	2.5 1.5	1×10^{17} 5×10^{16}	
C-13	$^{13}C(^3He,p)^{15}N$ / NRA $^{13}C(p,p)^{13}C$ / EPS $^{13}C(p,p)^{13}C$ / EPS	2.5 2.5 1.442 (resonance)	1×10^{17} 5×10^{16} 1×10^{16}	Quantitative for layers < 50 nm
Ni, Cr, Fe	H^+ / PIXE	2.5		
Re	$^4He^+$ / RBS H^+ / PIXE	2.5 2.5	3×10^{12}	

Table 3: Thickness of the deposits on the divertor tiles removed in 2009 after different exposure periods.

Tile	Sample	SIMS (μm)	Opt. Microscopy (μm)
1 (2004-2009)	2	28±1	33±3
	5	19±2	18±2
	8	60±3	58±3
	10		104±5
3 (2004-2009)	2	31±2	33±2
	4	37±2	36±4
	6	39±2	37±10
	8	46±5	47±5
3 (1998-2009)	2	93±4	89±5
	4	72±3	74±11
	6	28±3	46±7
	8	80±3	84±7
4 (2004-2009)	2		57±3
	4		49±8
	6		122±6
	7		247±5
	10		145±3
4 (2007-2009)	1	26±2	36±2
	3	7.4±0.8	102±4
	6		339±35
	10		73±4
6 (2004-2009)	2	4.3±0.2	2.8±0.4
	3		75±5
	4		144±20

	5		281±30
	6		325±40
	7		476±30
	8		119±29
6 (1998-2009)	1	25±3	24±3
	3		200±18
	6		402±60
	8		129±34

Table 4: Thickness (in µm) of the deposits measured on cores cut from Tiles 1 and 3 after different experimental campaigns and after different exposure periods.

TILE/SAMPLE	**1998-2001**	**2001-2004**	**1998-2004**	**2005-2007**	**1998-2007**	**2007-2009**
1/11		72	98			
1/10				115	119	51
1/8	28	31	32	49	46	17
1/5		6.5	11	9	6	6.5
1/4	13					
1/2		11	18	15	18	13
1/1	14					
3/8	55	41	56	26		22
3/4	35	31	63	20		24
3/2			43	13		27
3/1	31	29	14			

Table 5: Thickness (in µm) of the deposits on the samples from floor tiles exposed in 1991-2001, 2001-2004, 1998-2007 and 1998-2009. Layer thicknesses were determined with SIMS, micrometer and optical microscopy.

TILE/SAMPLE	**1999-2001**	**2001-2004**	**1998-2007**	**1998-2009**
4/1	14			
4/2		7	32	20
4/4	12	37	35	110
4/7	260	280	416	205
4/8				
4/9		110	430	
4/10	87			535
6/1		0.2		
6/3		3	2.5	
6/4		69	72	
6/7	160	300	822	
6/9	4.2	32	69	

Table 6: Amounts of ^{13}C found on divertor tiles (extrapolated to the whole divertor) following the puffing experiments in 2001 and 2004, expressed as a percentage of the ^{13}C-labelled methane gas input

Tile	^{13}C amount for 2004 (% of total input)	^{13}C amount for 2001 (% of total input)
1	1.3	21.0
3	0.7	24.0
4	3.7	0.8
6	2.6	0.1
7	7.0	0.3
8	6.0	<0.1

Table 7: Average film thicknesses for each tile in Module 2, and the volume of coatings obtained by integrating film thicknesses toroidally.

Tile	1998-2007		1998-2009		2007-2009	
	Average film (μm)	Integrated vol (cm^3)	Average film (μm)	Integrated vol (cm^3)	Average film (μm)	Integrated vol (cm^3)
1	30.8	83.7	56.6	151.9	23.9	65.6
3	55.0	122.0#	55.0	118.8	22.3	49.1
4	176.4	478.9	221.9	596.1	131.3	341.8
6	196.5	580.1	187.3	550.1	116.6	343.0
Total		1264.7		1462.2		799.5

 # This is the value for a tile exposed 1998-2004 since no Tile 3 exposed 1998-2007 exists

Figure Captions

Figure 1: Timeline for JET operations from the first plasma in 1983 until the removal of the carbon divertor in 2010

Figure 2: Interior of the JET vessel in the 1983-84 campaign

Figure 3: Interior of the JET vessel in 1987

Figure 4: Cross-section of JET showing the plasma configuration for discharges with an X-point inside the top of the vessel, close to the upper dump plates.

Figure 5: Cross-section of the JET MkI divertor (in use 1994-5) (top), and comparison of the D retention in the C and Be MkI divertor (bottom)

Figure 6: Deposition in the JET MkI divertor due to the "roof-top" design of the divertor elements (left, vertical scale exaggerated). The deposition is strongly peaked just inside the shadowed region (right).

Figure 7a-7d: Cross-sections of the JET MKI (1994-5), MkIIA (1996-8), MkII-GB (1998-2001) and MkII-SRP (2001-3) divertor configurations

Figure 8: Cross-section of the JET MkII-HD divertor, and the shape of the proposed ITER divertor for comparison

Figure 9: Left-hand side: view of the inside of JET in 1999 with the MkII-GB divertor. Right-hand side: view of the inside of JET in 2002 with the MkII-SRP divertor.

Figure 10: Poloidal cross-section of the Mk-IIGB divertor, the flux deposition profiles and distribution of mechanical measurement points

Figure 11: Histogram of the inner strike point positions (Z-coordinate) during the operational campaigns with the MkII-GB divertor. Position of inner divertor Tiles 1 and 3 is indicated with vertical dashed lines

Figure 12: Histogram of tile temperature in the inner target during the operation with the MkII-A and Gas Box (in 2000 and 2001) divertors.

Figure 13: The cross-section of the JET HD divertor showing the agreed s co-ordinate system for specifying the poloidal locations of the surfaces of the divertor tiles. When applied retrospectively to the MkII-SRP divertor, the SRP (which fits directly between Tiles 4 and 6) has co-ordinates for its top surface from 980 to 1260 mm.

Figure 14: Histogram showing the distribution of strike point positions in the divertor during the MkII-SRP operations 2001-4. The X-axis is the s co-ordinate: the changes from Tiles 1-3-4-5-6-7-8 occur at approximately 0.43, 0.7, 0.95, 1.32, 1.55 and 1.81 m

Figure 15: Cross-section of the JET-HD divertor installed in 2004 and used until 2009. (a) Plasma cross-section for the high-delta configuration with the inner strike-point on Tile 1 and the outer strike-point on the load bearing tile (sometimes referred to as Tile 5).
(b) Other configurations were also used during the 2005-7 campaign with strike-points more symmetrically placed, e.g. as here, on Tiles 3 and 7.

Figure 16: Histogram showing the distribution of strike point positions in the divertor during the MkII-HD operations 2005-7 and 2007-9, and comparison with the MkII-SRP operations 2001-4. The X-axis is the s co-ordinate: the changes from Tiles 1-3-4-5-6-7-8 occur at approximately 0.43, 0.7, 0.95, 1.32, 1.55 and 1.81 m

Figure 17: Floor plan of the divertor which consists of 24 modules, numbering anti-clockwise from Octant 1. Each module has Wide and Narrow carriers (the wide carrier has electrical connections), and there are Outer, Base and Inner carriers. So, for example, a tile designated as Tile 2IN G1A is in Module 2, the Inner carrier and is a Tile 1 (one of 4 with labels "A", "B", "C" or "D").

Figure 18: Tritium retention in JET following the DTE1 campaign in 1997

Figure 19: Flakes piled behind a divertor support leg, observed using an endoscope in 1999

Figure 20 Schematic view of a marker tile, and a diagram showing how the possible erosion/deposition scenarios would affect the markers.

Figure 21: Erosion or deposition on a poloidal set of divertor tiles following exposure from 1999-2001, as derived from micrometer measurements (see also Figure 10): grey shading shows the amount of compression in the micrometer measurements (only occurred at two points). Also included are film thicknesses measured by SIMS. The tile numbers are shown on the Figure.

Figure 22: SIMS spectra from a core cut from the bottom of Tile 1 exposed 1998-2001

Figure 23: SIMS spectra from a core cut from the middle of Tile 3 exposed 1998-2001

Figure 24: Structure of the Gas Box module viewed from the inner divertor. The location of narrow deposition belts on the support plates is indicated with arrows. Local re-deposition on Tiles 5 is indicated with shading

Figure 25: Tile 7 after removal from JET in 2004 and after cutting a poloidal set of samples at VTT

Figure 26: RBS spectrum from the W stripe near the bottom of the front face of Tile 8 exposed in JET 2001-4. The spectrum shows a continuous film of W at the surface, and is similar to the spectrum before exposure in JET.

Figure 27: An RBS spectrum from the W stripe about one-third the way up the Tile 7 surface as shown in the sketch, after exposure in JET 2001-4. Edges labelled W and ^{12}C are the high energy edge of the feature characteristic of that element. Small amounts of Be, ^{13}C and O are also present at the surface.

Figure 28: SEM photograph from a strongly eroded area of the W stripe on Tile 8 after exposure in JET 2001-4

Figure 29: The strike points and field lines for the series of discharges into which the ^{13}C was puffed in 2004.

Figure 30: Levels of D, Be and ^{13}C along Tile 7 (from bottom to top) after exposure in JET 2001-4 measured by NRA

Figure 31: Be/C ratios determined by NRA for Tile 1 - examples from different operational campaigns. The apron is between s-coordinates 162 and 222 mm and the front face of the tile from 222 to 431 mm.

Figure 32: Cross-section of deposit on Tile 3 exposed 2001-4. SIMS analysis shows bands of greater C/Be at the surface and near the centre of the film.

Figure 33: RBS spectra from the upper part of the front face of Tile 3 for tiles removed in 2001 and in 2004. The arrows indicate the high energy edge of the feature characteristic of that element.

Figure 34: NRA spectra from the upper part of the front face of Tile 3 for tiles removed in 2001 and in 2004, with peaks characteristic of each element indicated.

Figure 35: C, Be and D concentrations derived from NRA measurements on Tile 3BW G4B (Tile 4) exposed in JET 2001-4, plotted inboard to outboard

Figure 36: Section from shadowed region of Tile 4 exposed 2001-4

Figure 37: C, Be and D concentrations derived from NRA measurements across Tile 14BN G6B (Tile 6) exposed 2001-4, plotted inboard to outboard.

Figure 38: Section from sloping part of Tile 6 exposed 2001-4. Note the bright band between the deposit and the tile surface, which is the W marker layer coated onto the tile before exposure.

Figure 39: Cross-section of the JET MkII-HD divertor showing the positions of tritium retention diagnostics during the 2005-7 operational period.

Figure 40: The proposed coating scheme for tile LBSRP 14WR - two thicknesses of W (3 and 1.5 μm) and a 10 μm thick stripe of C (on a W interlayer), before mounting in JET in 2004. However, in brackets are the actual W film thicknesses found during subsequent analysis (0.7 and 1.3 μm) - the C stripe did not survive plasma operations.

Figure 41: View of the LBSRP Tiles 14WR and 14NL from the Octant 5 UMVP at the end of the 2005-7 operations. The W-coated stripes can be clearly seen on Tile 14WR. The deposition patterns can also be seen from the methane injected from the gas injection nozzle (the nozzle is visible between the two tiles).

Figure 42: RBS spectra from the centre (poloidally) of the W-coated stripes on LBSRP Tile 14WR (a) on the thinner coating (JET11822 – labelled “22”), (b) on the plasma-exposed part of the thicker coating (JET11832 – labelled “32”), (c) on the shadowed part of the thicker coating JET11838 – labelled “38”). The arrows indicate the high energy edge of the feature characteristic of that element.

Figure 43: RBS spectra from the thicker W stripe (JET11868 – labelled “68”), in the gap between stripes (JET11870 – labelled “70” and 11874 – labelled “74”), and downstream from both stripes (JET11890 - unlabelled). The arrows indicate the high energy edge of the feature characteristic of that element.

Figure 44: A photograph of the W-coated load-bearing tile after exposure 2007-9. The s co-ordinates indicate the inboard and outboard edges of the tile (1039 and 1289mm), and the area of maximum 12C and 13C (1189mm) for the puffing experiments on the last day of operations in 2009: the strike point was at ~1170mm during the inter-ELM periods.

Figure 45: View of part of the apron of a Tile 1 (right-hand side) and the upper front face of the tile (towards the left-hand side) during the 2007 JET shutdown inspection, showing spalling deposits. The tile had been exposed 1998-2007.

Figure 46: RBS spectra from the lower part of the front face (JET12924) and from the apron (JET12860, recorded for only half the beam fluence of JET12924 for clarity) of Tile 2IWG1A exposed 2005-7. The arrows indicate the high energy edge of the feature characteristic of that element.

Figure 47: The ratio Be/C and the D in the surface layer on Tiles 1 and 3 exposed 2007-9 from NRA data.

Figure 48: Comparison of Be/C ratios on Tile 4 for tiles removed after the last three JET campaigns (1999-2001 – Mk II Gas Box, 2001-4 – MkII SRP, 2005-7 – MkII HD divertors)

Figure 49: Comparison of Be/C ratios on Tile 6 for tiles removed after the last three JET campaigns (1999-2001 – Mk II Gas Box, 2001-4 – MkII SRP, 2004-7 – MkII HD divertors)

Figure 50: Photograph of the inner carrier 2IN after removal in 2007. The bottom of Tile 3 is at the top of the picture. Surfaces are covered with a thick deposit, which is showing signs of spalling in certain places. The front face of the mirror test unit (centre of picture) is so thickly coated that it is not possible to see where the third channel (with a sample flush to the face) is.

Figure 51: NRA concentrations of D and Be across Tile 6 (exposed 1998-2009). Region A is shadowed by the LBT, region B is the sloping part of the tile, and C is the region shadowed by Tile 7.

Figure 52: Rutherford Backscattering spectra from a divertor Tile 7 (2ON G7A, exposed 2005-7). The spectra were recorded from samples 10 mm below (spectrum 13926) and 10 mm above (spectrum 13924, recorded for only half the beam fluence of 13926 for clarity) the middle of the tile. The ^{12}C arrow indicates the high energy edge of the carbon feature – the D, ^{13}C and O are present at the surface.

Figure 53: Cross-section of the JET MkII-SRP divertor showing the principle $^{13}CH_4$ injection point (heavy red arrow) and a supposed leakage path (hollow red arrow).

Figure 54: D and ^{13}C concentrations plotted along the W-stripe seen in the panel above. The left-hand edge of the stripe in the picture is the top of Tile 7, the right-hand edge the bottom

Figure 55: RBS spectrum of the thin deposit comprising ^{12}C, ^{13}C and O on the W-stripe near the top of Tile 7 after exposure in JET 2001-2004 (where D and ^{13}C are maxima in Fig.32).

Figure 56: A 2-dimensional plot of the ^{13}C deposit of a Tile 7 (2ONG7A) as derived from RBS spectra, in the region adjacent to a gas injection nozzle between Tiles 7 and 8 at the top of the front surface. The maximum is in a region normally protected from incident ions by the

slightly prominent lower edge of Tile 8. The ^{13}C flow is in the direction of the arrow beneath "^{13}C injection".

Figure 57: Plot of ^{13}C and ^{12}C measured by NRA across Tile 2ONG7A, showing that the deposit at the top edge is almost exclusively ^{13}C and not ^{12}C

Figure 58: Maximum temperatures measured with an infra-red camera during selected pulses during the ^{13}C puffing experiments at the end of the 2002-4 campaign.The upper part shows the maximum temperature in the outer divertor during pulse 63415 (red curve) and 63438 (blue curve). The lower part shows the maximum temperature in the inner divertor during pulse 63415 (red curve) and 63438 (blue curve)

Figure 59: Cross-section of the JET MkII-HD divertor showing the tile numbering, some relevant s co-ordinates (see text), and the plasma configuration used during the ^{13}C (as methane) puffing experiments on the last day of the 2007-9 operational period.

Figure 60: Particle Sizing Data - Results given as weight in the particular size fraction multiplied by the total weight of the dust sample collected versus the particular size fraction in microns.

Figure 61: Film thicknesses from optical microscopy of sections for Tiles 1 removed after operational periods 1998-2004 (Module 22), 1998-2009 (Module 14) and 2004-9 (Module 14).

Figure 62: Film thicknesses from optical microscopy of sections for Tiles 6 removed from Module 2 after operational periods 1998-2007, 1998-2009 and 2007-9.

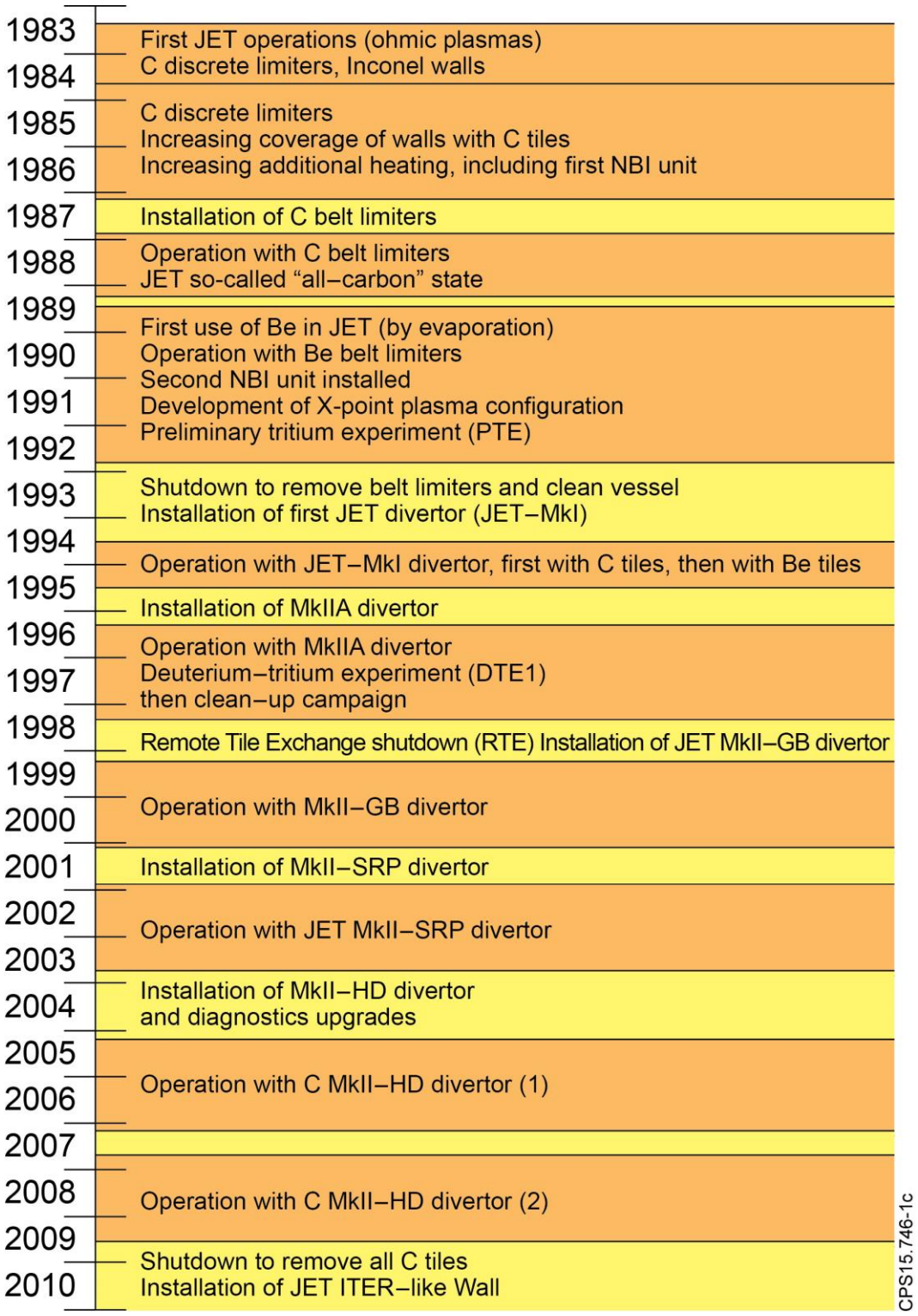

Figure 1: Timeline for JET operations from the first plasma in 1983 until the removal of the carbon divertor in 2010

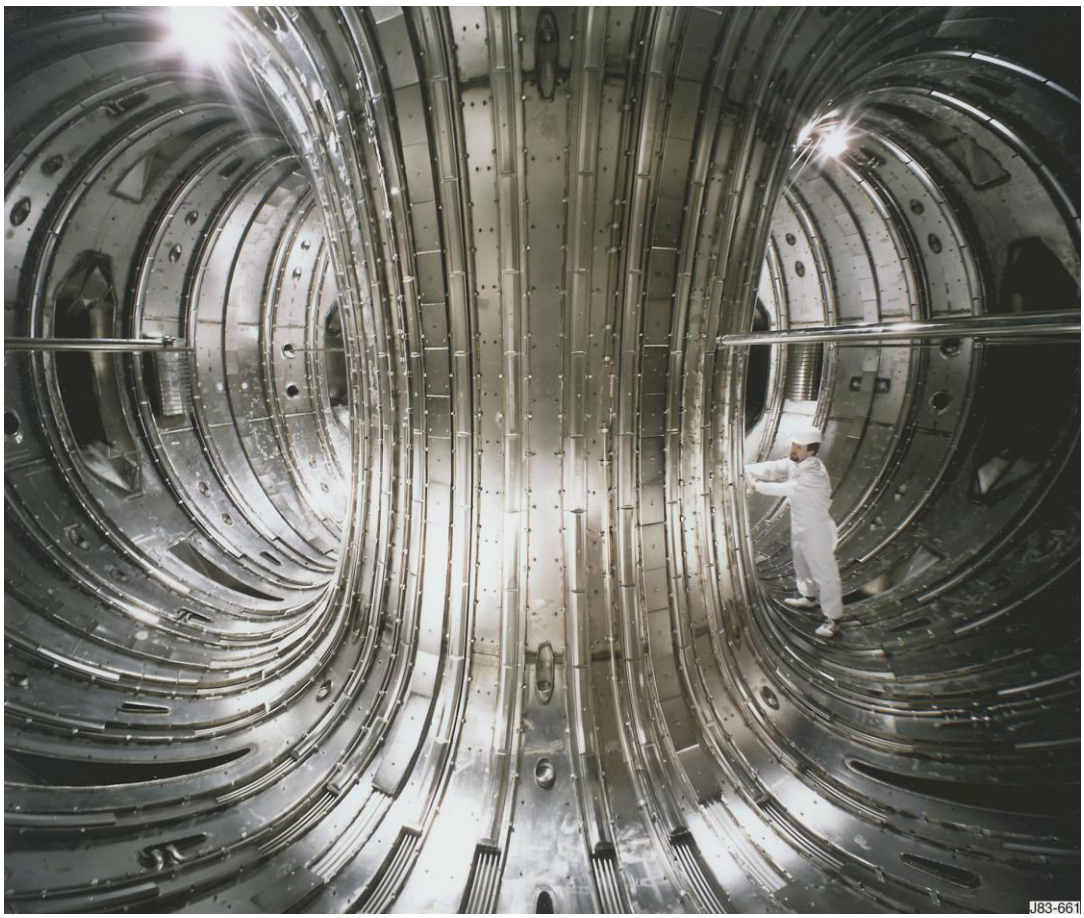

Figure 2: Interior of the JET vessel in the 1983-84 campaign

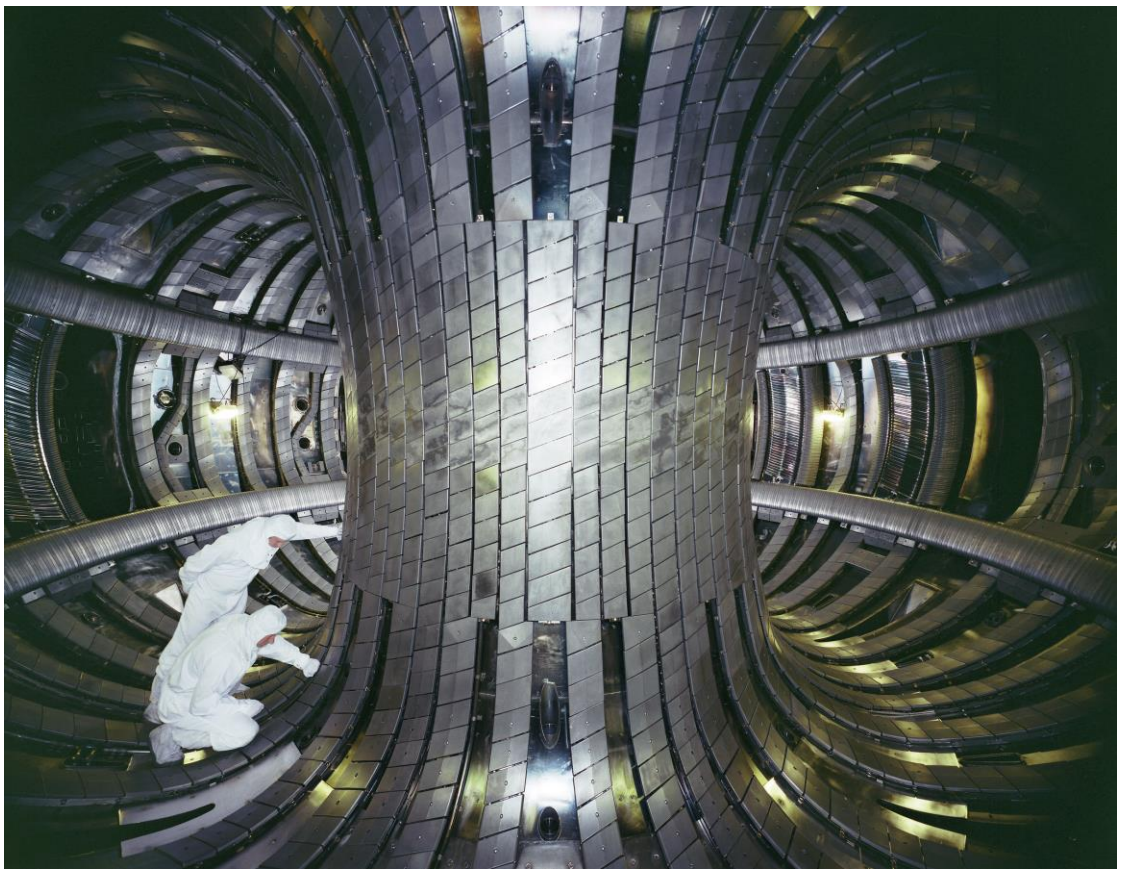

Figure 3: Interior of the JET vessel in 1987

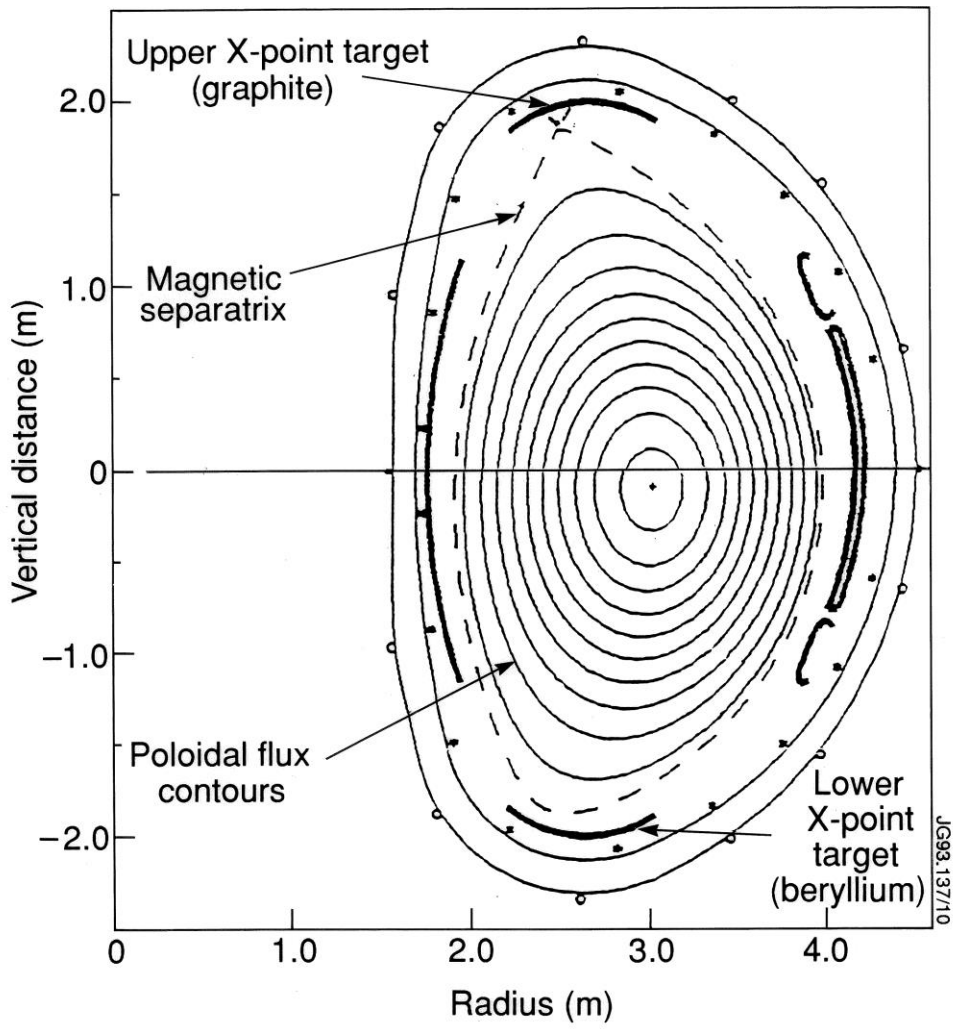

Figure 4: Cross-section of JET showing the plasma configuration for discharges with an X-point inside the top of the vessel, close to the upper dump plates.

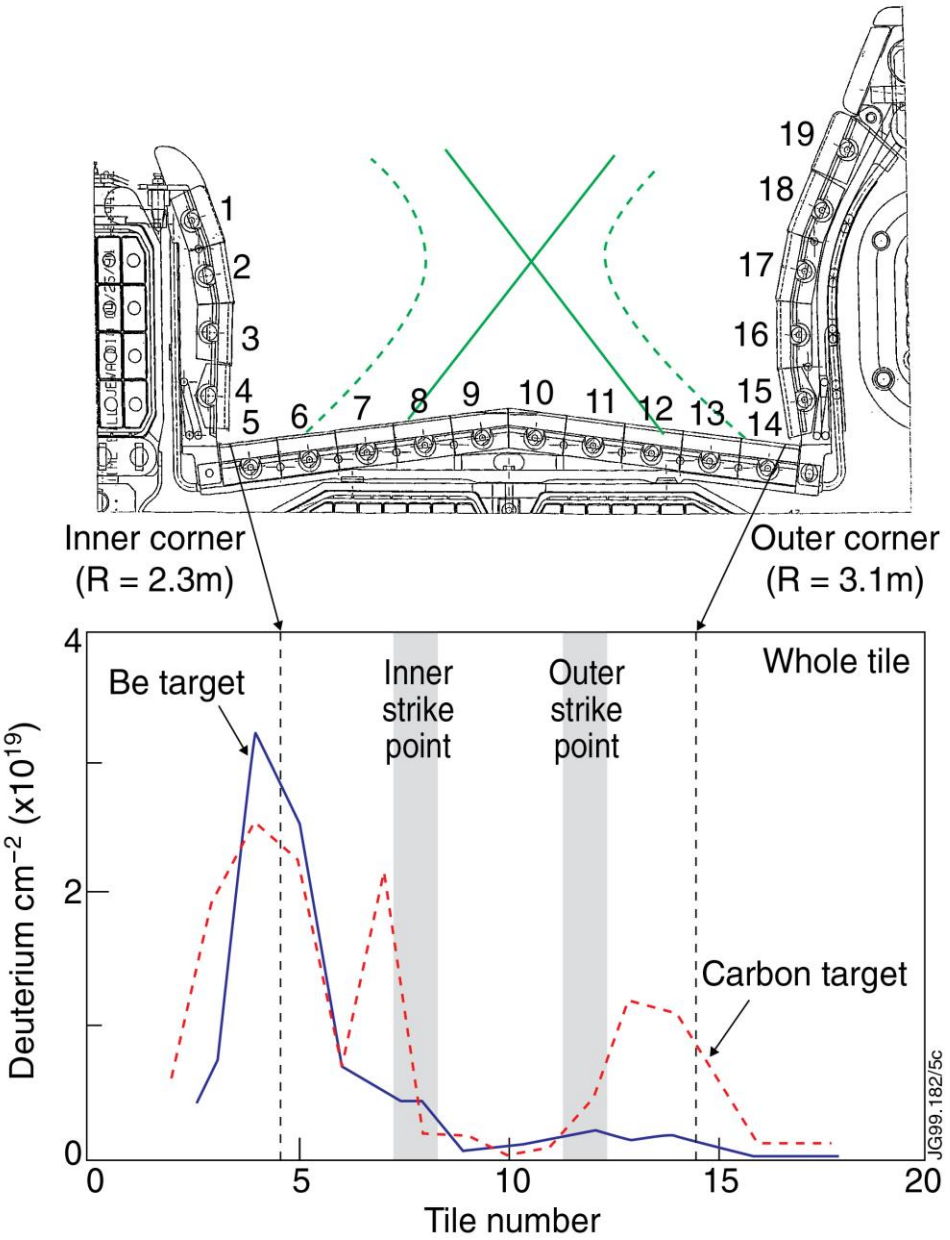

Figure 5: Cross-section of the JET MkI divertor (in use 1994-5) (top), and comparison of the D retention in the C and Be MkI divertor (bottom)

Divertor tiles are arranged in "roof-top" pattern to protect tile edges and prevent "blooms"

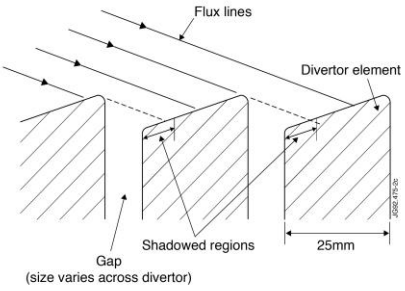

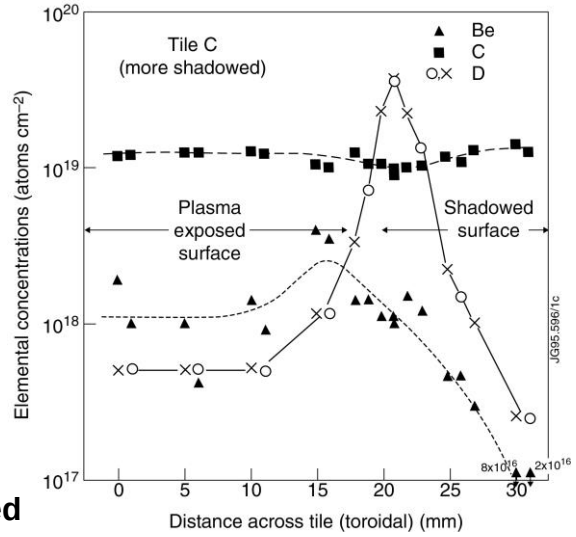

Heavy re-deposition of C in shadowed area of each tile adjacent to erosion zones

Figure 6: Deposition in the JET MkI divertor due to the "roof-top" design of the divertor elements (left, vertical scale exaggerated). The deposition is strongly peaked just inside the shadowed region (right).

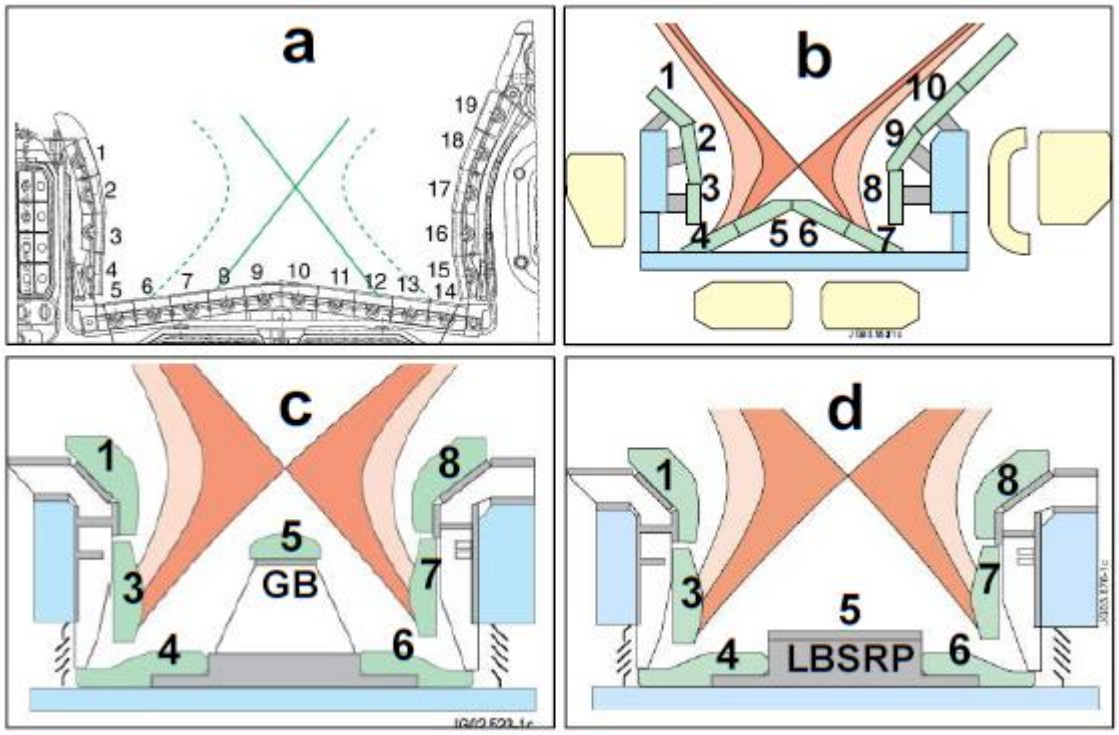

Figure 7a-7d: Cross-sections of the JET MKI (1994-5), MkIIA (1996-8), MkII-GB (1998-2001) and MkII-SRP (2001-3) divertor configurations.

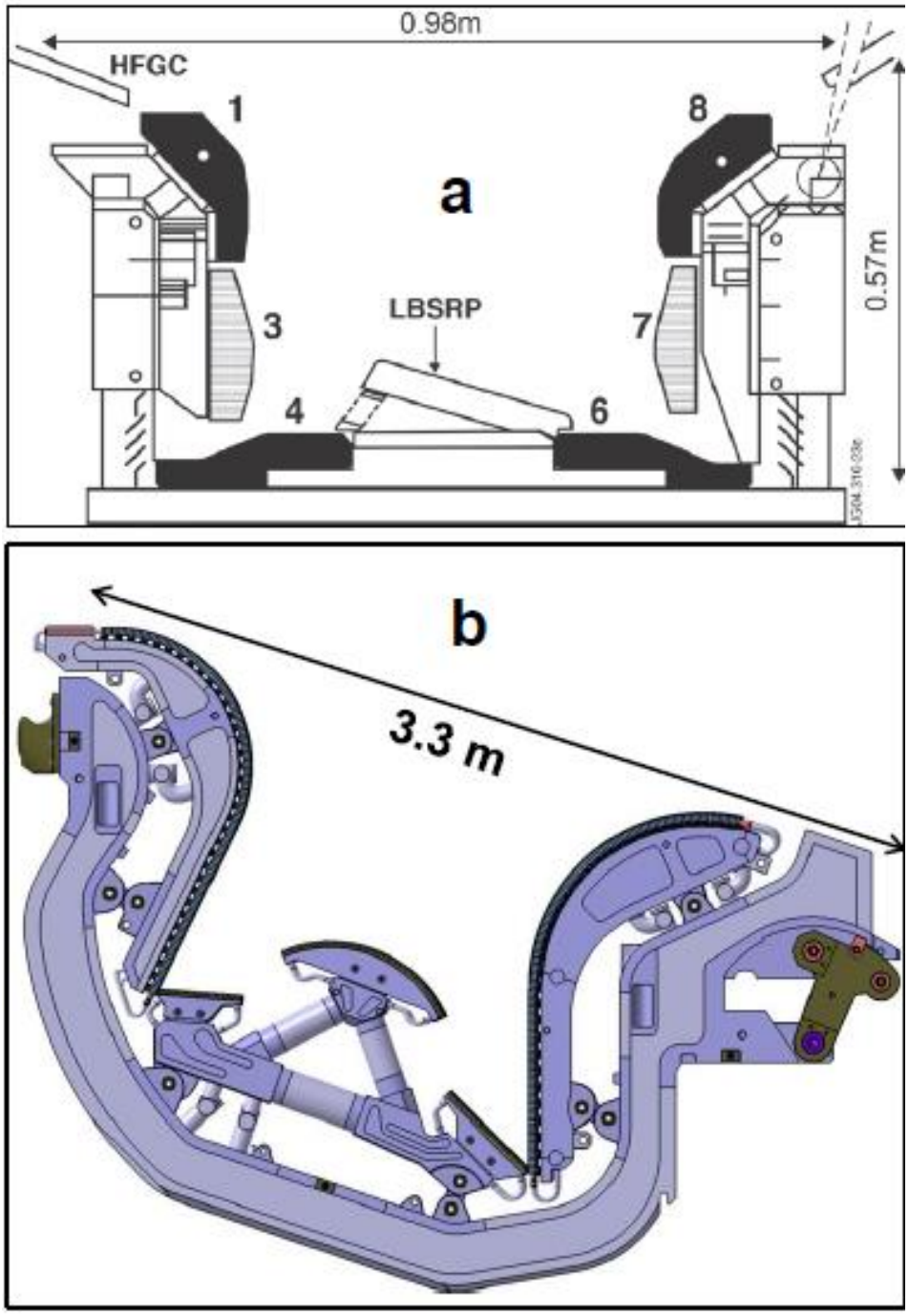

Figure 8: Cross-section of the JET MkII-HD divertor, and the shape of the proposed ITER divertor for comparison

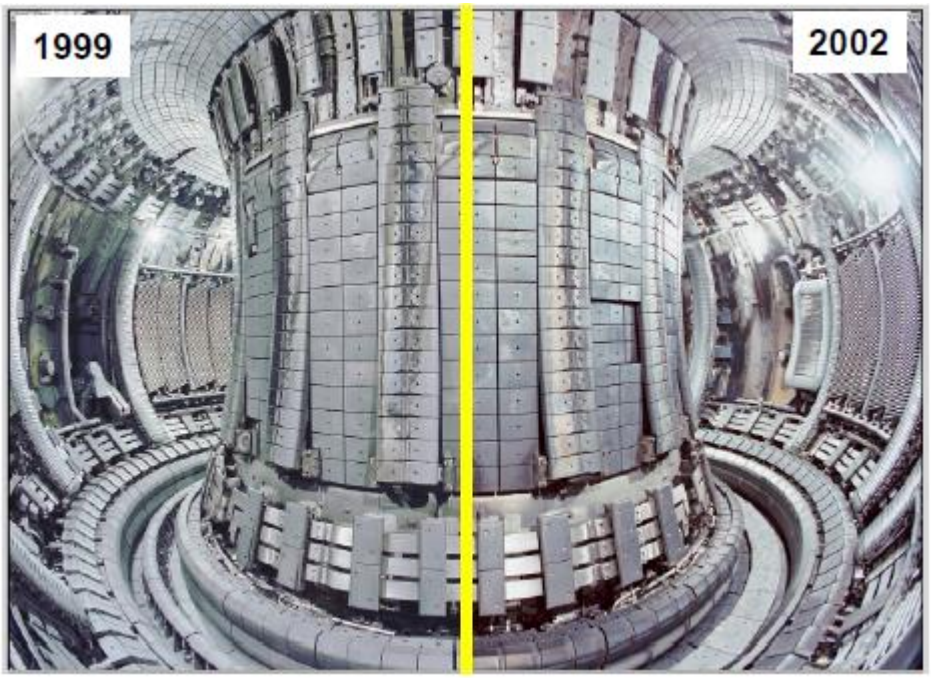

Figure 9: Left-hand side: view of the inside of JET in 1999 with the MkII-GB divertor. Right-hand side: view of the inside of JET in 2002 with the MkII-SRP divertor.

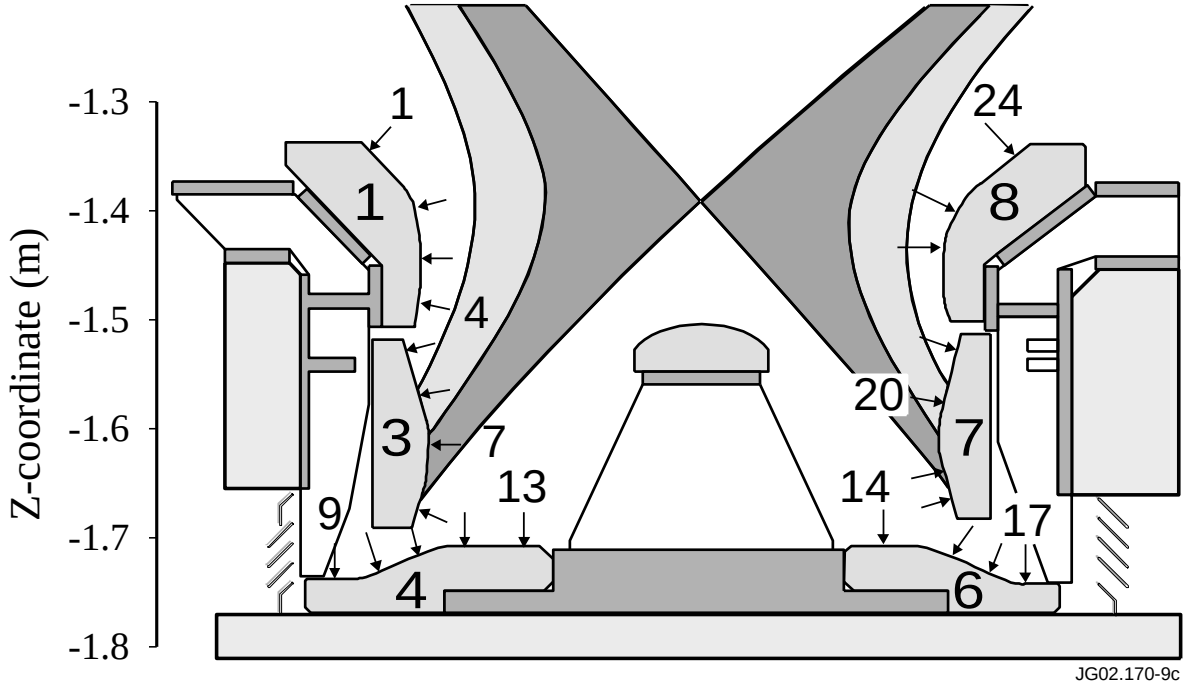

Figure 10: Poloidal cross-section of the Mk-IIGB divertor, the flux deposition profiles and distribution of mechanical measurement points. (All measurement points are numbered consecutively in a poloidal direction: some are omitted for clarity.)

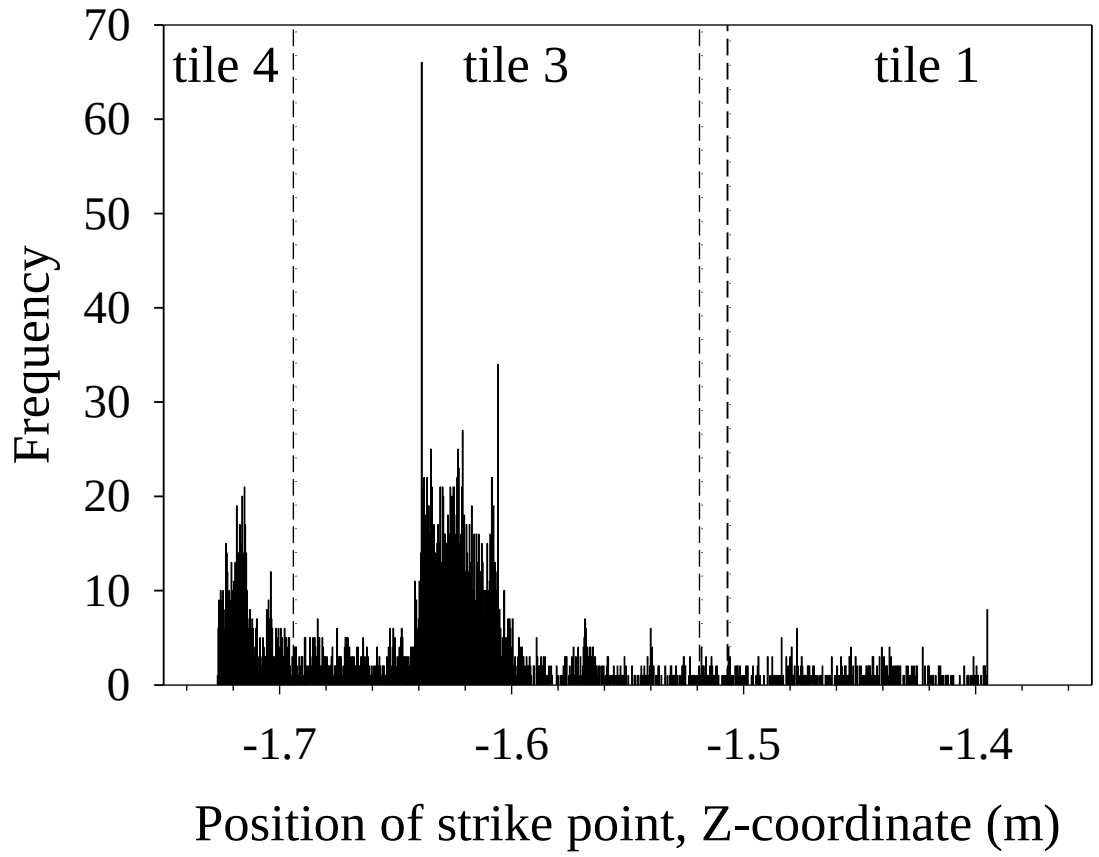

Figure 11: Histogram of the inner strike point positions (Z-coordinate) during the operational campaigns with the MkII-GB divertor. Position of inner divertor Tiles 1 and 3 is indicated with vertical dashed lines

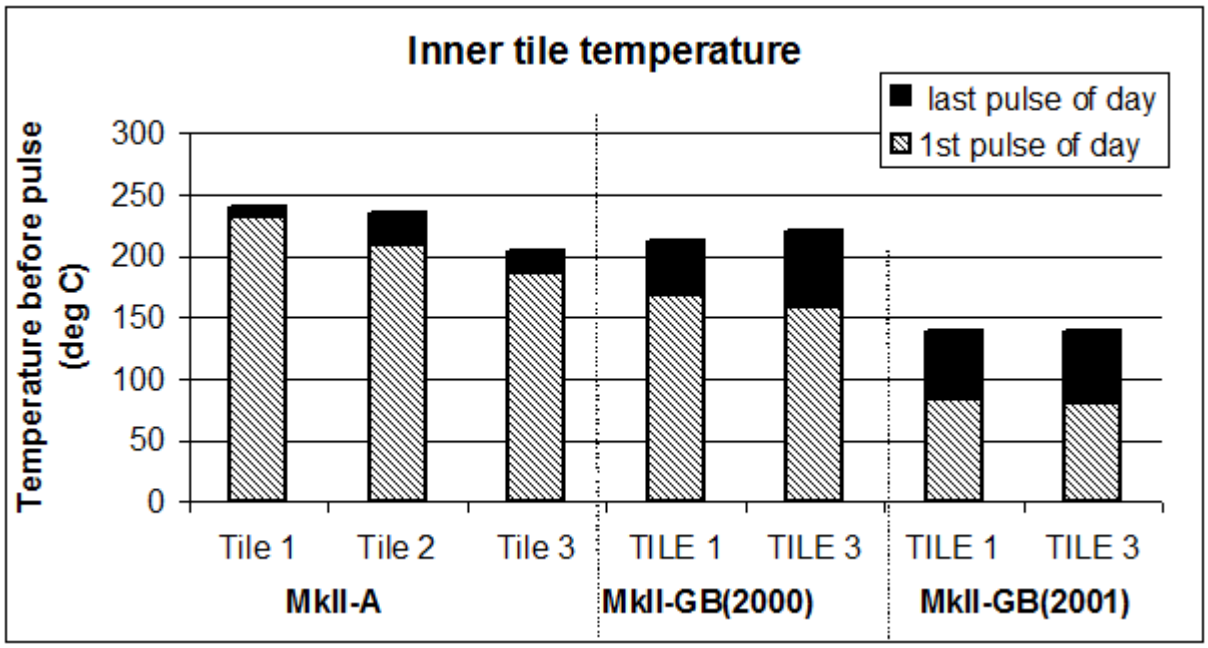

Figure 12: Histogram of tile temperature in the inner target during the operation with the MkII-A and Gas Box (in 2000 and 2001) divertors.

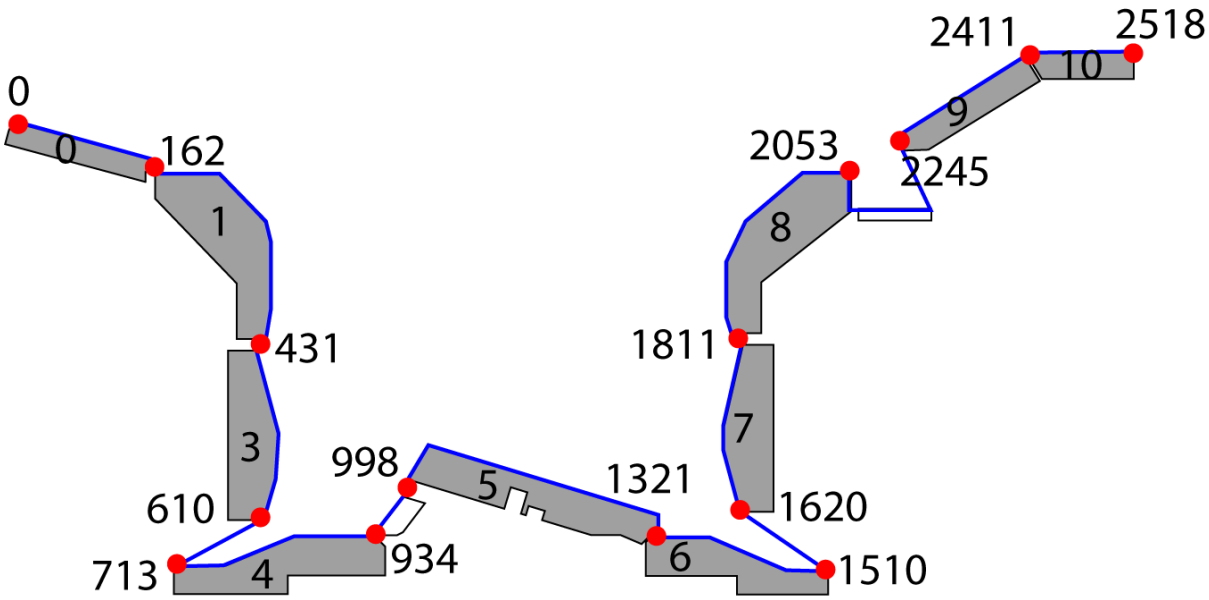

Figure 13: The cross-section of the JET HD divertor showing the agreed s co-ordinate system for specifying the poloidal locations of the surfaces of the divertor tiles. When applied retrospectively to the MkII-SRP divertor, the SRP (which fits directly between Tiles 4 and 6) has co-ordinates for its top surface from 980 to 1260 mm.

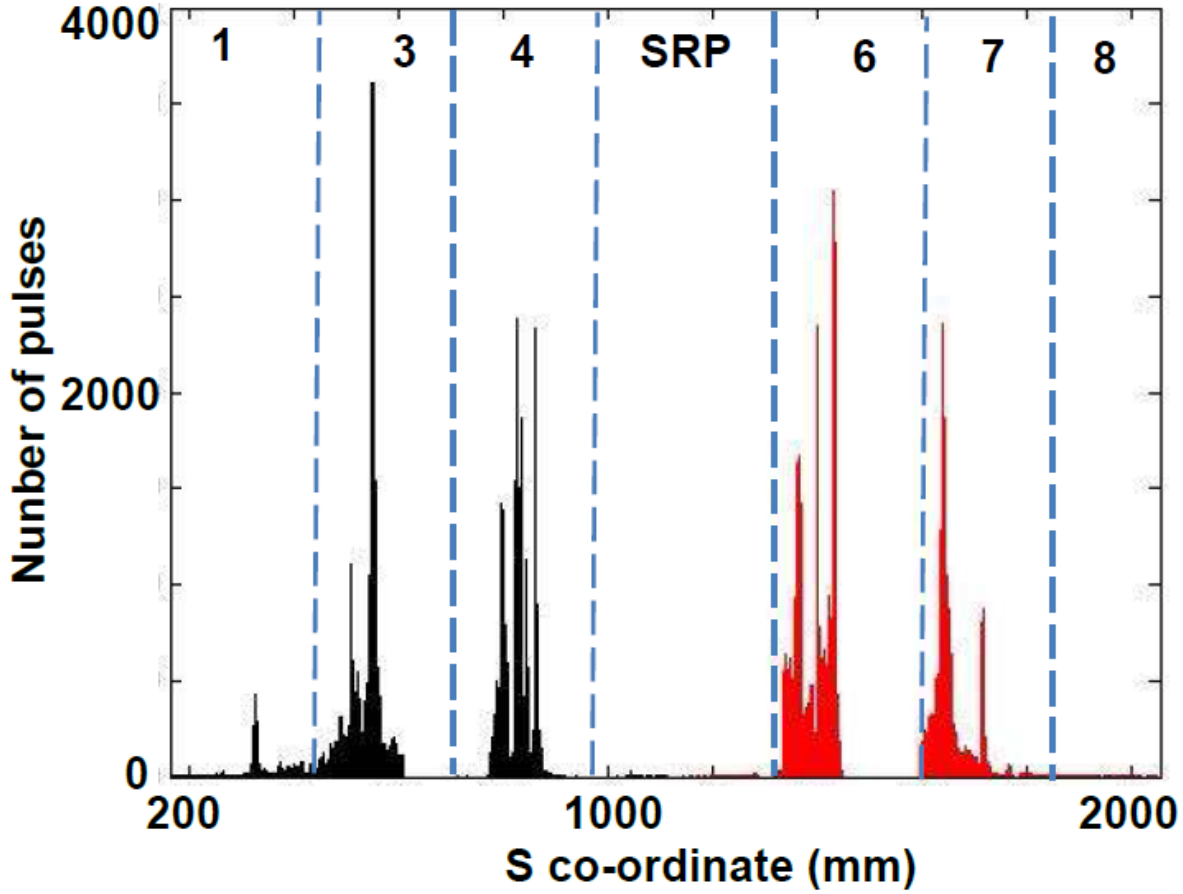

Figure 14: Histogram showing the distribution of strike point positions in the divertor during the MkII-SRP operations 2001-4. The X-axis is the s co-ordinate: the changes from Tiles 1-3-4-5-6-7-8 occur at approximately 0.43, 0.7, 0.95, 1.32, 1.55 and 1.81 m

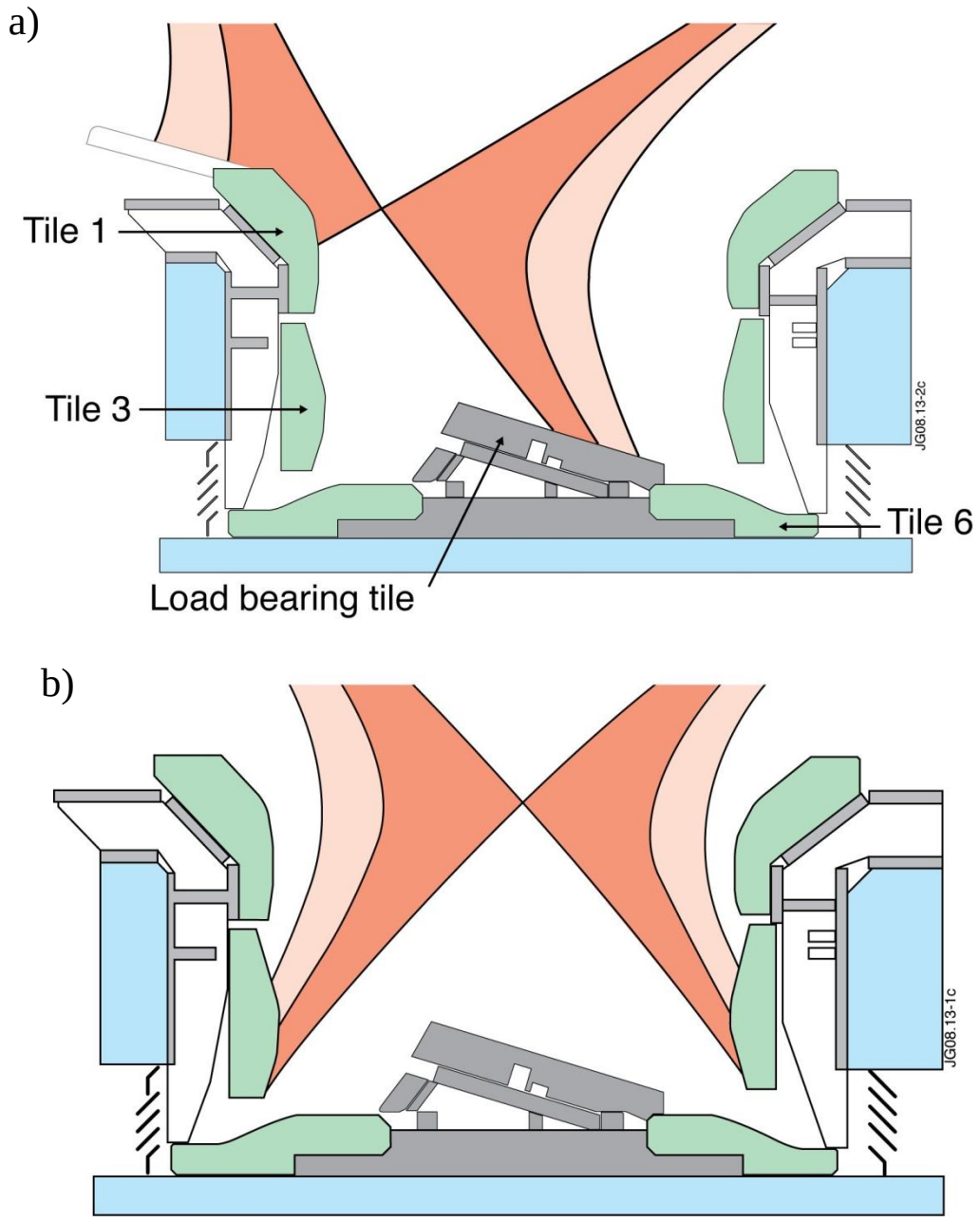

Figure 15: Cross-section of the JET-HD divertor installed in 2004 and used until 2009.
(a) Plasma cross-section for the high-delta configuration with the inner strike-point on Tile 1 and the outer strike-point on the load bearing tile (sometimes referred to as Tile 5).
(b) Other configurations were also used during the 2005-7 campaign with strike-points more symmetrically placed, e.g. as here, on Tiles 3 and 7.

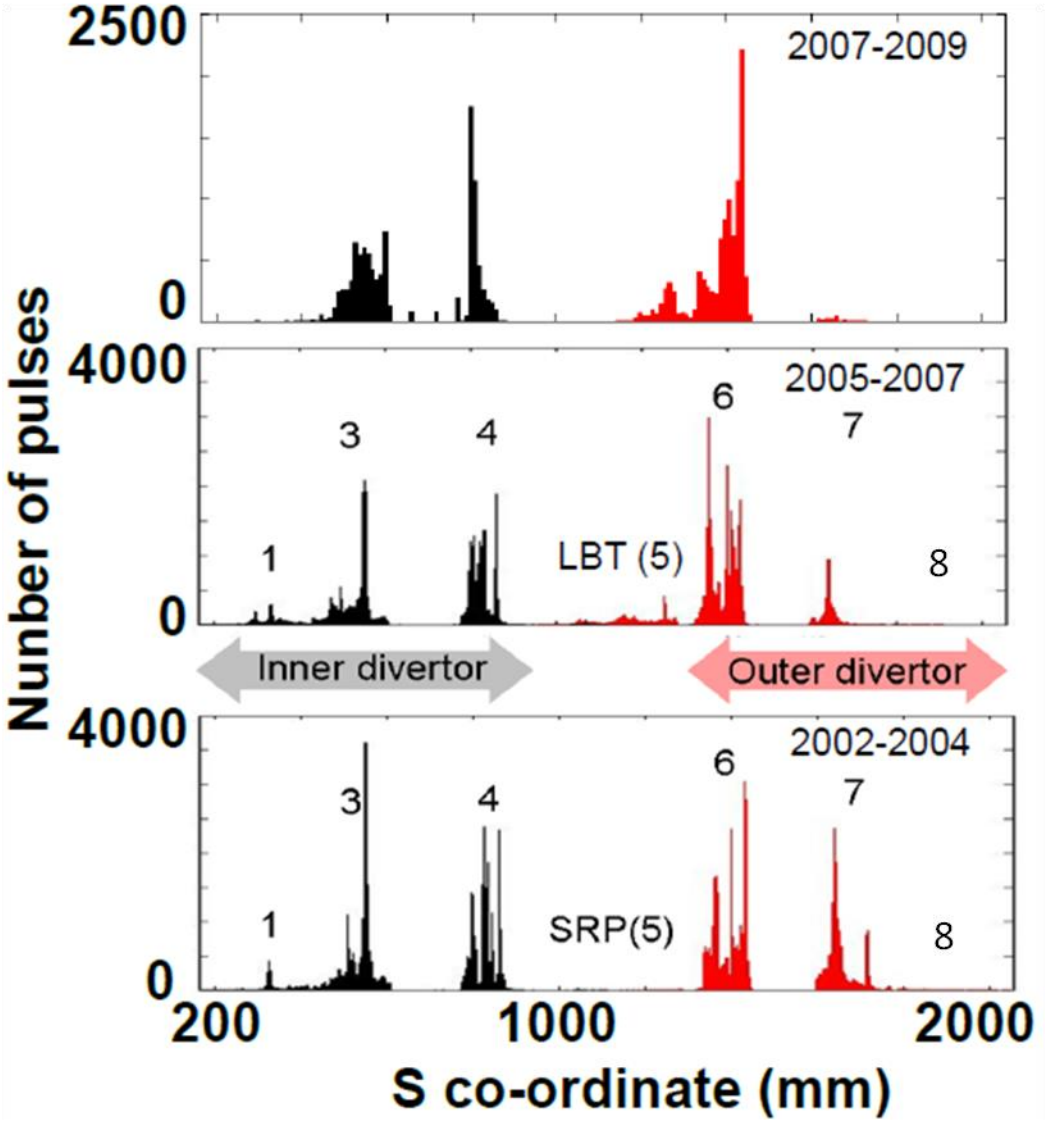

Figure 16: Histogram showing the distribution of strike point positions in the divertor during the MkII-HD operations 2005-7 and 2007-9, and comparison with the MkII-SRP operations 2001-4. The X-axis is the s co-ordinate: the changes from Tiles 1-3-4-5-6-7-8 occur at approximately 0.43, 0.7, 0.95, 1.32, 1.55 and 1.81 m

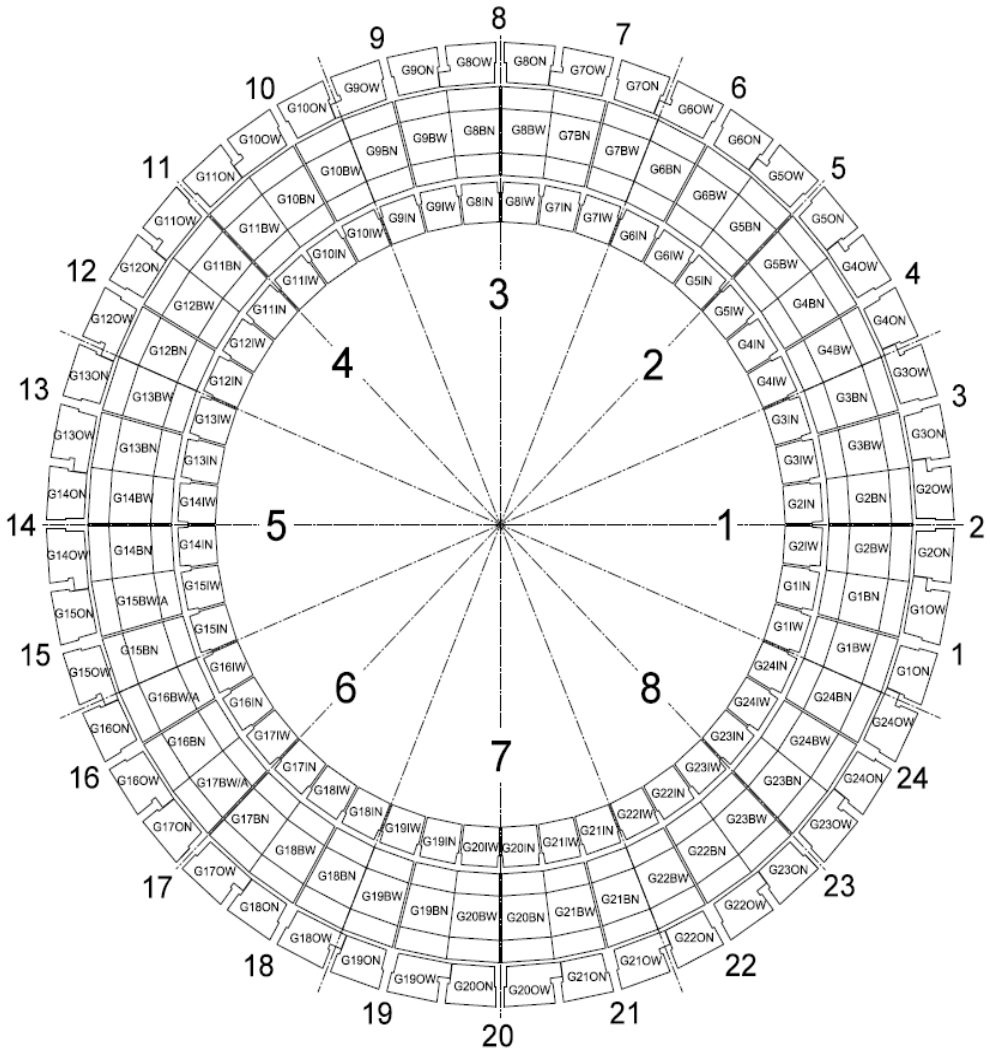

Figure 17: Floor plan of the divertor which consists of 24 modules, numbering anti-clockwise from Octant 1. Each module has Wide and Narrow carriers (the wide carrier has electrical connections), and there are Outer, Base and Inner carriers. So, for example, a tile designated as Tile 2IN G1A is in Module 2, the Inner carrier and is a Tile 1 (one of 4 with labels “A”, “B”, “C” or “D”).

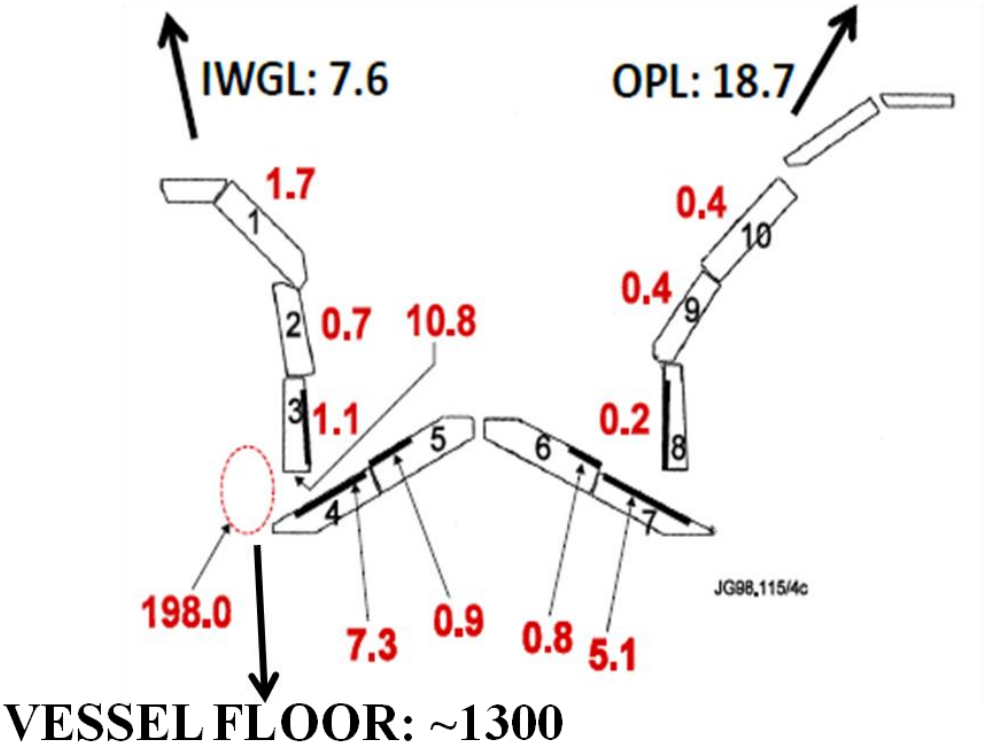

Figure 18: Tritium retention (in TBq) in JET following the DTE1 campaign in 1997

Figure 19: Flakes piled behind a divertor support leg, observed using an endoscope in 1999

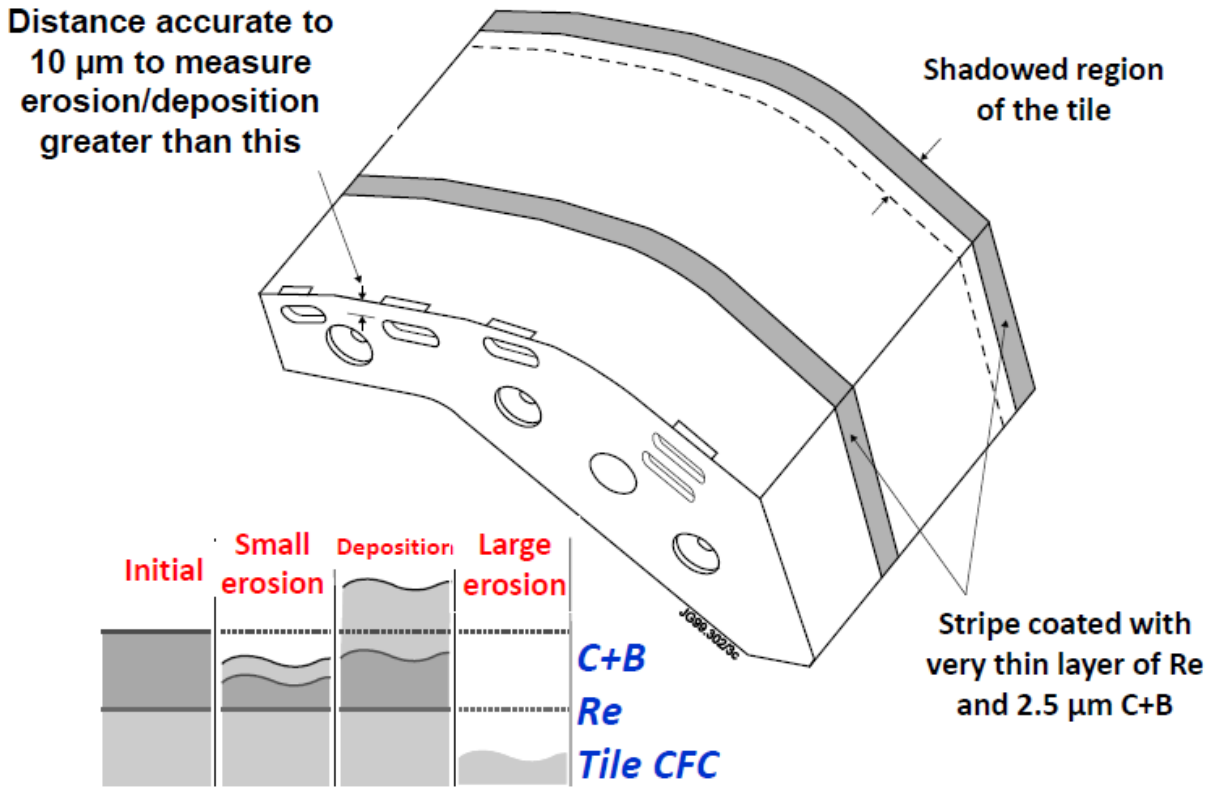

Figure 20: Schematic view of a marker tile, and a diagram showing how the possible erosion/deposition scenarios would affect the markers.

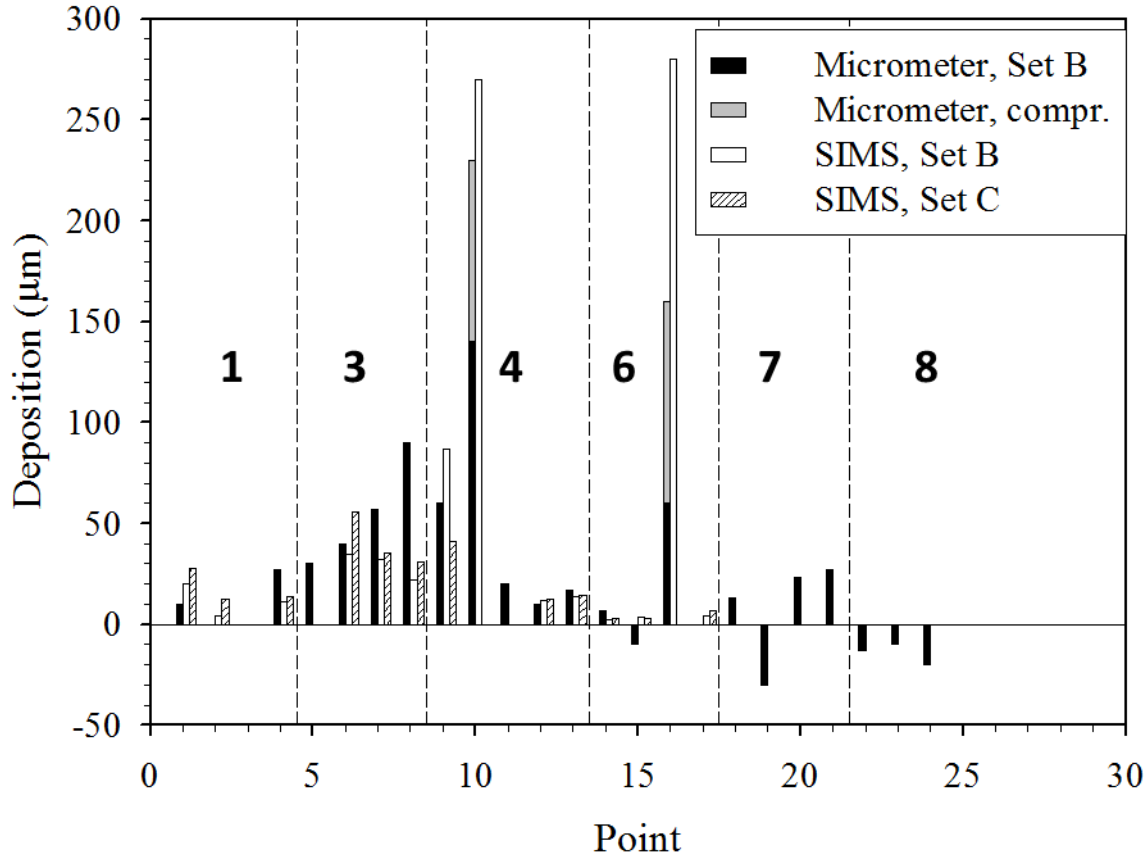

Figure 21: Erosion or deposition on a poloidal set of divertor tiles following exposure from 1999-2001, as derived from micrometer measurements (see also Figure 10): grey shading shows the amount of compression in the micrometer measurements (only occurred at two points). Also included are film thicknesses measured by SIMS. The tile numbers are shown on the figure.

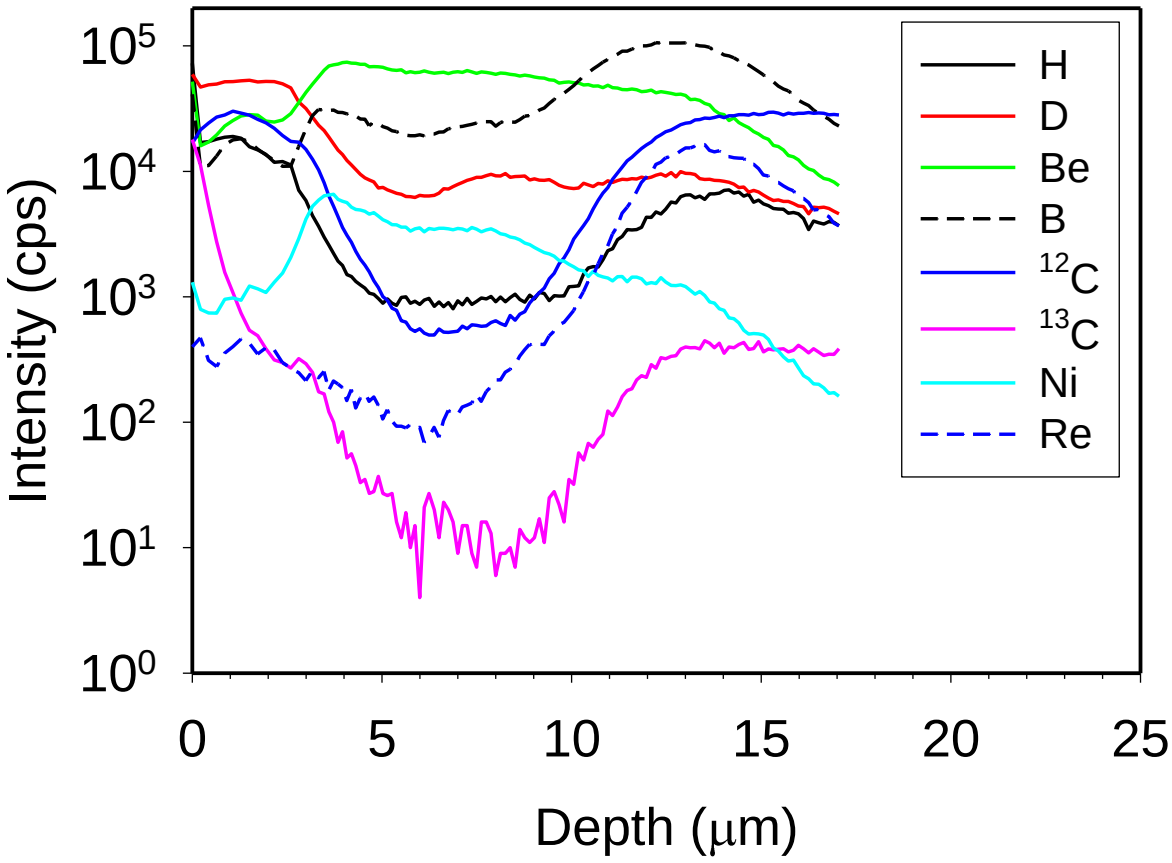

Figure 22: SIMS spectra from a core cut from the bottom of Tile 1 exposed 1998-2001

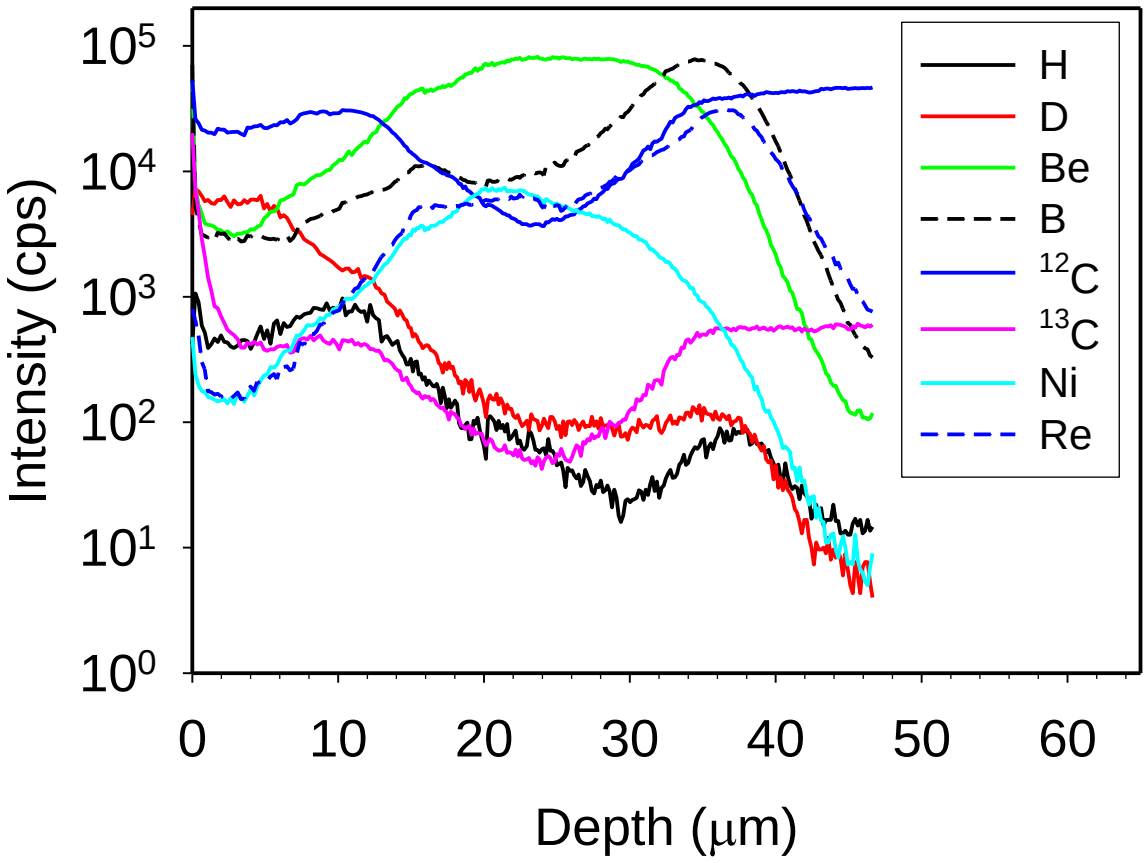

Figure 23: SIMS spectra from a core cut from the middle of Tile 3 exposed 1998-2001

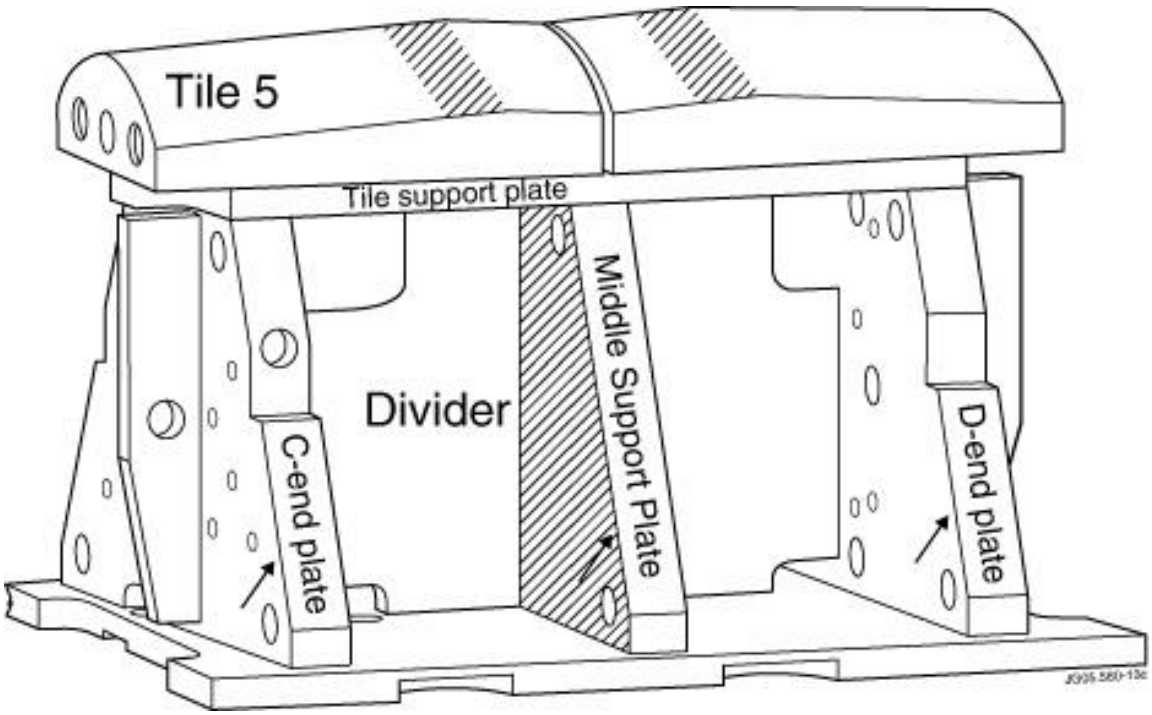

Figure 24: Structure of the Gas Box module viewed from the inner divertor. The location of narrow deposition belts on the support plates is indicated with arrows. Local re-deposition on Tiles 5 is indicated with shading

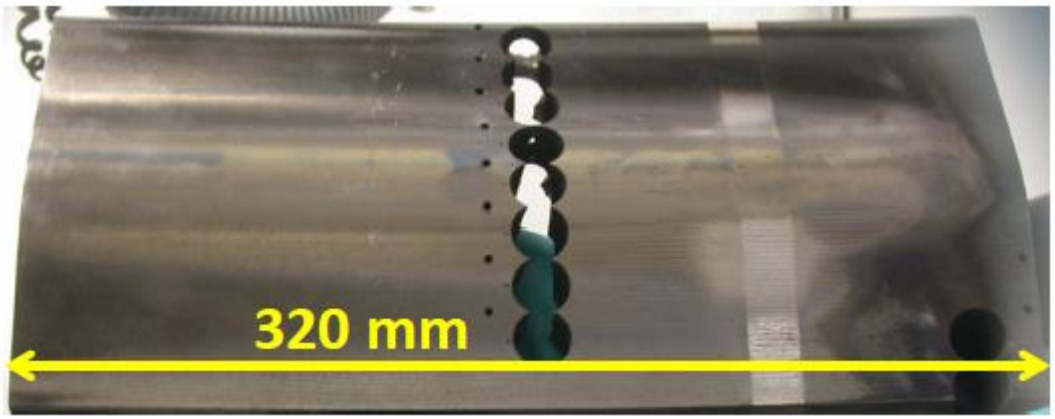

Figure 25: Tile 7 after removal from JET in 2004 and after cutting a poloidal set of samples at VTT

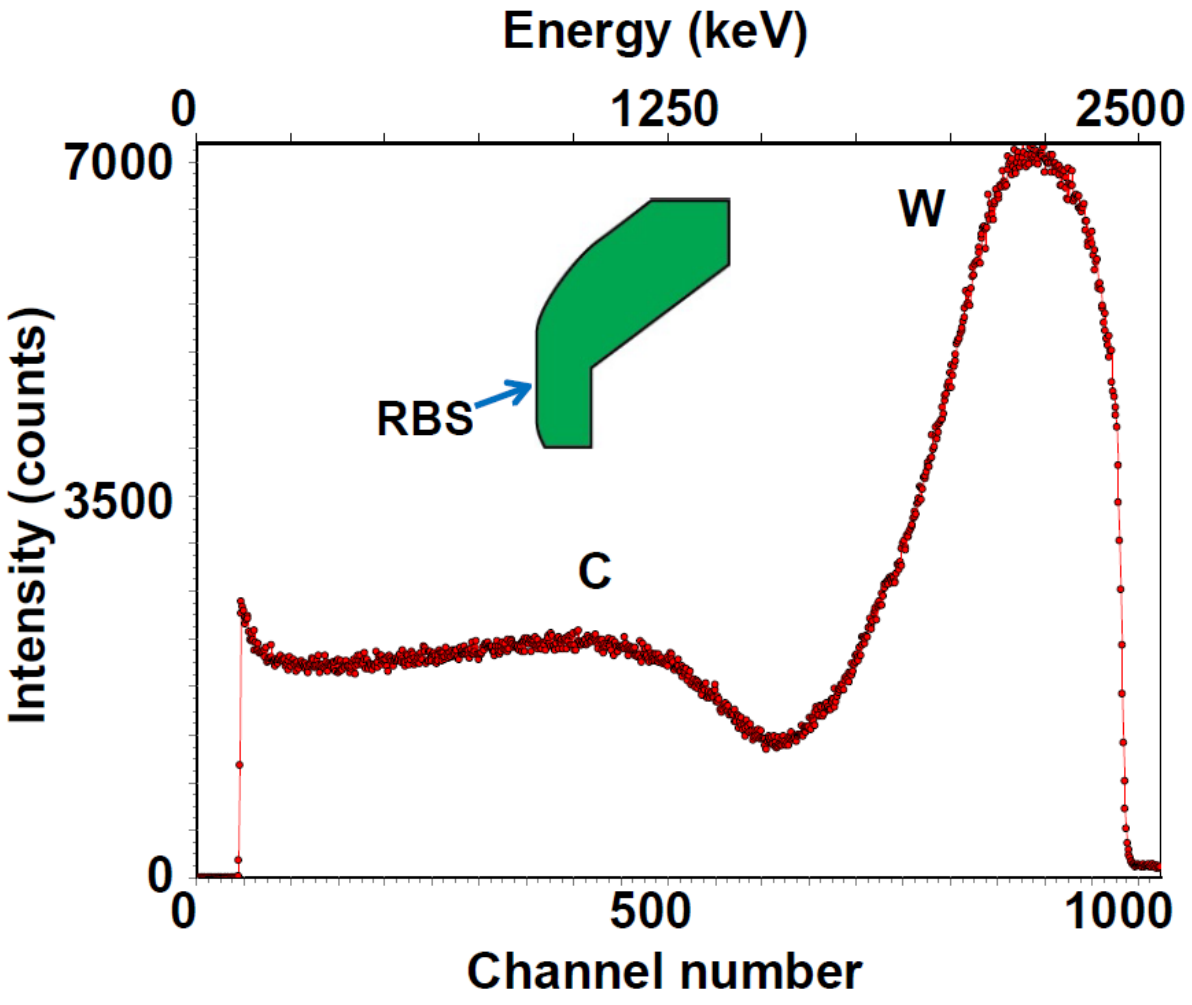

Figure 26: RBS spectrum from the W stripe near the bottom of the front face of Tile 8 exposed in JET 2001-4. The spectrum shows a continuous film of W at the surface, and is similar to the spectrum before exposure in JET.

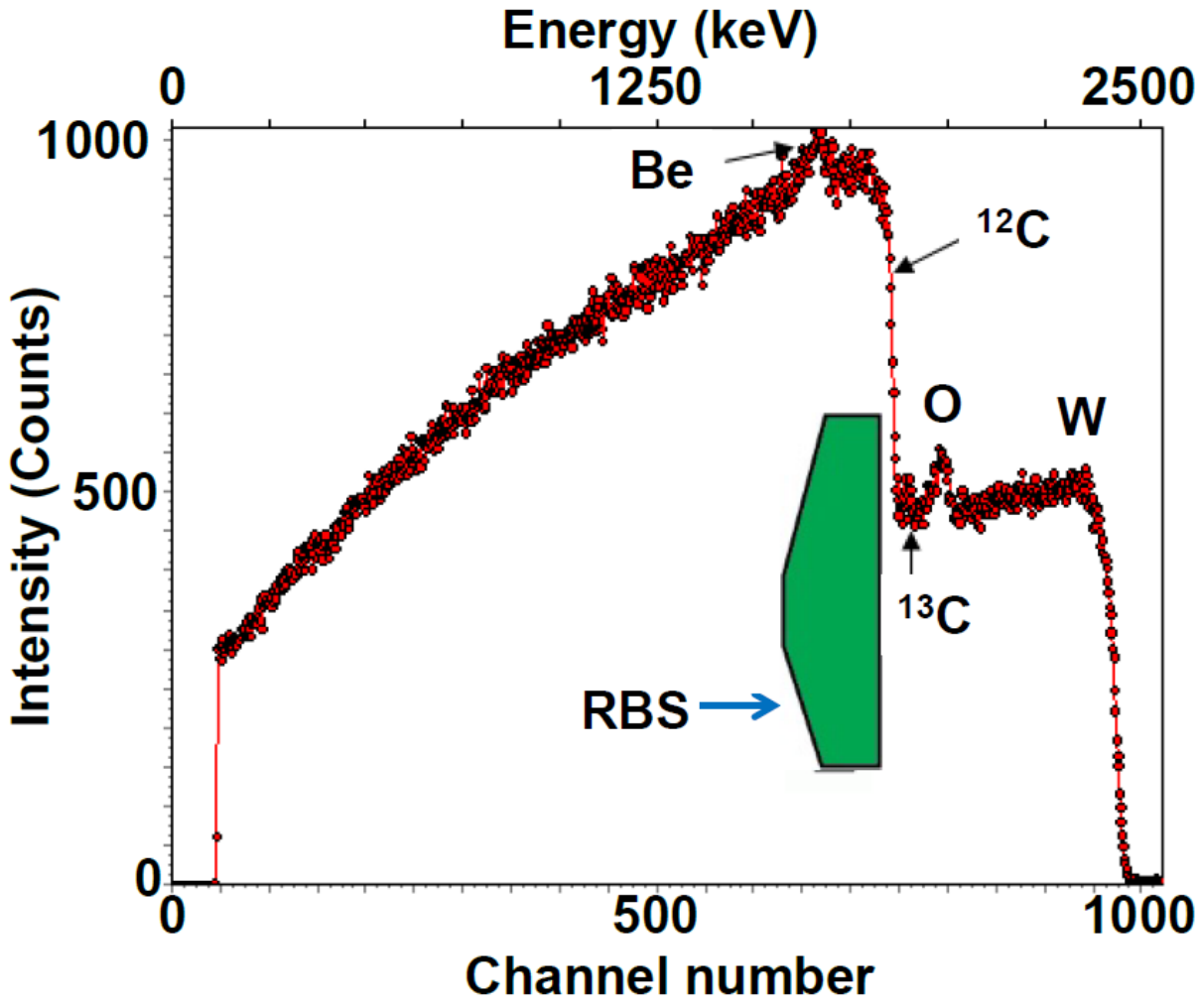

Figure 27: An RBS spectrum from the W stripe about one-third the way up the Tile 7 surface as shown in the sketch, after exposure in JET 2001-4. Edges labelled W and ^{12}C are the high energy edge of the feature characteristic of that element. Small amounts of Be, ^{13}C and O are also present at the surface.

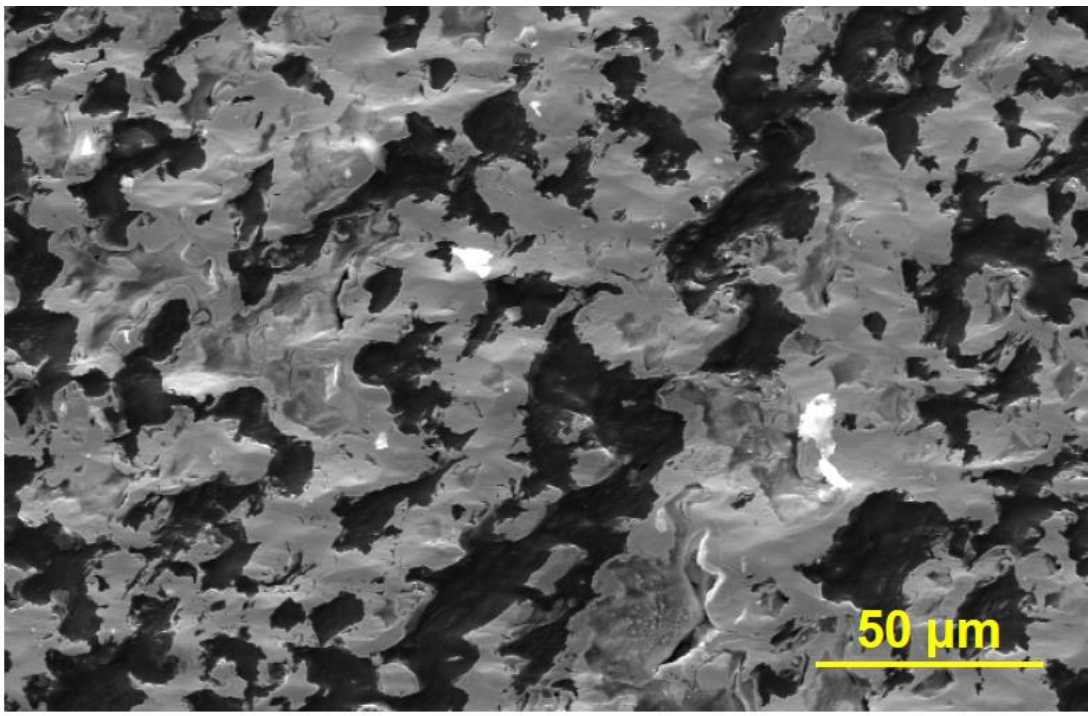

Figure 28: SEM photograph from a strongly eroded area of the W stripe on Tile 8 after exposure in JET 2001-4

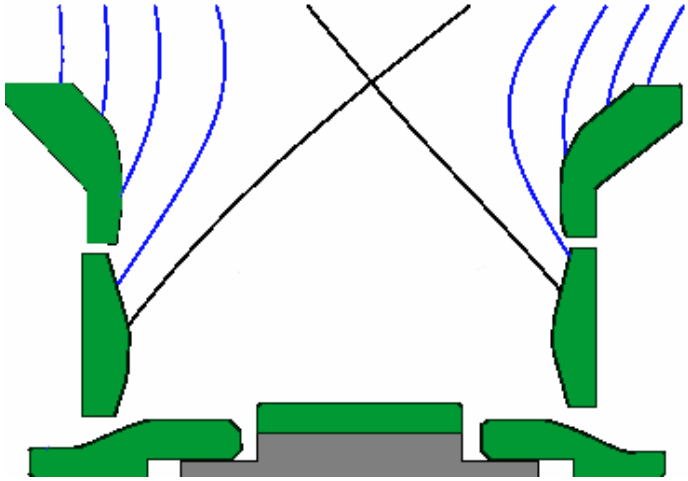

Figure 29: The strike points and field lines for the series of discharges into which the 13C was puffed in 2004.

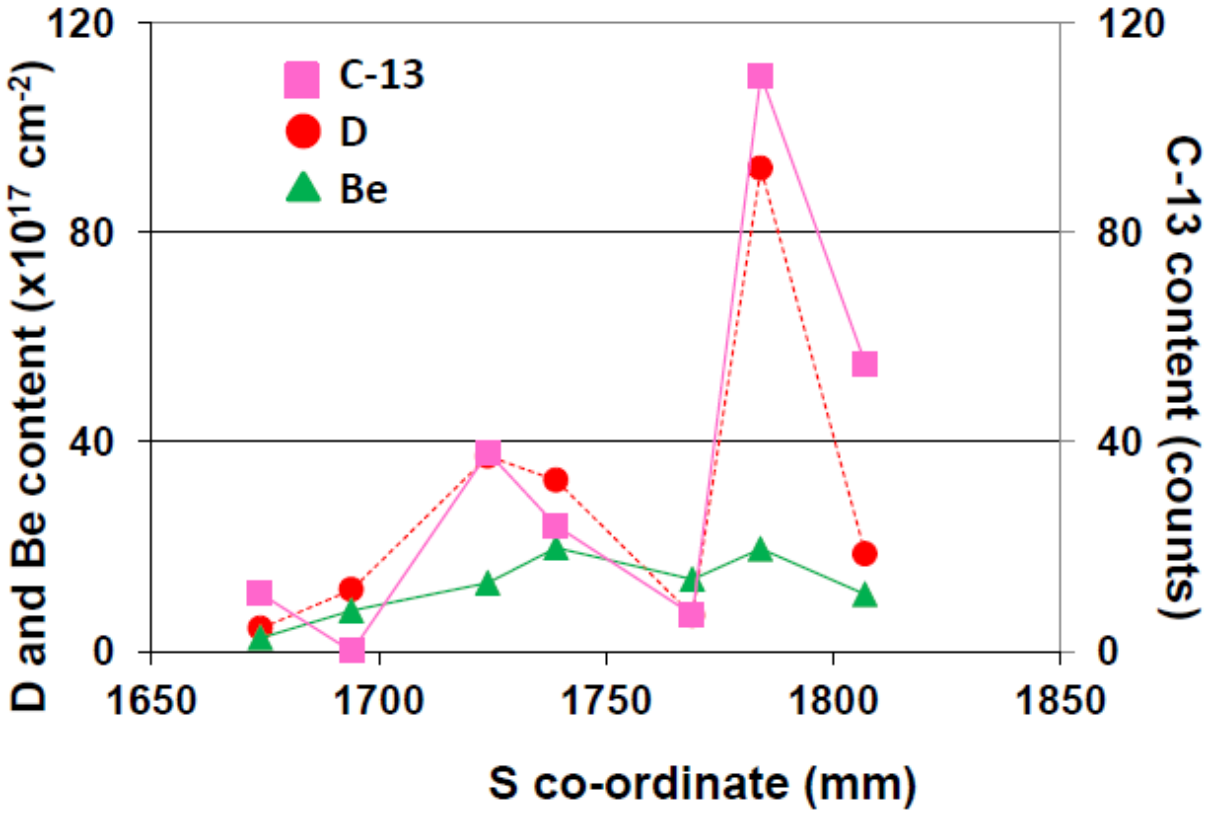

Figure 30: Levels of Be and D, and C^{13} counts, along Tile 7 (from bottom to top) after exposure in JET 2001-4 measured by NRA

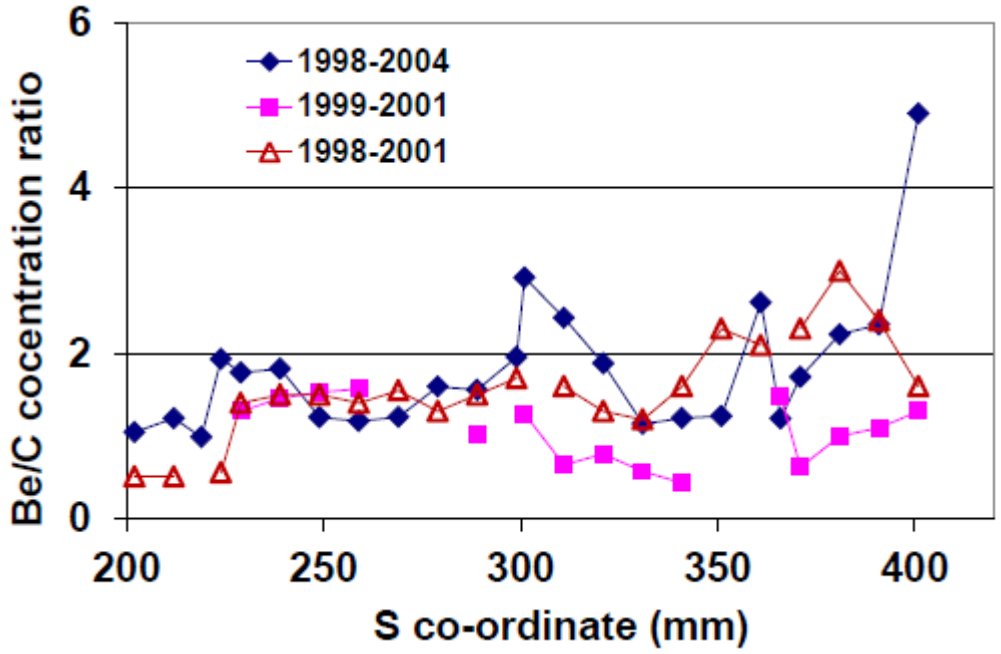

Figure 31: Be/C ratios determined by NRA for Tile 1 - examples from different operational campaigns. The apron is between s-coordinates 162 and 222 mm and the front face of the tile from 222 to 431 mm.

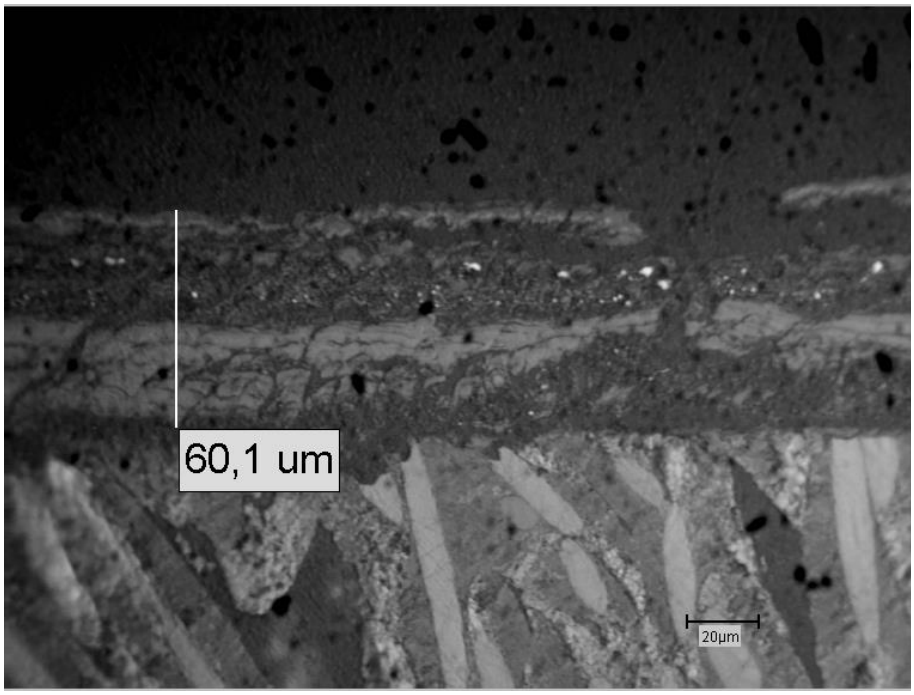

Figure 32: Cross-section of deposit on Tile 3 exposed 2001-4. SIMS analysis shows bands of greater C/Be at the surface and near the centre of the film.

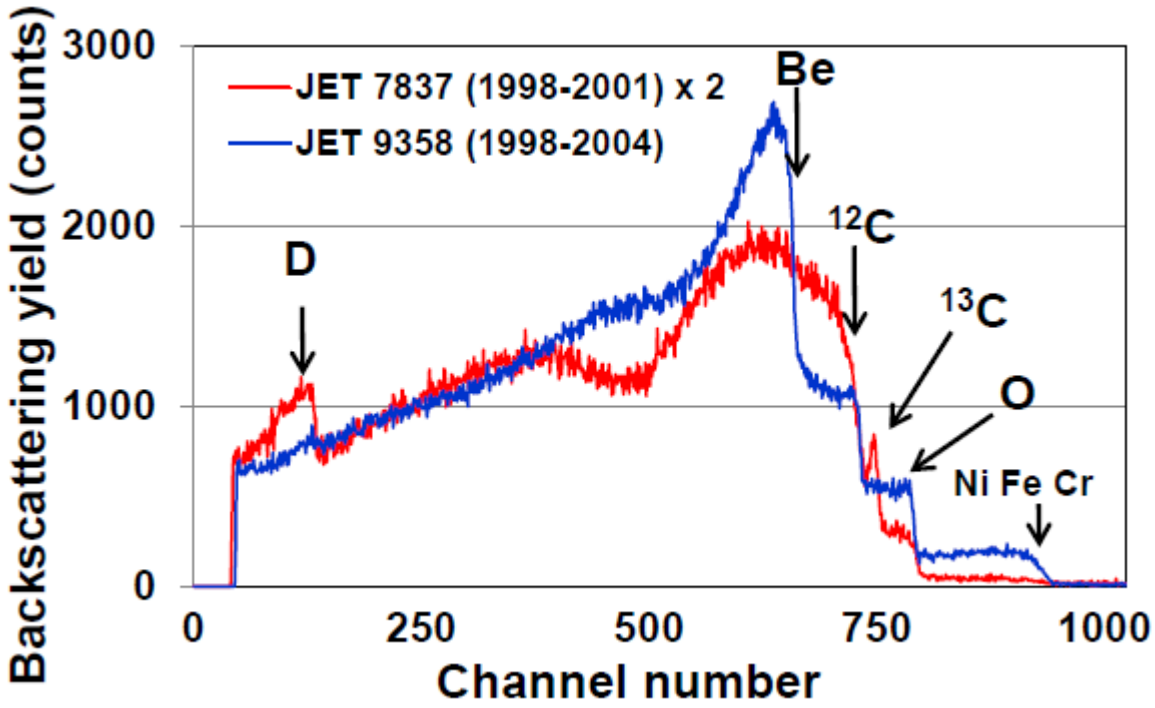

Figure 33: RBS spectra from the upper part of the front face of Tile 3 for tiles removed in 2001 and in 2004. The arrows indicate the high energy edge of the feature characteristic of that element.

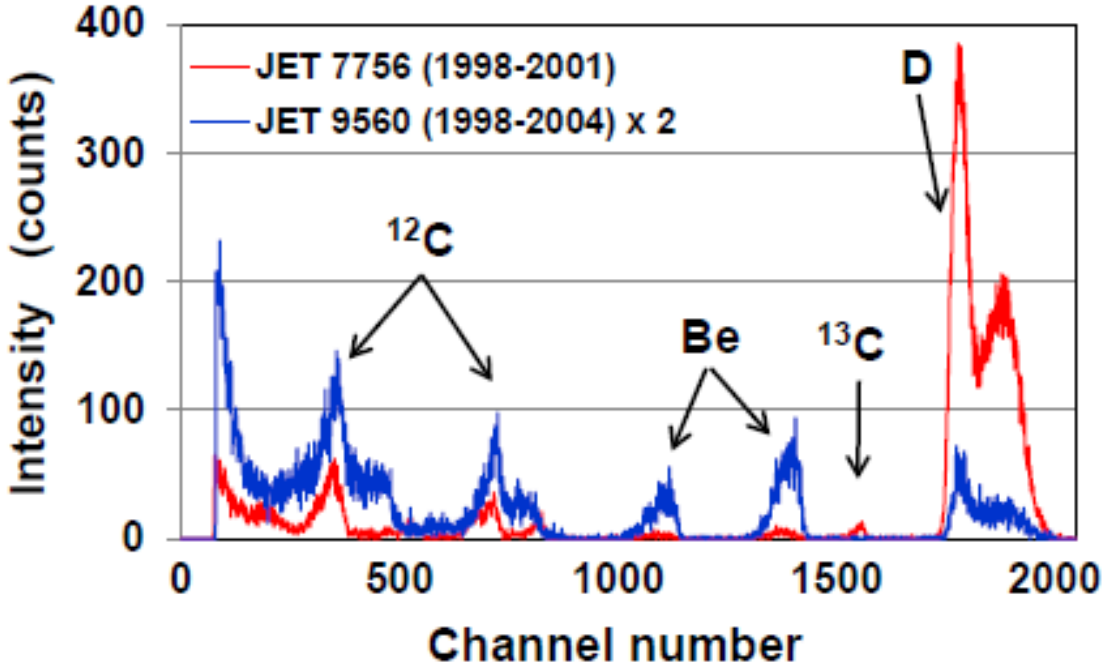

Figure 34: NRA spectra from the upper part of the front face of tile 3 for tiles removed in 2001 and in 2004, with peaks characteristic of each element indicated.

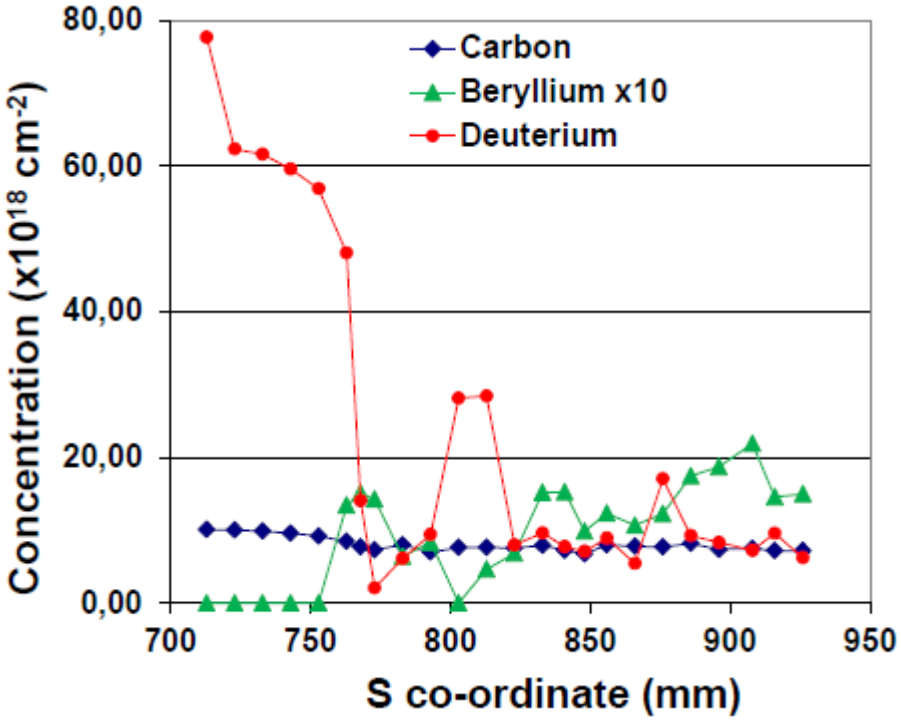

Figure 35: C, Be and D concentrations derived from NRA measurements on Tile 3BW G4B (Tile 4), plotted inboard to outboard

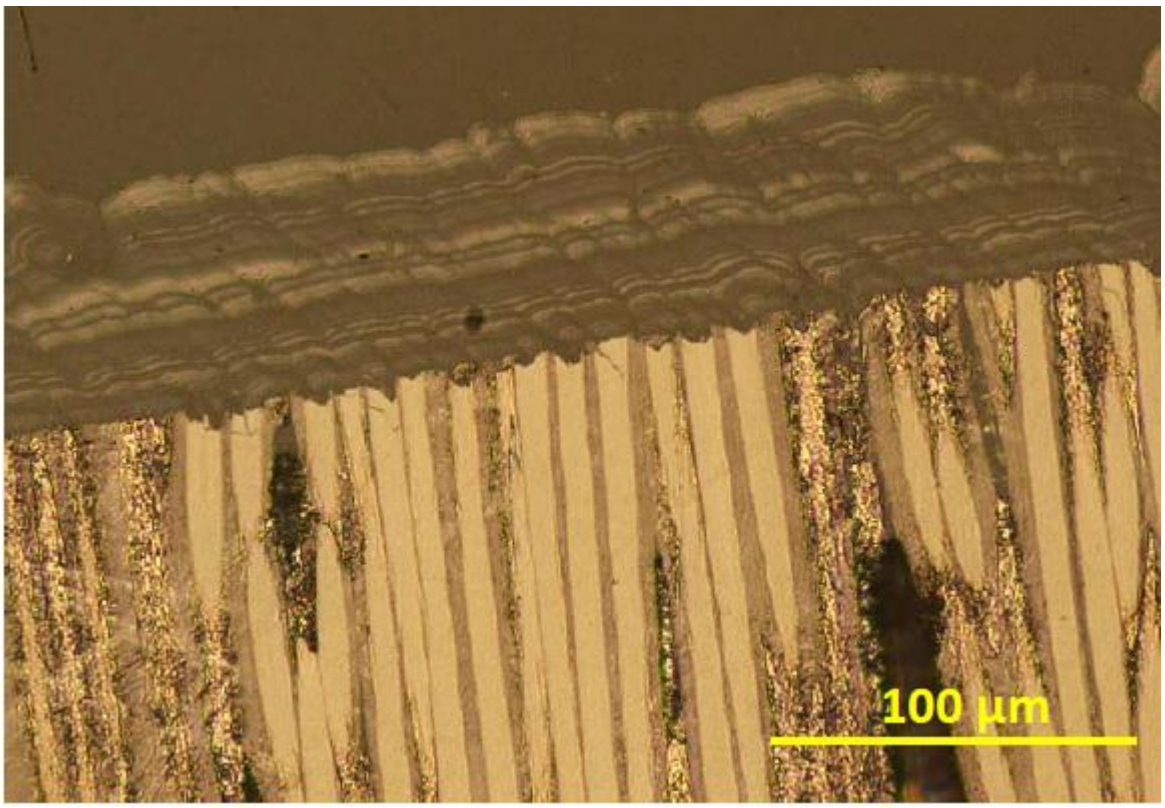

Figure 36: Section from shadowed region of Tile 4 exposed 2001-4

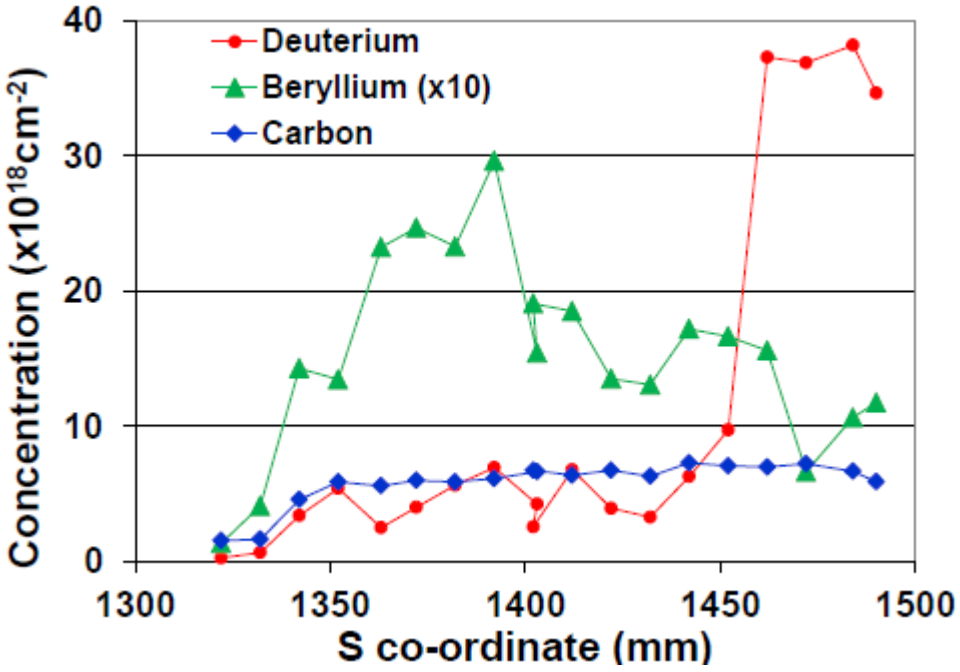

Figure 37: C, Be and D concentrations across Tile 14BN G6B (Tile 6) exposed 2001-4, plotted inboard to outboard.

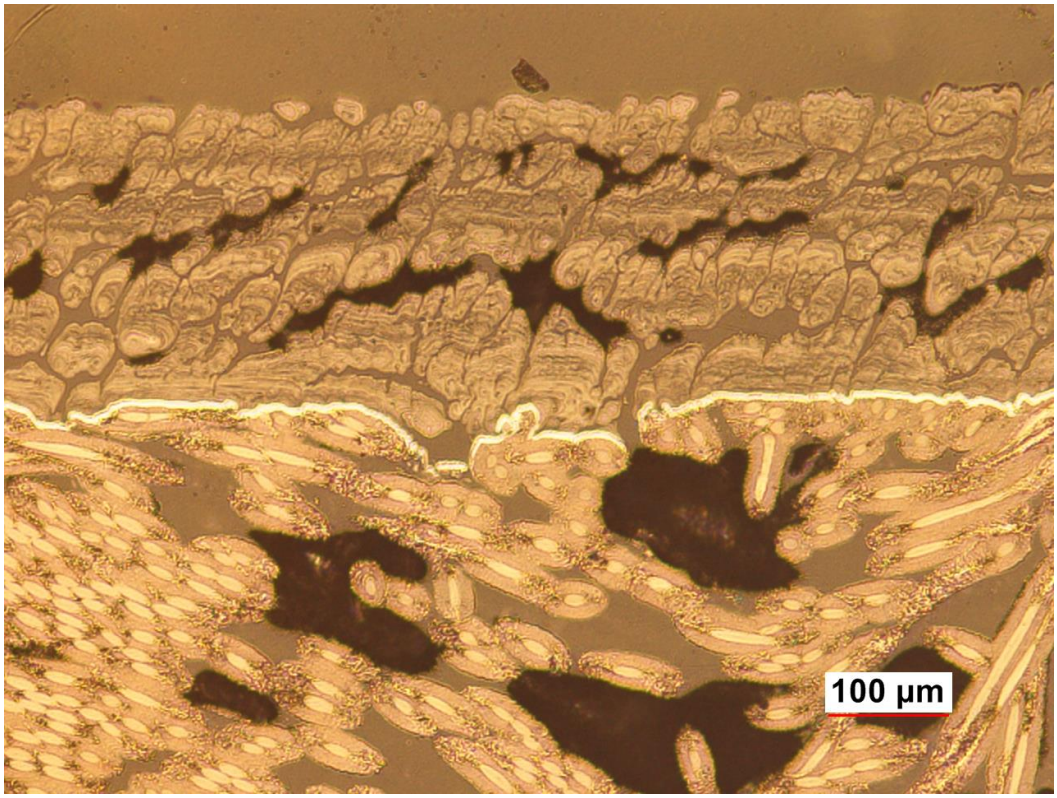

Figure 38: Section from sloping part of Tile 6 exposed 2001-4. Note the bright band between the deposit and the tile surface, which is the W marker layer coated onto the tile before exposure.

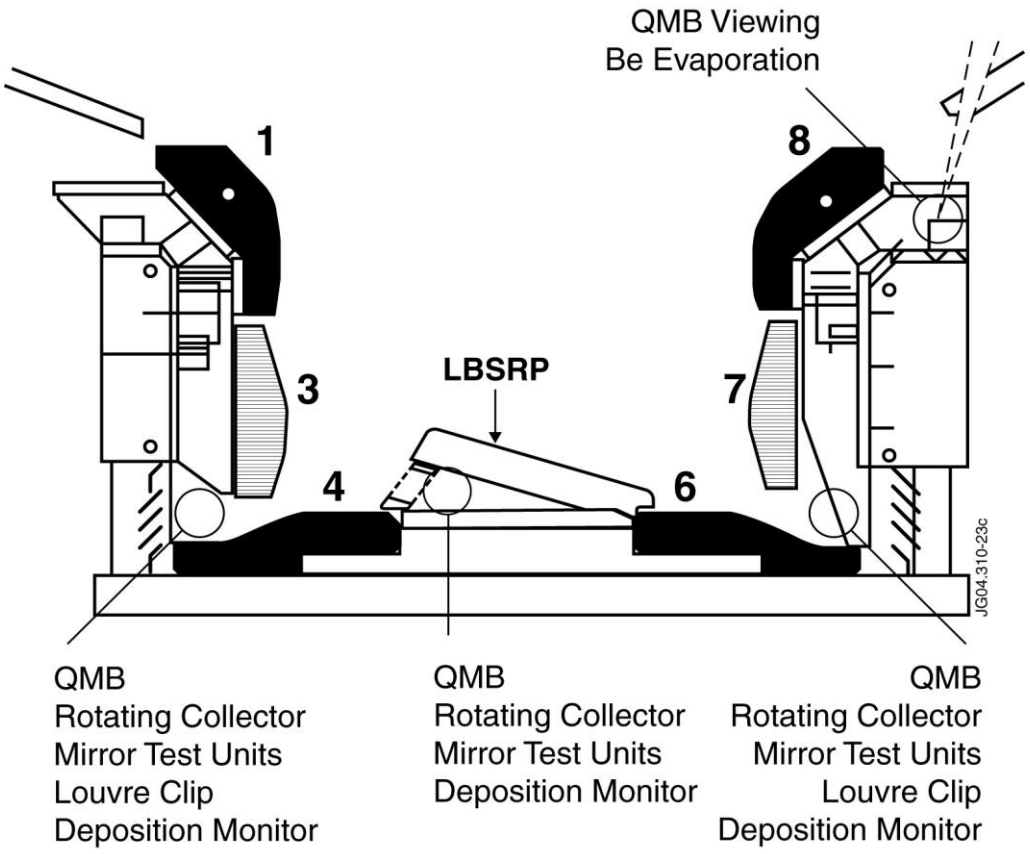

Figure 39: Cross-section of the JET MkII-HD divertor showing the positions of tritium retention diagnostics during the 2005-7 operational period.

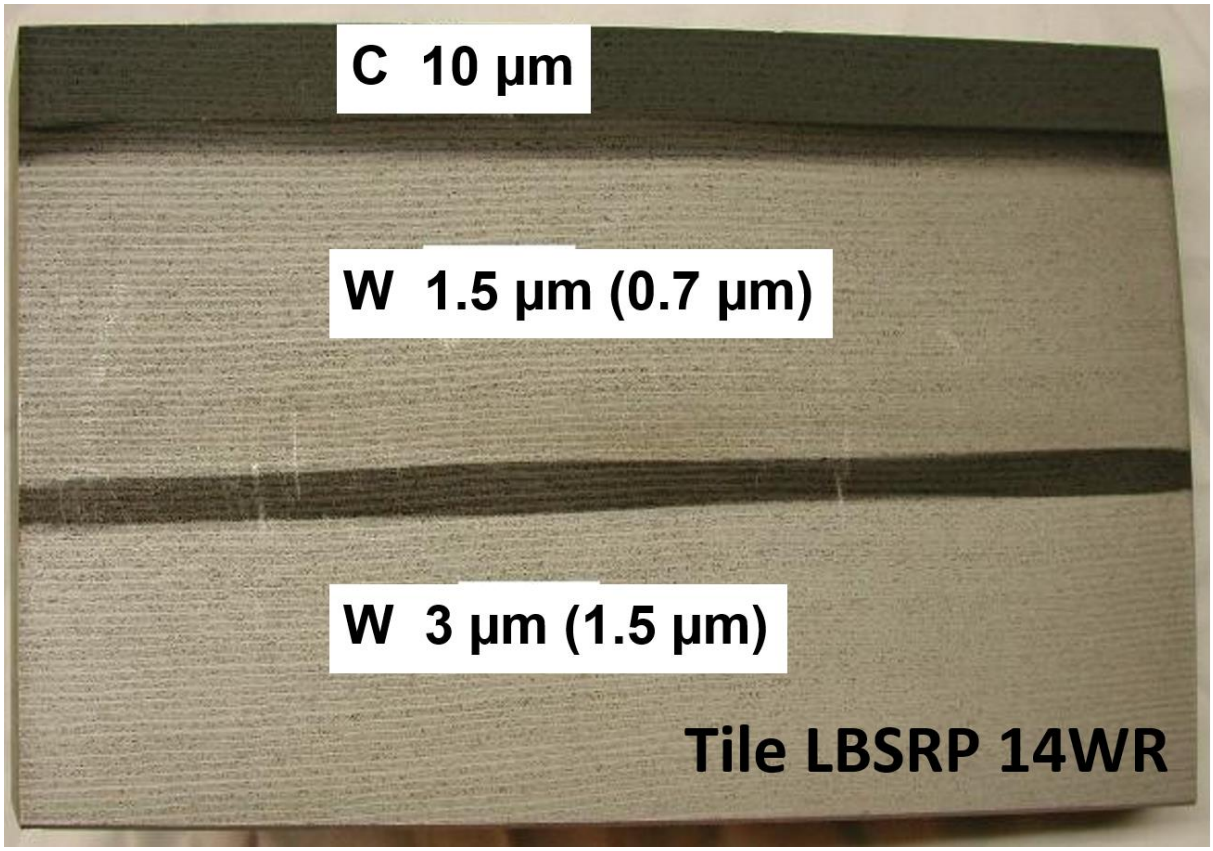

Figure 40: The proposed coating scheme for tile LBSRP 14WR - two thicknesses of W (3 and 1.5 µm) and a 10 µm thick stripe of C (on a W interlayer), before mounting in JET in 2004. However, in brackets are the actual W film thicknesses found during subsequent analysis (0.7 and 1.3 µm) - the C stripe did not survive plasma operations.

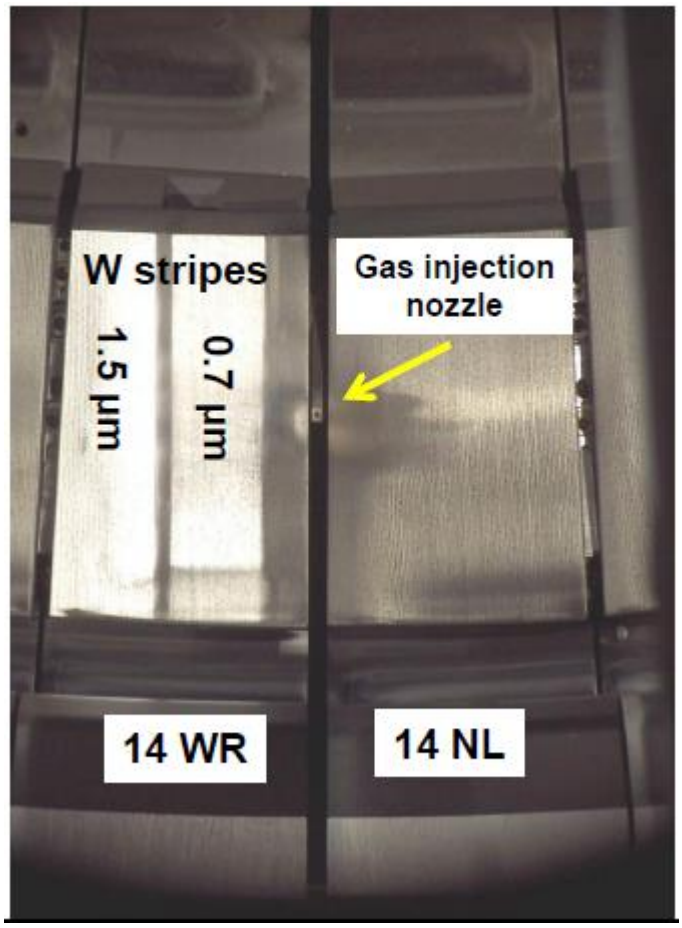

Figure 41: View of the LBSRP Tiles 14WR and 14NL from the Octant 5 UMVP at the end of the 2005-7 operations. The W-coated stripes can be clearly seen on Tile 14WR. The deposition patterns can also be seen from the methane injected from the gas injection nozzle (the nozzle is visible between the two tiles).

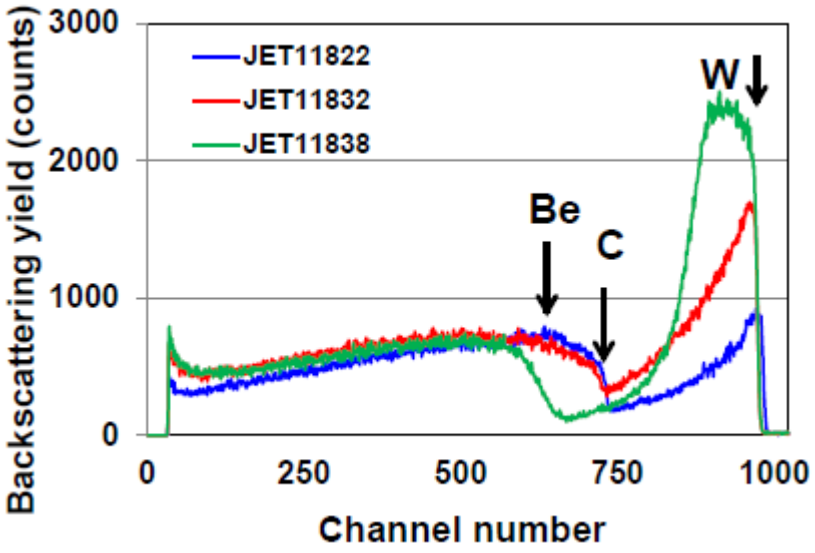

Figure 42: RBS spectra from the centre (poloidally) of the W-coated stripes on LBSRP Tile 14WR (a) on the thinner coating (JET11822), (b) on the plasma-exposed part of the thicker coating (JET11832), (c) on the shadowed part of the thicker coating JET11838). The arrows indicate the high energy edge of the feature characteristic of that element.

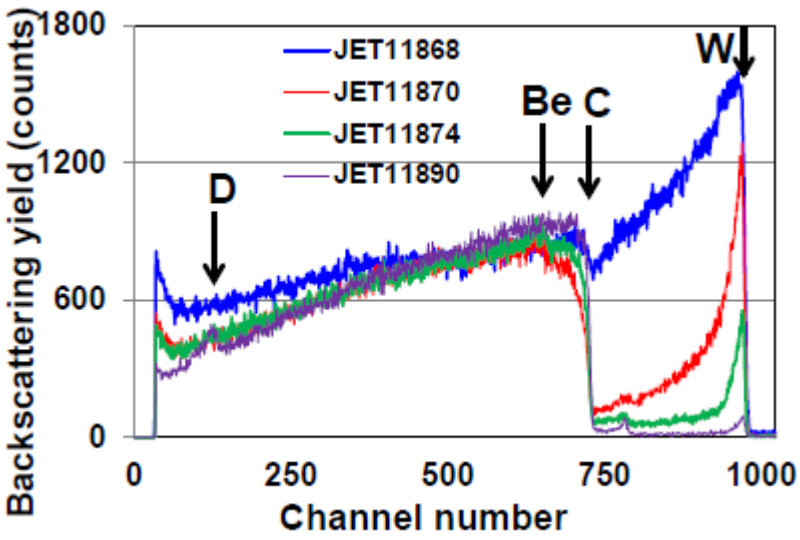

Figure 43: RBS spectra from the thicker W stripe (JET11868), in the gap between stripes (JET11870 and 11874), and downstream from both stripes (JET11890). The arrows indicate the high energy edge of the feature characteristic of that element.

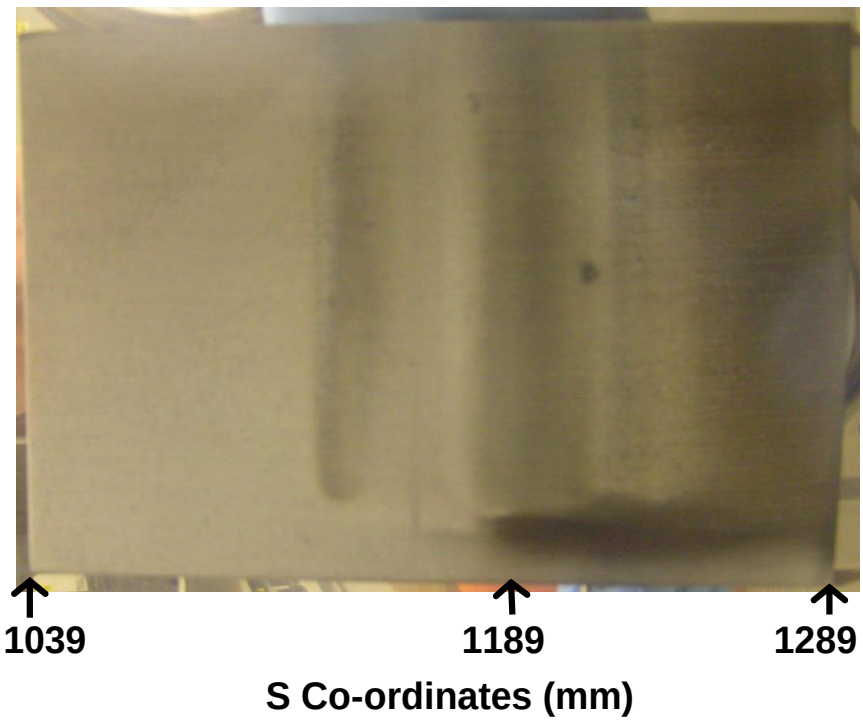

Figure 44: A photograph of the W-coated load-bearing tile after exposure 2007-9. The s co-ordinates indicate the inboard and outboard edges of the tile (1039 and 1289mm), and the area of maximum ^{12}C and ^{13}C (1189mm) for the puffing experiments on the last day of operations in 2009: the strike point was at ~1170mm during the inter-ELM periods.

Figure 45: View of part of the apron of a Tile 1 (right-hand side) and the upper front face of the tile (towards the left-hand side) during the 2007 JET shutdown inspection, showing spalling deposits. The tile had been exposed 1998-2007.

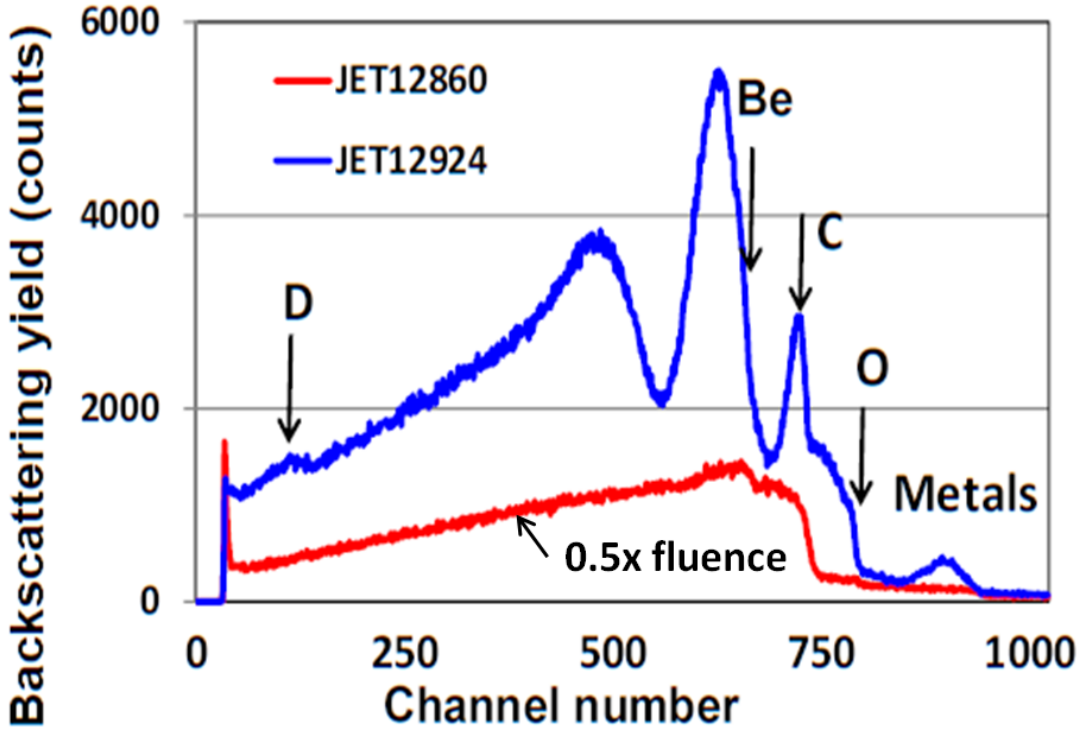

Figure 46: RBS spectra from the lower part of the front face (JET12924) and from the apron (JET12860, recorded for only half the beam fluence of JET12924 for clarity) of Tile 2IWG1A exposed 2005-7. The arrows indicate the high energy edge of the feature characteristic of that element.

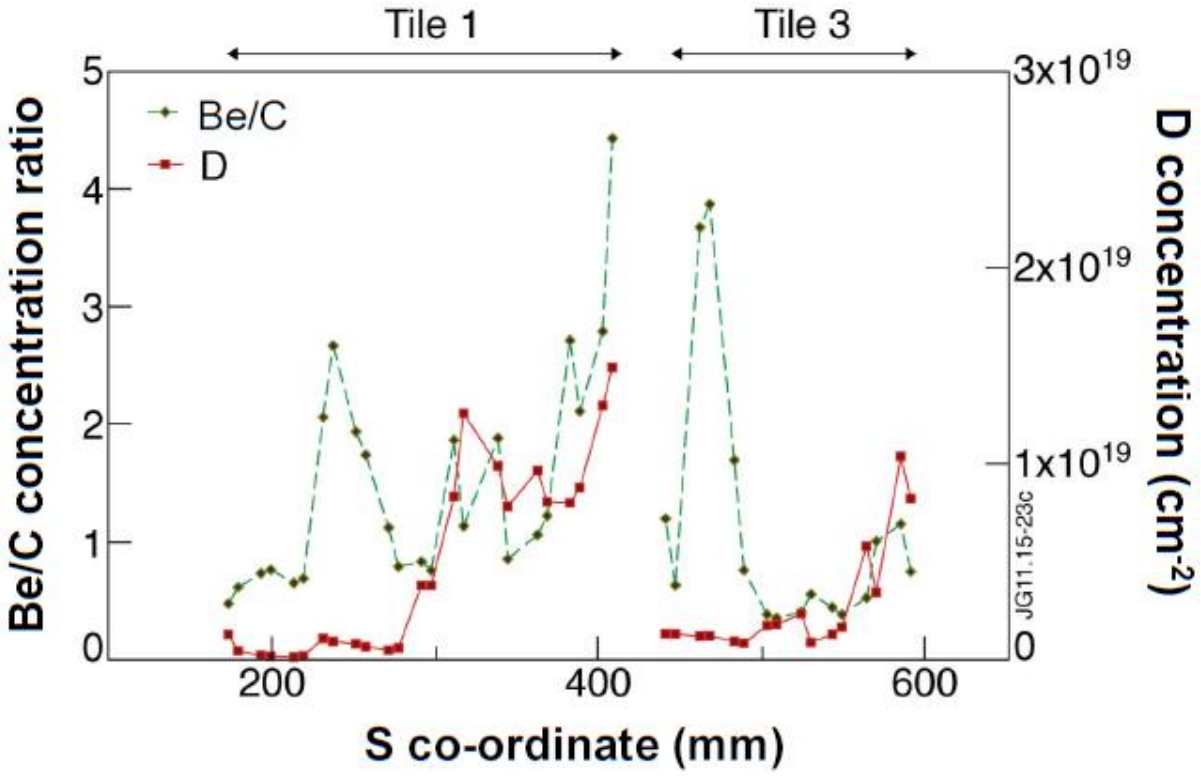

Figure 47: The ratio of Be/C and the D in the surface layer on Tiles 1 and 3 exposed 2007-9 from NRA data.

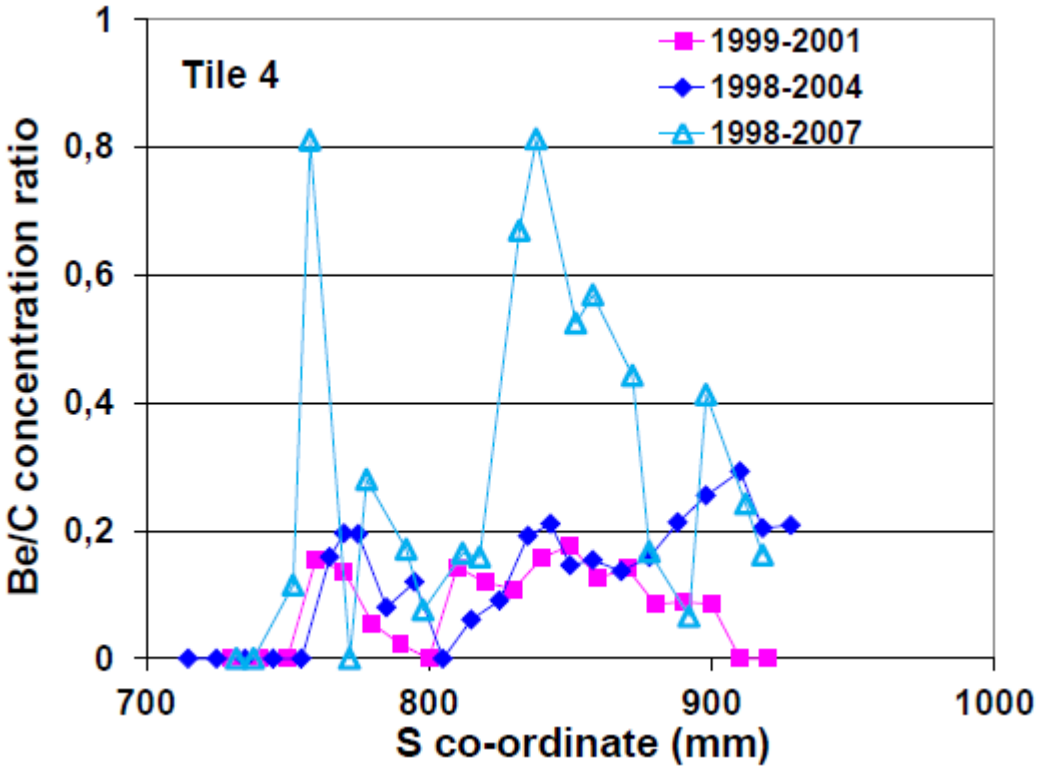

Figure 48: Comparison of Be/C ratios on Tile 4 for tiles removed after the last three JET campaigns (1999-2001 – Mk II Gas Box, 2001-4 – MkII SRP, 2005-7 – MkII HD divertors)

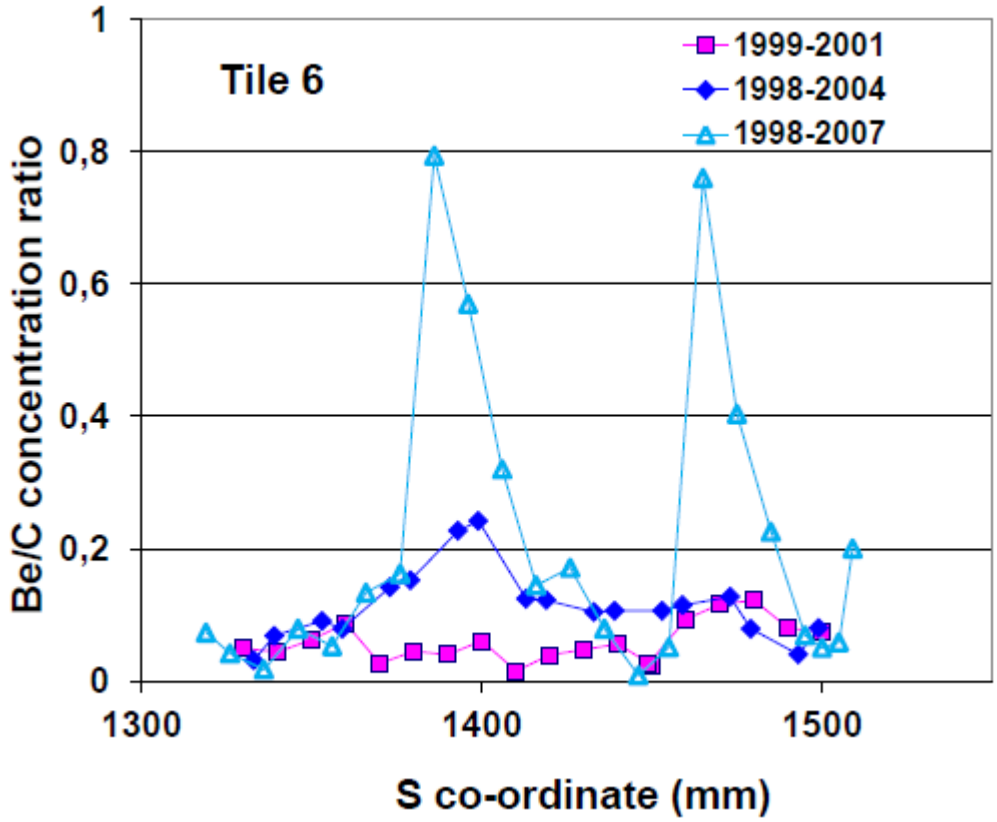

Figure 49: Comparison of Be/C ratios on Tile 6 for tiles removed after the last three JET campaigns (1999-2001 – Mk II Gas Box, 2001-4 – MkII SRP, 2004-7 – MkII HD divertors)

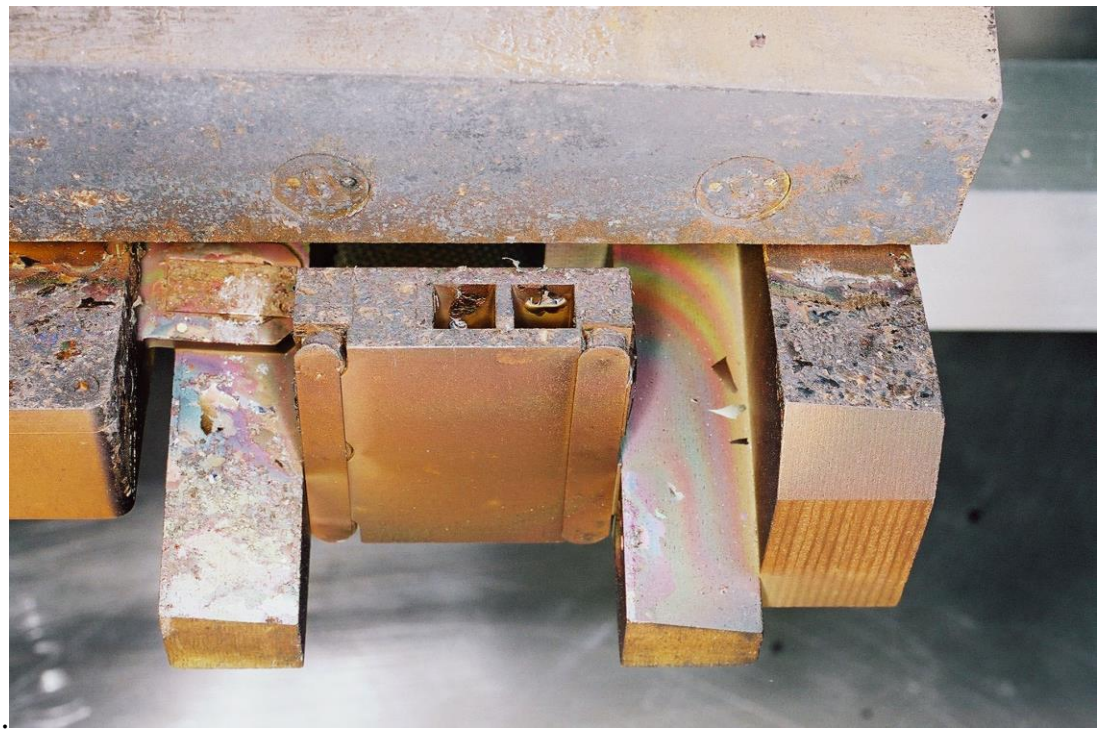

Figure 50: Photograph of the inner carrier 2IN after removal in 2007. The bottom of Tile 3 is at the top of the picture. Surfaces are covered with a thick deposit, which is showing signs of spalling in certain places. The front face of the mirror test unit is so thickly coated that it is not possible to see where the third channel (with a sample flush to the face) is.

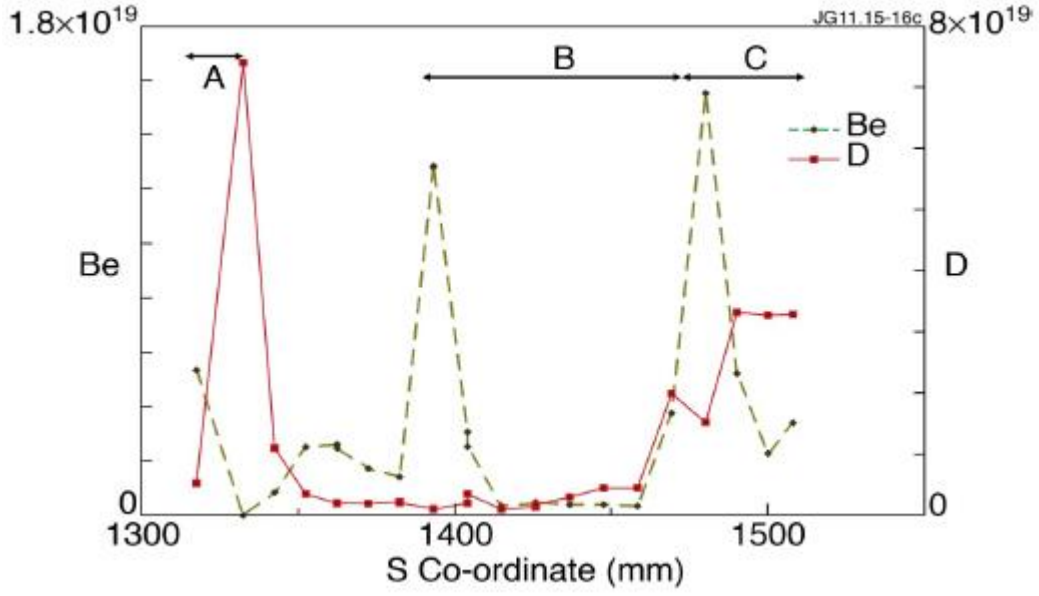

Figure 51: NRA concentrations of D and Be across Tile 6 (exposed 1998-2009). Region A is shadowed by the LBT, region B is the sloping part of the tile, and C is the region shadowed by Tile 7.

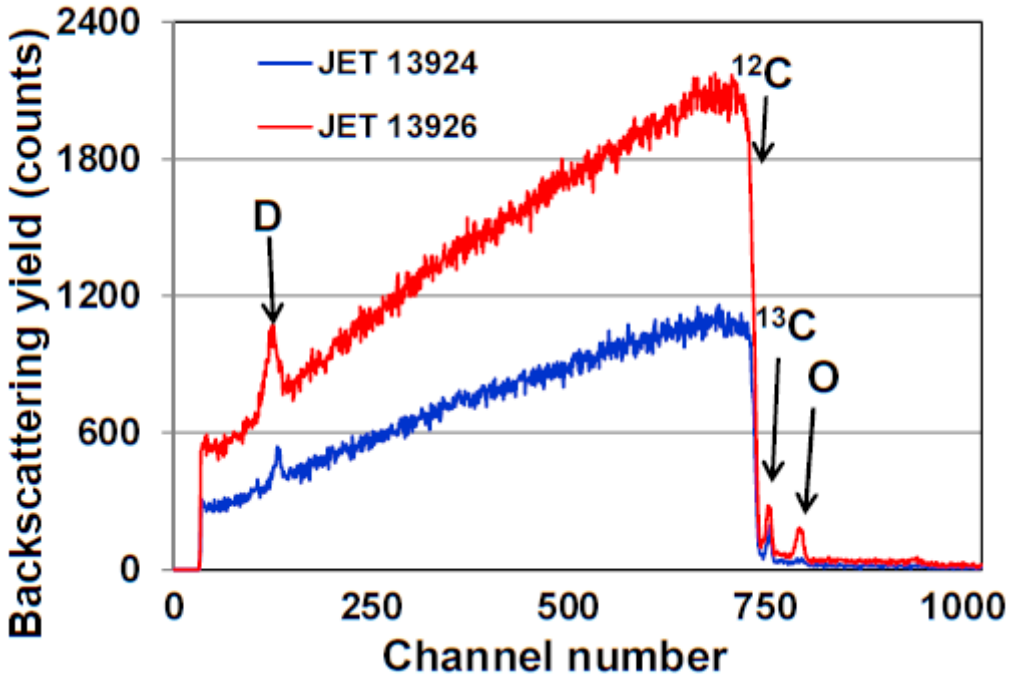

Figure 52: Rutherford Backscattering spectra from a divertor Tile 7 (2ON G7A, exposed 2005-7). The spectra were recorded from samples 10 mm below (spectrum 13926) and 10 mm above (spectrum 13924, recorded for only half the beam fluence of 13926 for clarity) the middle of the tile. The ^{12}C arrow indicates the high energy edge of the carbon feature – the D, ^{13}C and O are present at the surface.

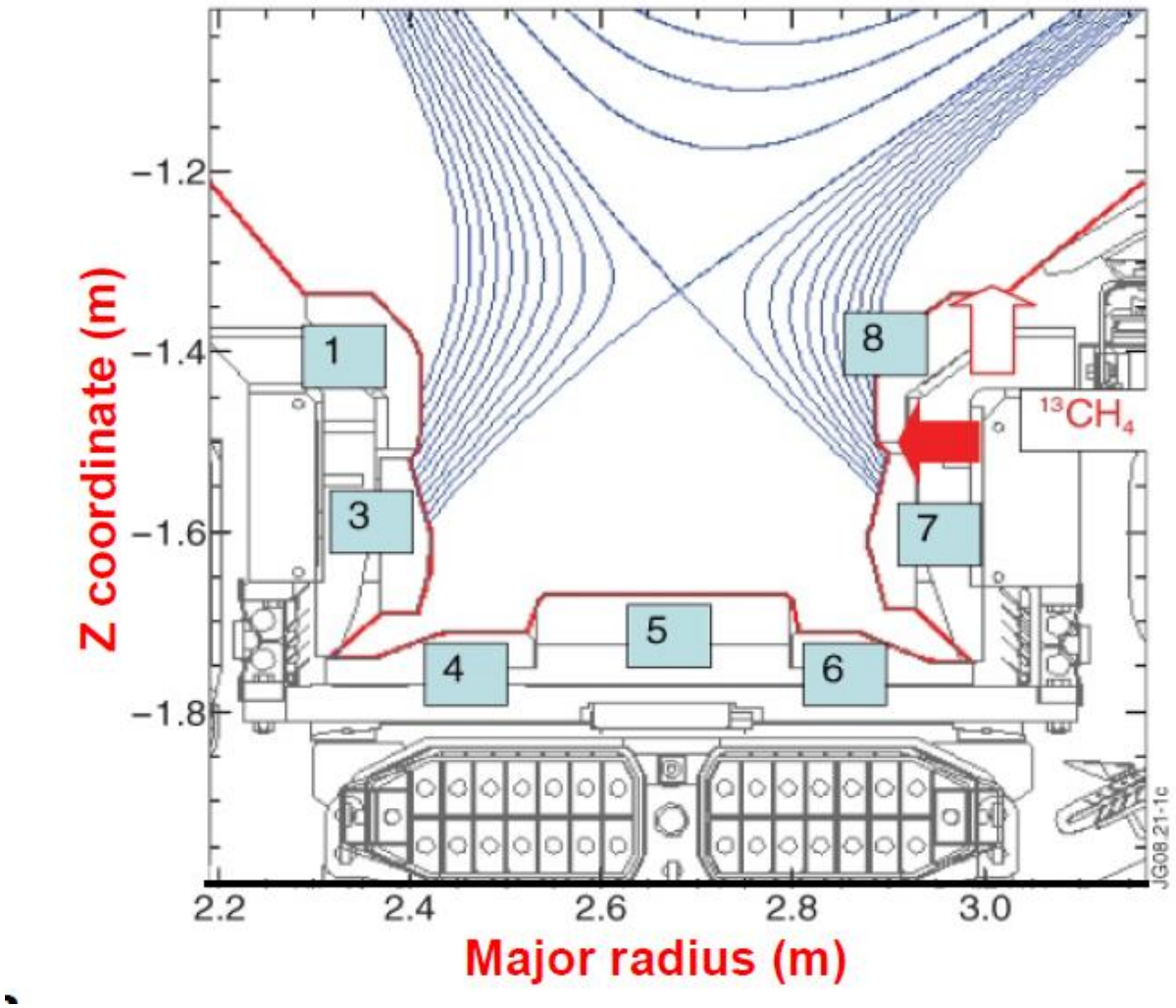

Figure 53: Cross-section of the JET MkII-SRP divertor showing the principle $^{13}CH_4$ injection point (heavy red arrow) and a supposed leakage path (hollow red arrow).

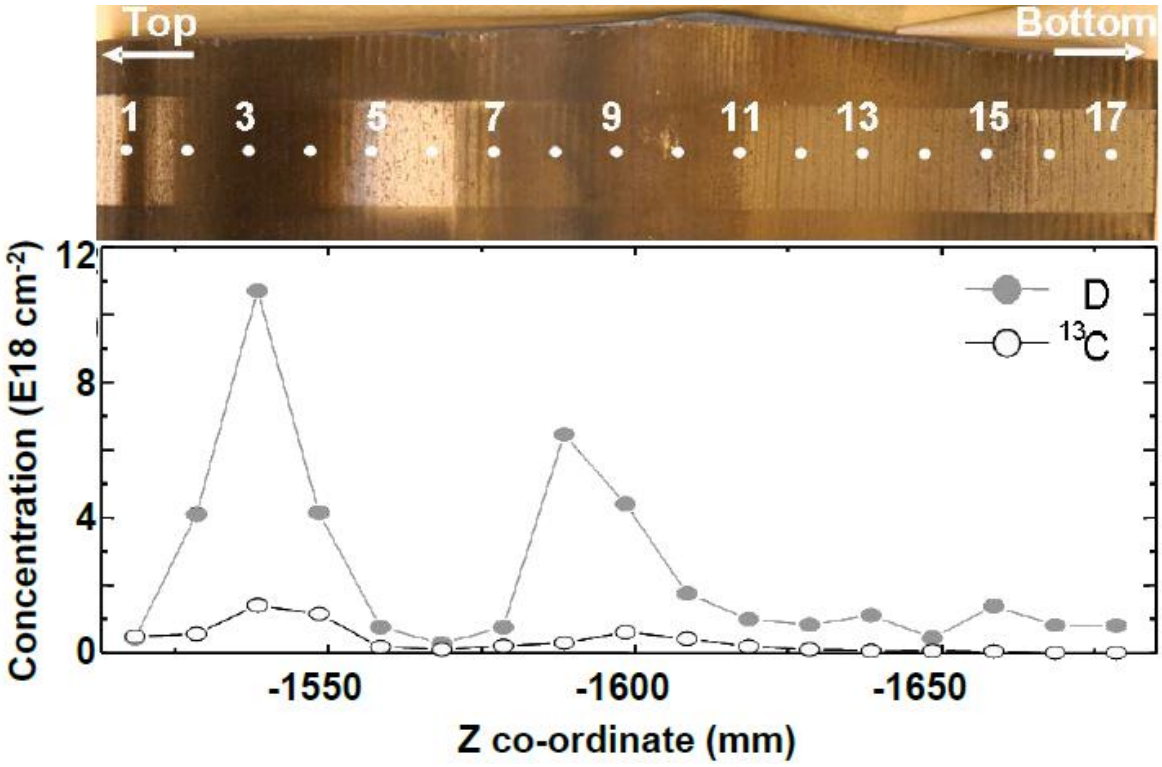

Figure 54: D and ^{13}C concentrations plotted along the W-stripe seen in the panel above. The left-hand edge of the stripe in the picture is the top of Tile 7, the right-hand edge is the bottom

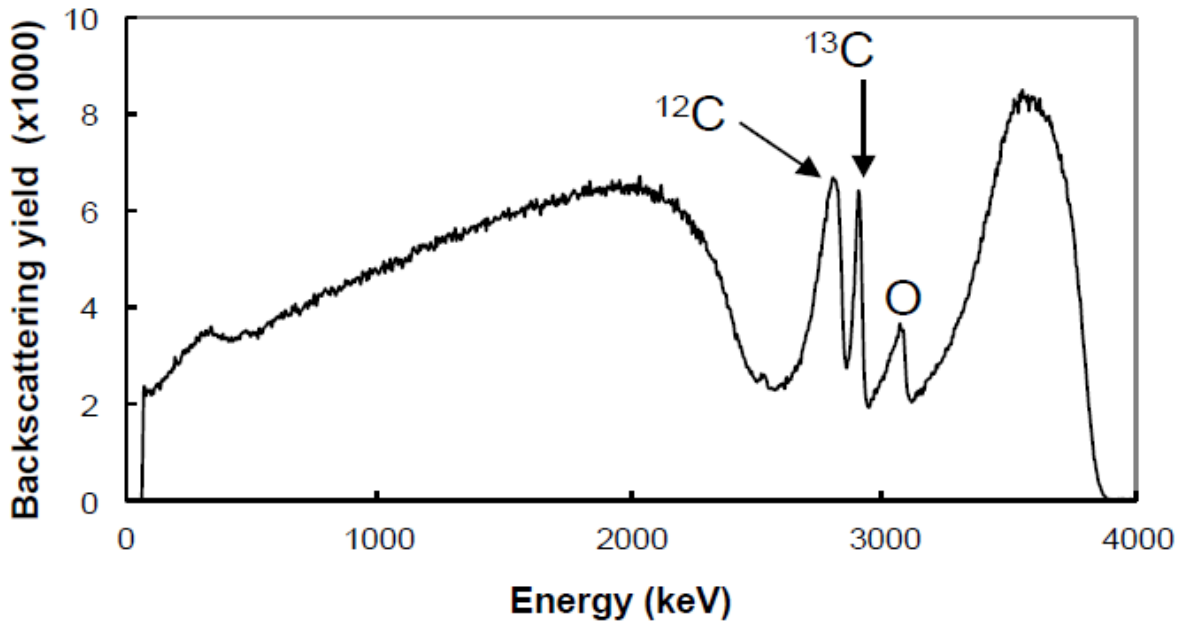

Figure 55: RBS spectrum of the thin deposit comprising ^{12}C, ^{13}C and O on the W-stripe near the top of Tile 7 after exposure in JET 2001-2004 (where D and ^{13}C are maxima in Fig.32).

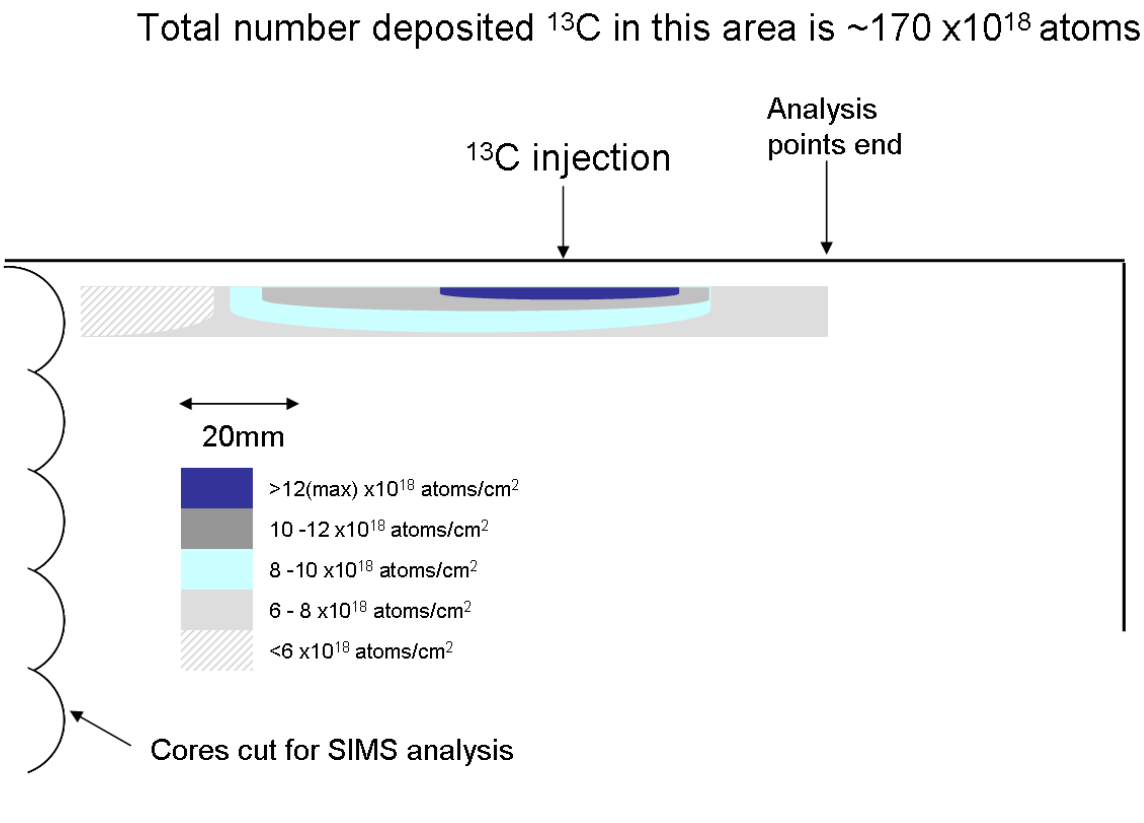

Figure 56: A 2-dimensional plot of the ^{13}C deposit of a Tile 7 (2ONG7A) as derived from RBS spectra, in the region adjacent to a gas injection nozzle between Tiles 7 and 8 at the top of the front surface. The maximum is in a region normally protected from incident ions by the slightly prominent lower edge of Tile 8. The ^{13}C flow is in the direction of the arrow beneath "^{13}C injection".

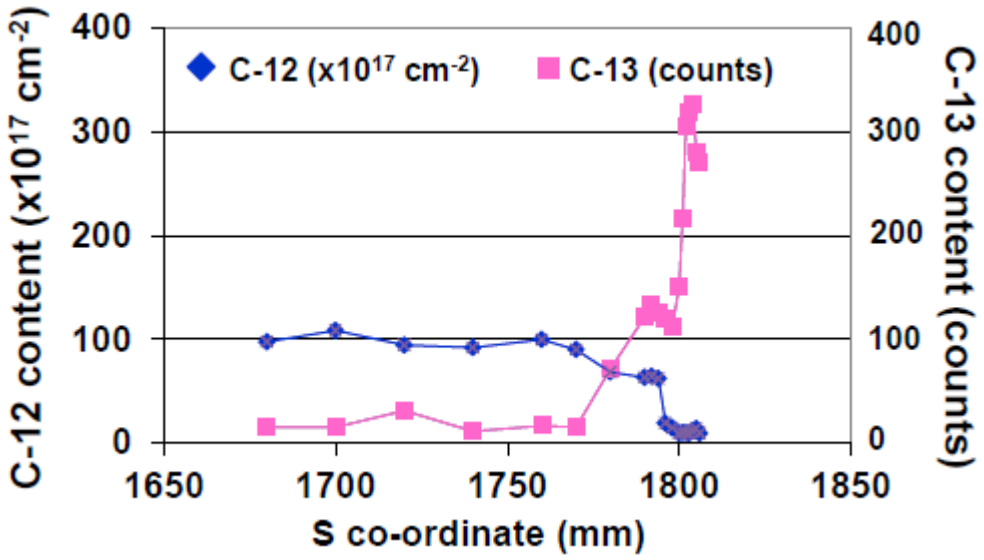

Figure 57: Plot of ^{13}C and ^{12}C measured by NRA across Tile 2ONG7A, showing that the deposit at the top edge is almost exclusively ^{13}C and not ^{12}C

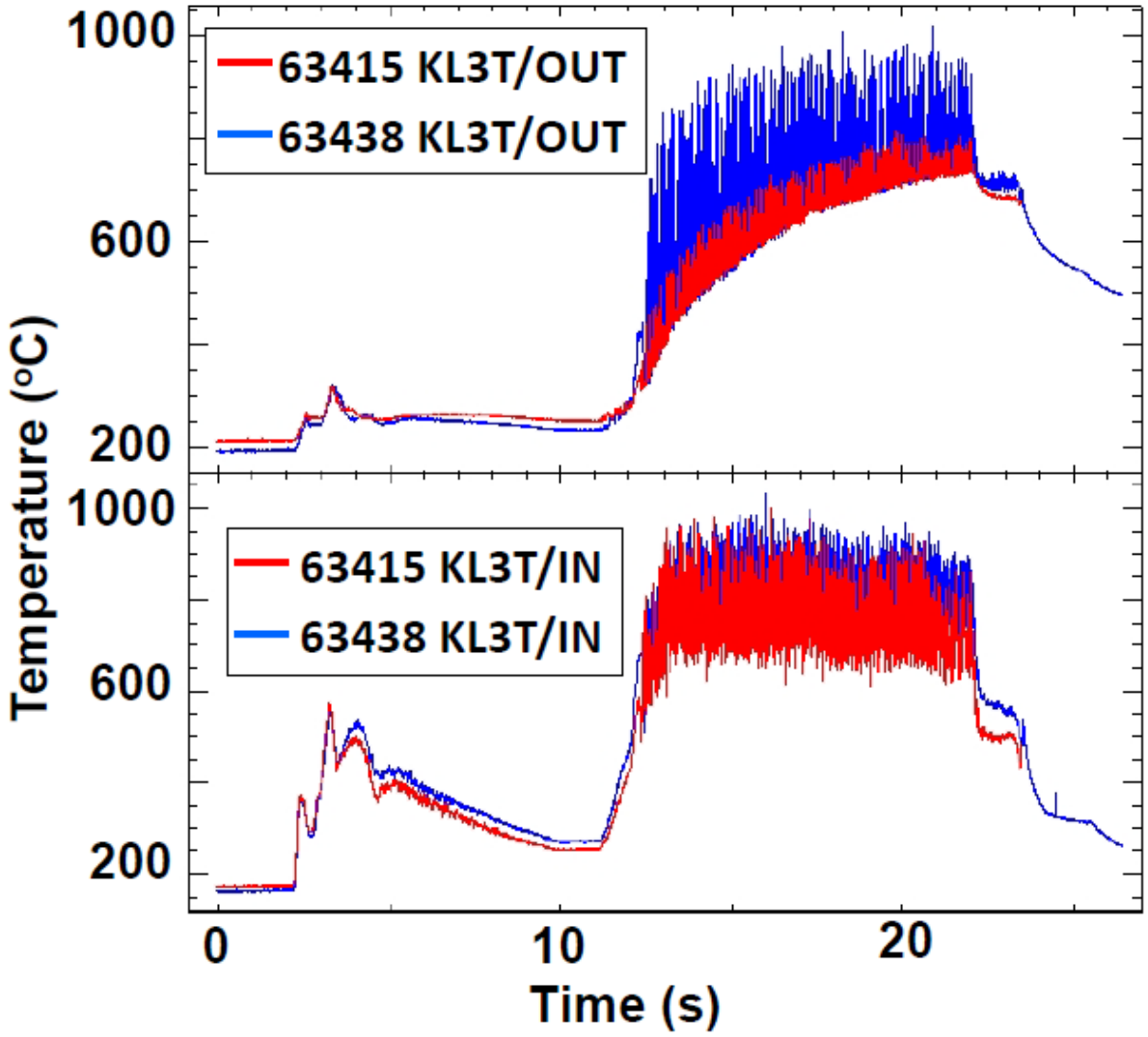

Figure 58: Maximum temperatures measured with an infra-red camera during selected pulses during the ^{13}C puffing experiments at the end of the 2002-4 campaign.The upper part shows the maximum temperature in the outer divertor during pulse 63415 (red curve) and 63438 (blue curve). The lower part shows the maximum temperature in the inner divertor during pulse 63415 (red curve) and 63438 (blue curve)

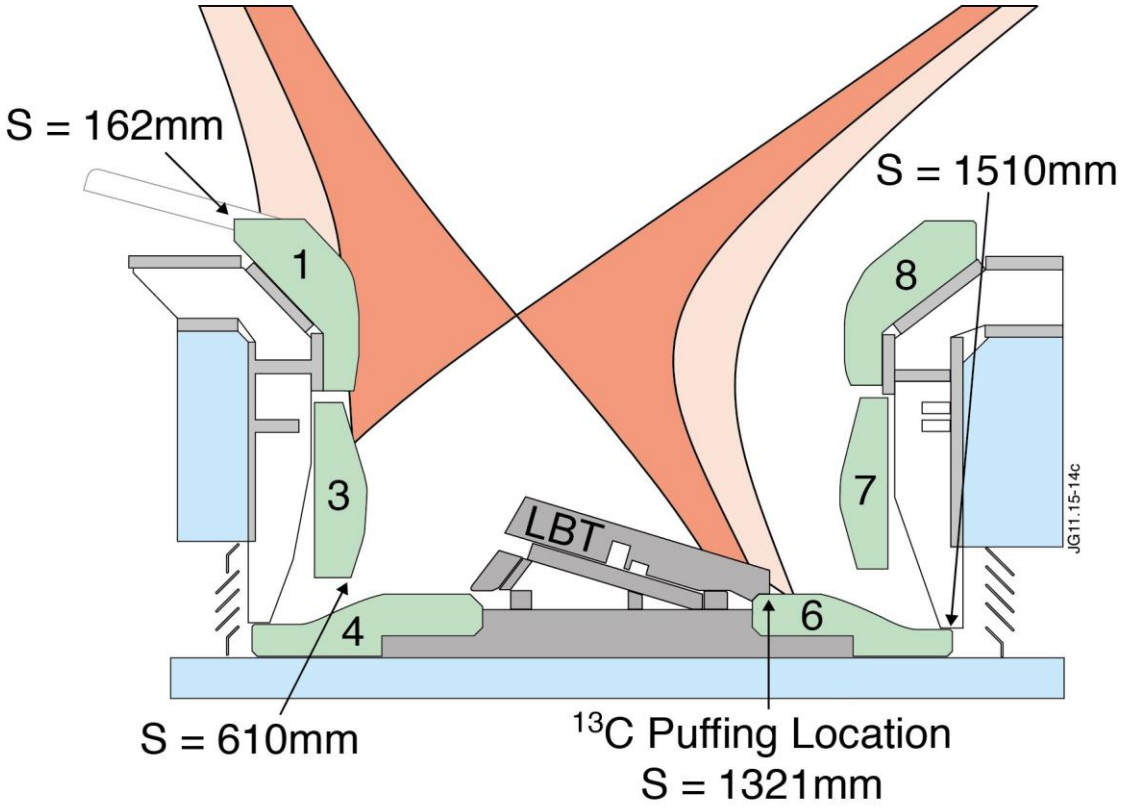

Figure 59: Cross-section of the JET MkII-HD divertor showing the tile numbering, some relevant s co-ordinates (see text), and the plasma configuration used during the ^{13}C (as methane) puffing experiments on the last day of the 2007-9 operational period.

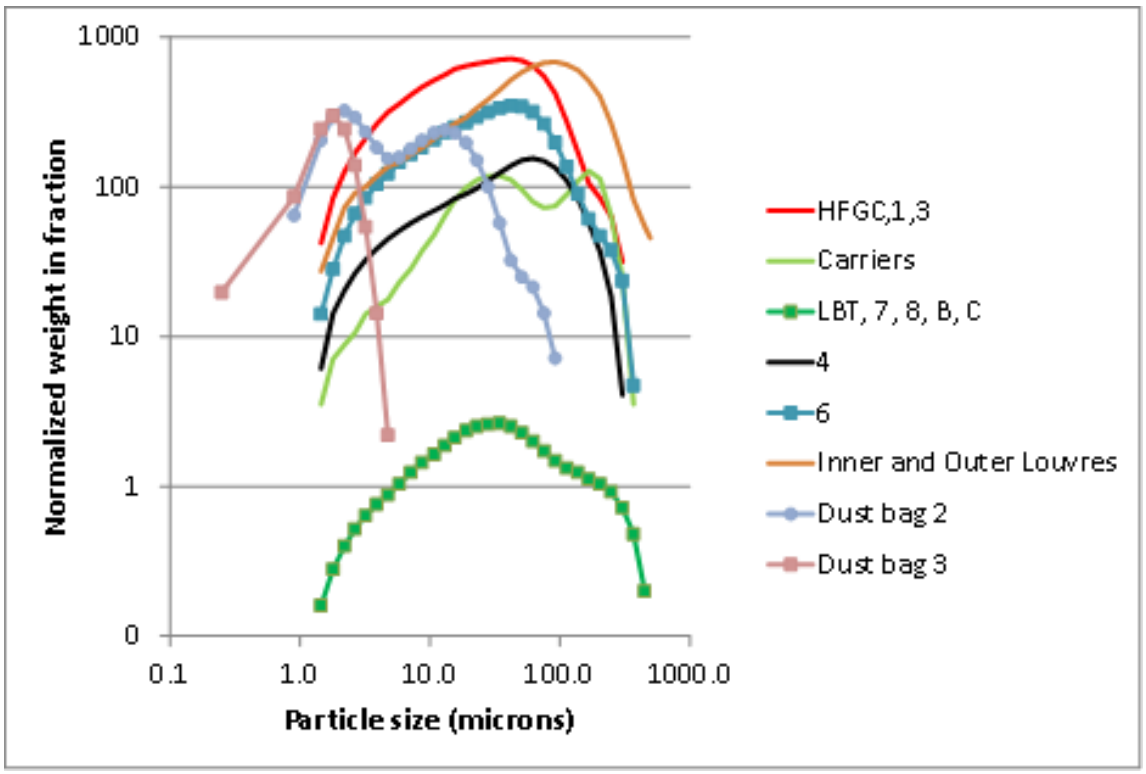

Figure 60: Particle Sizing Data - Results given as weight in the particular size fraction multiplied by the total weight of the dust sample collected versus the particular size fraction in microns.

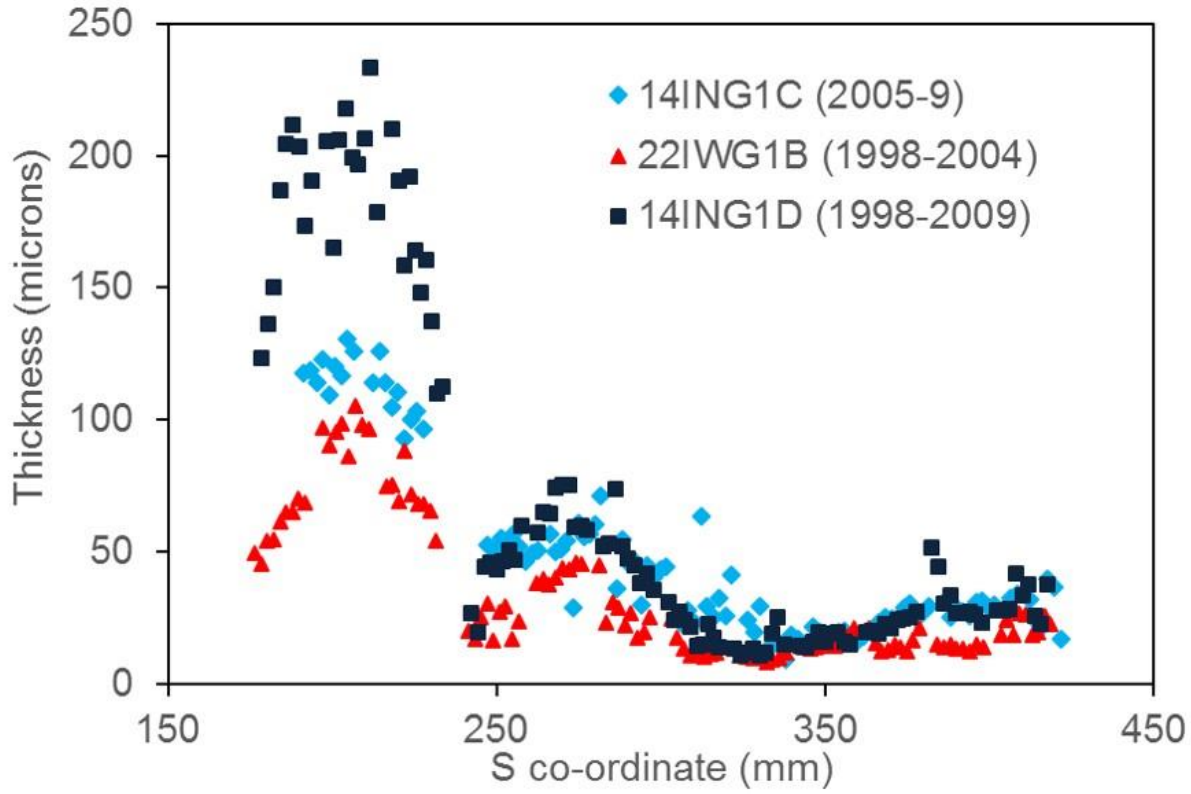

Figure 61: Film thicknesses from optical microscopy of sections for Tiles 1 removed after operational periods 1998-2004 (Module 22), 1998-2009 (Module 14) and 2004-9 (Module 14).

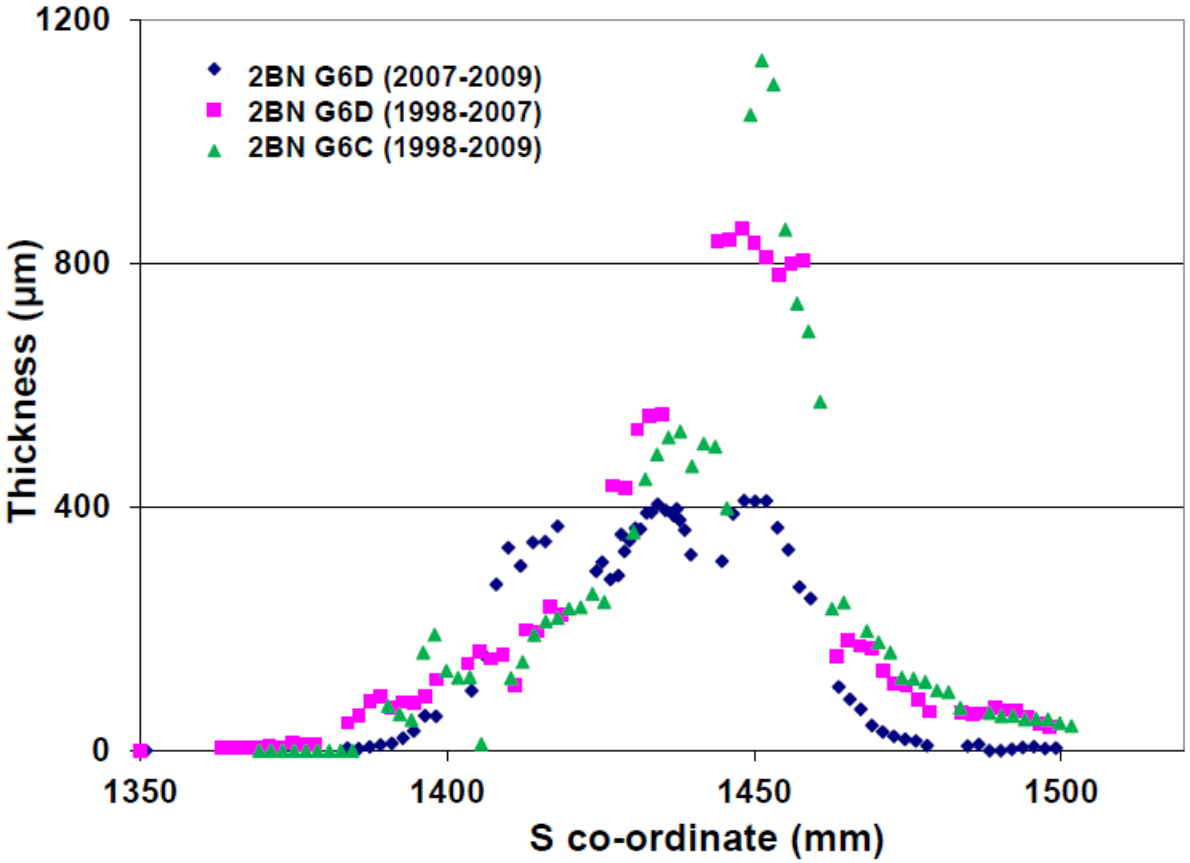

Figure 62**:** Film thicknesses from optical microscopy of sections for Tiles 6 removed from Module 2 after operational periods 1998-2007, 1998-2009 and 2007-9.